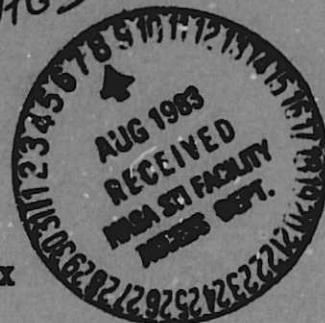


General Disclaimer

One or more of the Following Statements may affect this Document

- This document has been reproduced from the best copy furnished by the organizational source. It is being released in the interest of making available as much information as possible.
- This document may contain data, which exceeds the sheet parameters. It was furnished in this condition by the organizational source and is the best copy available.
- This document may contain tone-on-tone or color graphs, charts and/or pictures, which have been reproduced in black and white.
- This document is paginated as submitted by the original source.
- Portions of this document are not fully legible due to the historical nature of some of the material. However, it is the best reproduction available from the original submission.

DRA
NAG 74



**TURBULENCE MEASUREMENTS IN A COMPLEX
FLOWFIELD USING A CROSSED HOT-WIRE**

By

BRIAN EUGENE MCKILLOP

Bachelor of Science in Mechanical Engineering

Oklahoma State University

Stillwater, Oklahoma

1981

(NASA-CR-173080) TURBULENCE MEASUREMENTS IN
A COMPLEX FLOWFIELD USING A CROSSED HOT-WIRE
M.S. Thesis (Oklahoma State Univ.,
Stillwater.) 132 p HC A07/MF A01 CSCL 20D

N83-35316

Unclas
G3/34 36656

**Submitted to the Faculty of the Graduate College
of the Oklahoma State University
in partial fulfillment of the requirements
for the Degree of
MASTER OF SCIENCE
July, 1983**

**TURBULENCE MEASUREMENTS IN A COMPLEX
FLOWFIELD USING A CROSSED HOT-WIRE**

By

BRIAN EUGENE MCKILLOP

Bachelor of Science in Mechanical Engineering

Oklahoma State University

Stillwater, Oklahoma

1981

**Submitted to the Faculty of the Graduate College
of the Oklahoma State University
in partial fulfillment of the requirements
for the Degree of
MASTER OF SCIENCE
July, 1983**

Name: Brian Eugene McKillop

Date of Degree: July, 1983

Institution: Oklahoma State University Location: Stillwater, Oklahoma

Title of Study: TURBULENCE MEASUREMENTS IN A COMPLEX FLOWFIELD USING A
CROSSED HOT-WIRE

Pages in Study: 120

Candidate for Degree of Master of Science

Major Field: Mechanical Engineering

Scope and Method of Study: Measurements of turbulence quantities in complex axisymmetric, nonreacting, nonswirling, flowfields have been carried out using a crossed hot-wire anemometer. Mean velocity, turbulence intensities, turbulent viscosity and Reynolds stress are measured in a round free jet and confined jet flowfields. The free jet measurements provide an independent check on the data acquisition and interpretation techniques. Measurements were made in the confined jet, a model of an axisymmetric can combustor, with an expansion ratio $D/d=2$, an expansion angle α of 90° and axial location increments of 0.5 diameters. The confined jet was investigated with and without a contraction nozzle of an area ratio of 4 located at $L/D=2$.

Findings and Conclusions: The free jet measurements validated the experimental technique and data reduction. The results show good agreement with those of previous research. Measurements in the confined jet indicate that the crossed hot-wire used cannot handle axial flow reversal and that the experimental technique is inadequate for the measurement of time-mean radial velocity. Other quantities show a high level of comparability. Time-mean and turbulence characteristics with the contraction nozzle at $L/D=2$ show little change from that of the corresponding flowfield without a contraction nozzle.

ADVISER'S APPROVAL

David G. Lilley.

TURBULENCE MEASUREMENTS IN A COMPLEX
FLOWFIELD USING A CROSSED HOT-WIRE

Thesis Approved:

David G. Hilkey.

Thesis Adviser

A. J. Ghajar

R. L. Lawrence

Dean of the Graduate College

ACKNOWLEDGMENTS

The author wishes to express his appreciation to his major adviser, Dr. David G. Lilley for his advice and guidance. Gratitude is also extended to Dr. Richard L. Lowery and Dr. Afshin J. Ghajar of the committee who provided helpful suggestions and Dr. John A. Wiebelt for his guidance on data acquisition.

Further appreciation is extended to Ms. Rhonda Smith for her expert typing skills and advice in the preparation of this thesis.

Finally, the author wishes to express sincere gratitude for the financial support of the National Aeronautics and Space Administration and Air Force Wright Aeronautical Laboratories through Grant No. NAG 3-74.

TABLE OF CONTENTS

Chapter	Page
I. INTRODUCTION	1
1.1 Investigation of Combustor Flowfields.	1
1.2 The Problem of Turbulence Measurement.	2
1.3 Previous Experimental Studies.	3
1.3.1 Recent Studies at O.S.U.	3
1.3.2 Free Jet.	4
1.3.3 Confined Jet.	5
1.4 The Present Contribution	7
II. EXPERIMENTAL FACILITIES.	9
2.1 Idealized Flowfields	9
2.2 Free Jet	10
2.3 Confined Jet	10
2.4 Hot-wire Instrumentation and A/D Conversion.	12
III. EXPERIMENTAL TECHNIQUES AND DATA REDUCTION	14
3.1 Experimental Techniques.	14
3.2 Turbulent Viscosity Formulation.	19
IV. RESULTS.	23
4.1 Measurement Procedures	23
4.2 Free Jet Results	24
4.2.1 Mean Velocity	24
4.2.2 Turbulence Intensities.	25
4.2.3 Shear Stress.	25
4.2.4 Turbulent Viscosity	25
4.3 Confined Jet Results	26
4.3.1 Mean Velocity	26
4.3.2 Turbulence Intensities.	27
4.3.3 Shear Stress.	27
4.3.4 Turbulent Shear	28
V. CLOSURE.	29
5.1 Summary and Conclusions.	29
5.2 Recommendations for Further Work	30
REFERENCES.	31

Chapter	Page
APPENDIXES.	35
APPENDIX A - TABLES.	35
APPENDIX B - FIGURES	54
APPENDIX C - COMPUTER PROGRAM USER'S GUIDE	84
APPENDIX D - COMPUTER PROGRAM LISTING.	104

LIST OF TABLES

Table	Page
I. Free Jet Flowfield Data	36
II. Confined Jet Flowfield Data	42
III. Confined Jet With Contraction Nozzle Flowfield Data	48

LIST OF FIGURES

Figure	Page
1. Axisymmetric Combustor of a Gas Turbine	5
2. Different Regions in a Turbulent Jet.	56
3. The Confined Jet Flowfield.	57
4. Free Jet Apparatus.	58
5. Schematic of the Overall Experimental Facility.	59
6. The Contraction Nozzle with Area Ratio of 4	60
7. Hot-wire Orientation.	61
8. Constant Temperature Anemometer	61
9. Schematic of the Constructed Devices.	62
10. Instrumentation Layout.	63
11. Hot-wire Probe Mounted on the Confined Jet Test Section	64
12. Hot-wire Calibration Curves	65
13. Sensitivity Parameters D_m and B_ϕ Versus \bar{u}	66
14. Angulation Test Coordinate System	67
15. Calibration Plot for Sensitivity to Angulation.	68
16. Free and Confined Jet Coordinate System	69
17. Free Jet Radial Distribution of Time-Mean Velocities.	70
18. Free Jet Radial Distribution of Turbulence Intensities.	72
19. Free Jet Radial Distribution of Turbulent Shear Stress.	74
20. Free Jet Radial Distribution of Turbulent Viscosity	75
21. Confined Jet Radial Distribution of Time-Mean (a) Axial and (b) Radial Velocities	76

Figure	Page
22. Confined Jet Radial Distribution of (a) Axial and (b) Radial Turbulence Intensities	77
23. Confined Jet Radial Distribution of Turbulent Shear Stress. . .	78
24. Confined Jet Radial Distribution of Turbulent Viscosity	79
25. Confined Jet with Contraction Nozzle Radial Distribution of Time-Mean (a) Axial and (b) Radial Velocities	80
26. Confined Jet with Contraction Nozzle Radial Distribution of (a) Axial and (b) Radial Turbulence Intensities	81
27. Confined Jet with Contraction Nozzle Radial Distribution of Turbulent Shear Stress.	82
28. Confined Jet with Contraction Nozzle Radial Distribution of Turbulent Viscosity	83

NOMENCLATURE

A, B, C	calibration constants
A_m	axial velocity fluctuation sensitivity coefficient
A_v	radial velocity fluctuation sensitivity coefficient
B_ϕ	$(E_1 A_{v_1} + E_2 A_{v_2})$
C_u	eddy viscosity factor
D	confined jet tube diameter
D_m	$(E_1 A_{m_1} + E_2 A_{m_2})$
d	nozzle exit diameter
dBA	attenuation of channel A
dBB	attenuation of channel B
E	time-mean voltage of hot-wire = \bar{e}
e	voltage of hot-wire = $\bar{e} + e'$
j	radial position indicator; j=1 on the centerline
j_{\max}	maximum radial position indicator
K	free jet parameter
L	distance from nozzle exit to contraction nozzle
R_w	hot-wire resistance
u	axial velocity component = $\bar{u} + u'$
$\overline{u'v'}$	turbulent Reynolds shear stress
v	radial velocity component = $\bar{v} + v'$
x, r	axial and radial coordinates
Z	effective cooling velocity

l	single mixing length scale
α	expansion angle
ϕ	yaw angle
ν_t	turbulent viscosity
ν_t^*	nondimensionalized turbulent viscosity

Subscripts

1, 2	refer to hot-wires 1 or 2
0	value at $x = 0$
rms	root-mean-square value

Superscripts

(\quad)	time-mean average
$(\quad)'$	fluctuating quantity

CHAPTER I

INTRODUCTION

1.1 Investigation of Combustor Flowfields

A renewed interest in gas turbine combustor analysis has been initiated by new emphasis on pollutant and noise suppression and fuel economy. The combustor, shown in Figure 1, see Appendix B, must fulfill several requirements (1) including:

1. Burn fuel efficiently.
2. Maintain stable combustion over a wide range of operating conditions.
3. Uniform distribution of temperature in product gases.
4. Minimum size and weight.
5. Minimum pressure drop.

Flowfields within such combustors are very complex due to the corner and central recirculation regions produced by a rapid expansion and strong swirl imparted to the incoming air. Thus, the flow is a swirling, recirculating, turbulent one and is, therefore, difficult to analyze. Aerothermochemistry is another formidable problem facing the designer, and more thorough and accurate procedures can yield the design objectives more quickly and less expensively.

The general aim of this investigation is to provide information on combustor phenomena so that combustion characteristics can be determined. These characteristics either in the form of experimental or

theoretical analysis are useful to designers. Theoretical investigators can also compare the experimental data with the data from a numerical solution of the appropriate governing partial differential equations. With this general knowledge, combustor development time and cost will be reduced.

The research presently being investigated involves several methods of analysis for both swirling and nonswirling flows. It consists of flow visualization, computer simulation, and time-mean and fluctuating velocity measurements with the emphasis on nonreacting, steady turbulent flow in axisymmetric geometries. Two simplified flowfields are being investigated: a free round jet issuing horizontally into a quiescent atmosphere and a confined jet. In the confined jet, flow enters through a nozzle of exit diameter d and proceeds via a sudden expansion into a tube of diameter D . A swirler may be located upstream of the inlet of the tube to swirl the flow. Also, a contraction nozzle may be positioned at some downstream location in the tube.

1.2 The Problem of Turbulence Measurement

Complex flowfield turbulence measurements have always been a difficult process. Several authors have discussed turbulence phenomena in detail and suggested various methods of turbulence measurement (2-5). The hot-wire anemometer is the most broadly used instrument to obtain turbulence quantities. A single hot-wire in a two-dimensional flow can measure the streamwise components of the time-mean velocity and the root-mean-square velocity fluctuation at a particular location in the flowfield when used at a single orientation. By using multi-orientations of a single hot-wire, the three components of the mean

and fluctuating velocity vector can be determined (6-8). The problems associated with this method are that extensive data reduction is required to calculate the desired turbulence quantities and, because the wire has to be positioned several times, the data obtained is not truly simultaneous. A multi-wire probe can be employed using a single orientation to determine flowfield quantities. In a two-dimensional flow, the time-mean velocities, streamwise and cross stream velocity fluctuations and their cross correlation can be determined with a two-wire probe. A crossed hot-wire probe was used in this study in which the wires were inclined at $\pm 45^\circ$ to the flow direction and parallel to the probe axis. This probe should give more accurate turbulence intensities and cross correlation than a single wire multi-orientation method because it is used at only one orientation and thus the data acquired is nearly simultaneous.

1.3 Previous Experimental Studies

1.3.1 Recent Studies at O.S.U.

As mentioned previously, the research presently being investigated involves several methods. Still (9) and movie (10) photography of neutrally-buoyant helium-filled soap bubbles and injected smoke has aided in the visualization of various combustor flowfields. A five-hole pitot probe has been used to measure time-mean velocities at different swirl strengths (9, 11). Turbulence quantities have been determined with a six-orientation single hot-wire technique (12) in swirling and non-swirling flowfields. Predictions of confined swirling flows corresponding to the ones studied experimentally have been

achieved using a computer code that solves the appropriate partial differential equations (13). These predictions (14) are now supplemented by predictions deduced from downstream nozzle effects (15) and realistic inlet conditions (16).

1.3.2 Free Jet

Corrsin and Uberoi (17) measured the power spectra of velocity and temperature fluctuations in heated and unheated jets using a crossed hot-wire similar to the one used in the present study. They concluded, from their measurements of the shear-correlation spectrum, that the fine structure in the shear flow in a round turbulent jet is isotropic.

Single and double hot-wires were used by Kolpin (18) to determine turbulence intensity and shear stress in the mixing region of a round jet. He found that, above a certain Reynolds number, the jet diameter plays no role in the description of the turbulent field and that the generation of turbulence, governed by the interaction of the large eddies and the mean flow, is a local phenomenon. Davies et al. (19) also conducted experiments in the mixing region in which the turbulence intensity, turbulence spectra, and shear stress were measured. Results indicated that the local intensity of the turbulence is equal to 0.2 times the shear velocity, where this velocity is defined as the product of the local integral length-scale of the turbulence with the local shear.

Measurements in the self-preserving region of a jet were performed by Wygnanski and Fiedler (20) and Rodi (21) using hot-wire probes. The mean velocities, normal stresses and shear stress measured by Wygnanski and Fiedler were also obtained by Rodi as a check. Rodi processed the

signals from the hot-wire anemometer using two different methods: the conventional method and a new method which determines the fluctuating velocities from the squared electrical signal. The results agree between the two studies when the conventional processing is used but higher values are indicated in Rodi's investigation with the squared data processing. Unfortunately, this new method is not applicable to low-intensity flows, that is, flows with less than 25% turbulence intensities.

Bradshaw et al. (22) conducted measurements of turbulence properties in the noise producing region of a free round jet. It was found that the flow in this region is dominated by a group of large eddies, containing nearly a quarter of the turbulent shear stress in the quasi-plane region of the shear layer.

Corrsin (23) and Sami et al. (24) performed turbulence measurements that can be compared with the results of the present study because of the close geometric similarity and experimental conditions. In his experiment, Corrsin used a four hot-wire probe to measure the turbulence quantities and a pitot tube to measure the mean velocity in a heated round jet. Mean axial and radial velocities, turbulence intensities and turbulent shear were determined by Sami et al. using single and crossed hot-wire probes in the flow-establishment region of an air jet issuing into still air. The data of Sami et al. (24) is presented because of the similarity in measurement techniques.

1.3.3 Confined Jet

Flow separation behind an orifice in an electrically heated tube was investigated by Krall and Sparrow (25). The peak Nusselt number

was presumed to be at the reattachment point. They concluded that the local heat-transfer coefficients in the separated, reattached, redevelopment regions are several times as large as those for a fully developed flow. Also, they found that the reattachment length was unaffected by Reynolds number in the turbulent range. This result was verified by Phaneuf and Netzer (26) who measured mean axial velocity and wall static pressure behind abrupt pipe steps. It was concluded that the reattachment zone spreads out with increasing Reynolds number and increasing step height, provided the Reynolds number is in the appropriate range.

Back and Roschke (27, 28) measured the reattachment length downstream of a pipe step by dye visualization in water flows. A conical contraction section was placed just upstream of a sudden expansion to reduce the boundary layer thickness. Dye was injected through holes positioned along the larger diameter tube at intervals of one step height. Reattachment locations were then observed by inspecting the direction of dye flow. Visual observation of small buoyant particles in a fluid in the redevelopment region was accomplished by Feuerstein et al. (29). The length of reattachment found by Feuerstein is slightly different than predicted by Back and Roschke probably due to dissimilar inlet profiles.

Pitot probe and hot-wire measurements in various sudden expansion flowfields were made by Ha Minh and Chassaing (30). The time-mean axial velocity was determined with both instruments and good agreement was exhibited. A rotating, inclining, single hot-wire technique was employed to measure the Reynolds stresses. One of their expansion ratios matched the one used in the present study but the axial locations of their measurements were not comparable.

Moon and Rudinger (31) and Johnson and Bennett (32) developed laser-Doppler Systems to measure mean velocities and recirculation region geometries, but the expansion ratios differed from the one used in the present experiments.

Because of the differences in geometry, comparisons between the results of the cited experiments and the present experimental study are not possible. However, the experiments of Chaturvedi (33) are comparable. Mean velocity and pressure downstream of a sudden expansion of a diameter ratio of 2.0 were measured with a stagnation tube and pitot probe. A single and crossed hot-wire were used to measure the turbulence intensities and turbulent shear stress. Mean velocity was also measured with the single hot-wire. Also comparable are six-orientation single hot-wire measurements recently obtained by Jackson and Lilley (34) in the same test facility as in the present study.

1.4 The Present Contribution

To further develop combustor flowfield prediction techniques, including turbulence modeling, there is a strong need to obtain experimental estimates of the mean and turbulent flow quantities and the turbulent viscosity. In the present study, a crossed hot-wire single orientation technique is employed to measure mean velocity, turbulence intensities and Reynolds stress in a round free jet and in a combustor simulation confined jet flowfield. The free jet measurements provide an independent check on the data acquisition and interpretation techniques. Measurements in the confined jet are carried out for nonswirling flow with a sudden expansion.

Chapter II describes the experimental facilities and hot-wire and

raw data acquisition instrumentation. This chapter also explains the concept of fluid flow at abrupt expansions. Experimental techniques, data reduction scheme and turbulent viscosity formulation are given in Chapter III. The computer program utilized in the data reduction and user's guide are contained in Appendixes D and C respectively. Measurement procedures and results for free jet and confined sudden expansion flows are discussed in Chapter IV. Tables of output quantities are contained in Appendix A and Appendix B consists of the figures. Some of the turbulence quantities are compared with measurements done by Sami et al. (24) in the free jet and Chaturvedi (33) and Jackson and Lilley (34) in the confined jet facilities. Chapter V concludes by summarizing the results of the present study and suggests further research.

CHAPTER II

EXPERIMENTAL FACILITIES

2.1 Idealized Flowfields

A round free jet issuing into a still ambient fluid, shown in Figure 2, has been the subject of many experimental investigations. The flow may be separated into three regions, each having a distinct set of characteristics. Region I contains a potential core of uniform mean velocity bounded by a shear layer. This region starts at the nozzle exit and extends to four or five nozzle diameters downstream. In region II, the velocity on the jet centerline decreases with increasing distance. Region II is also characterized by the lack of similarity in the mean velocity distribution. After about eight nozzle diameters, region III starts and the jet flow becomes fully developed in which the mean velocity flow patterns in consecutive sections become similar.

Confined flow at abrupt expansions, as in an actual gas turbine combustor, is a typical example of the problem of fluid flow separation from the boundary. A region of reverse flow is caused by this separation at the sudden expansion. This region, called the corner recirculation zone (CRZ), is associated with a large pressure drop which adversely affects the performance of a can-type combustion chamber. The turbulence levels are high on the shear layer between the two regions which indicates that, at this position, good combustion would occur. Flows in actual reacting can combustors have an area of high

heat transfer at the location of the reattachment of the dividing streamline which could lead to rapid deterioration of the walls of the combustor. A schematic of the test section geometry and expected recirculation zones are shown in Figure 3. The central torroidal recirculation zone (CTRZ) is present only with swirling flow.

2.2 Free Jet

The free jet facility, shown in Figure 4, consists of a seamless contoured nozzle fed by a thermally stabilized compressed air generator which delivers the desired flow rate through a small pressure regulator and a Fisher and Porter Model 10A1735A rotameter. The nozzle has a throat diameter of 3.4 cm and an effective flow management section just upstream.

It is necessary to calibrate the crossed hot-wires in a flow of known characteristics. The potential core of the free jet was utilized for this calibration. The sensitivity to angulation (see Section 3.1) was obtained by the use of a rotary table on the jet centerline to rotate the probe inside the potential core from -10° to $+10^\circ$ to the free stream flow direction. An "L" shaped probe bracket holds the probe while it is being calibrated.

2.3 Confined Jet

The Oklahoma State University Confined Jet Test Facility is used in this experimental study. It is a simulation of a typical axisymmetric combustion chamber of a gas turbine engine. Figure 5 shows a schematic of the overall facility. Ambient air enters the low-speed wind tunnel through a foam rubber air filter. The air then flows through an axial

flow fan driven by a 5 h.p. varidrive motor which allows the flow rate to be varied for different test conditions. Next, the flow passes into a flow conditioning section which reduces the intensity of the turbulence caused by the driving fan. This turbulence management section consists of a perforated aluminum plate, followed by a fine mesh screen, a 12.7 cm length of packed straws, and five more fine mesh screens. The flow then enters a contoured nozzle designed by the method of Morel (35) to produce a minimum adverse pressure gradient on the boundary layer to avoid local separation and flow unsteadiness. The ratio of the turbulence management cross section to that of the nozzle throat, by area, is approximately 22.5. The nozzle throat diameter d is 15 cm.

Finally, the flow enters the test section, which is an idealized combustion chamber model. It is composed of a swirler (optional), an expansion block and a long plexiglass tube. The expansion block is a 30 cm diameter disk of wood that has a 15 cm diameter hole centered on its axis and is attached after the swirler. In this study, the swirler is not used. Thus, the expansion block is mounted directly onto the throat of the wind tunnel nozzle. The flow expands into a plexiglass tube of diameter D of 30 cm, thus giving a diameter expansion ratio (D/d) of 2. The test section is constructed of plexiglass for flow visualization and ease of location of measuring probes. Holes are located at multiples of $x/D = 0.5$ along the length of the tube, so that the hot-wire probe can radially traverse the airflow. A contraction nozzle with an area ratio of 4, shown in Figure 6, may be positioned downstream of the expansion block to simulate the confining wall of a real gas turbine combustor. The test section does not have film cooling holes or dilution air holes, typical in a real

combustor. The ample size of the test section used in this study provides good probe resolution for the hot-wire measurements.

2.4 Hot-wire Instrumentation and A/D Conversion

As mentioned earlier, a crossed hot-wire probe, DISA Type 55P63, is used in this experimental study in which the wires are inclined at $\pm 45^\circ$ to the flow direction and parallel to the probe axis. The probe orientation in the flowfield is illustrated in Figure 7. Each hot-wire has a separate constant temperature anemometer for complex flow measurement. A circuit diagram for the DISA 55M01 main frame with a 55M10 standard bridge anemometer is given in Figure 8. To obtain the turbulence intensities in the axial and radial directions, it is necessary to instantaneously add and subtract the anemometer voltage outputs. The adder and subtractor circuits were constructed of commercially available 741 op amps and are shown in Figure 9. The multiplication of the voltages by a Saicor Model SAI 43 correlation and probability analyzer will give the shear stress. Because the fluctuating signals are small, each signal is amplified by a Hewlett Packard Amplifier with a 20 dB gain. The frequency response of the hot-wires and the associated electronics is approximately 40 kHz based on square wave response tests. The use of linearizers was judged unnecessary from experience in the use of crossed hot-wire anemometry gained previously at Oklahoma State University by researchers such as Morrison (36) and Swearingen (37).

To increase the accuracy of the measurements, a microprocessor with 12-bit analog to digital (A/D) conversion is employed to acquire the data. A schematic of the hot-wire and data acquisition equipment layout is shown in Figure 10. Because the A/D converter, an Octogon

Sys-2, has a maximum input voltage of 2.5 V, the incoming mean voltages are stepped down by a factor of four. The rms signals from the adder and subtractor are changed from AC to DC signals so that the A/D converter can read them. Accuracy with 12-bit conversion is:

$$\frac{1}{2^{12}-1} \times 2.5 \text{ V} \times 4 \approx 0.0024 \text{ V} \quad \text{for mean voltages}$$

$$\frac{1}{2^{12}-1} \times 2.5 \text{ V} \approx 0.006 \text{ V} \quad \text{for fluctuation voltages}$$

The sampling rate is 100 per second if the microprocessor with A/D conversion is just reading the input signals. In this experimental study, however, the microprocessor calculates an average of 625 voltages for each input signal and thus the sampling is impaired to the point of reading 12 voltages per second.

A traversing mechanism shown in Figure 11, supports the hot-wire in the confined jet test facility. The hot-wire probe is inserted into the flow through a rotary vernier and a base that mounts on the outside of the plexiglass tube. With the rotary vernier, it is possible for the probe to be traversed to any radial position at selected axial locations.

CHAPTER III

EXPERIMENTAL TECHNIQUES AND DATA REDUCTION

3.1 Experimental Techniques

The hot wires are assumed to obey an extension of King's Law. That is:

$$E^2 = A + BZ^{1/2} + CZ$$

where A, B and C are constants determined a priori by a calibration experiment and Z is the effective cooling velocity. Thus for each wire:

$$\begin{aligned} E_1^2 &= A_1 + B_1 Z_1^{1/2} + C_1 Z_1 \\ E_2^2 &= A_2 + B_2 Z_2^{1/2} + C_2 Z_2 \end{aligned} \tag{1}$$

The calibration is accomplished prior to every experiment by placing the crossed hot-wire on the free jet centerline within the potential core region. The flow rate through the nozzle and thus the exit velocity is varied by an upstream control valve and determined by a rotameter. For each rotameter setting, there is a corresponding axial velocity. Thus the voltage from each of the wires is recorded for each rotameter setting and calibration curves of voltage, E, versus velocity, \bar{u} , can then be drawn. These are presented in Figure 12.

If Equation (1) is inverted, the effective cooling velocity on

each wire is obtained.

$$Z_1 = [(-B_1 + (B_1^2 - 4C_1(A_1 - E_1^2))^{1/2})/2C_1]^2$$

$$Z_2 = [(-B_2 + (B_2^2 - 4C_2(A_2 - E_2^2))^{1/2})/2C_2]^2$$

Therefore, with a mean voltage from wire 1 or 2, the corresponding velocity can be found. Using the geometry shown in Figure 7, the mean axial and radial velocities are given respectively by:

$$\bar{u} = \frac{Z_1 + Z_2}{2}$$

$$\bar{v} = \frac{Z_1 - Z_2}{2}$$

These velocities are nondimensionalized with respect to the nozzle exit velocity, u_o .

The instantaneous velocity fluctuations measured from an inclined hot-wire can be defined by the following expression derived by Corrsin and Uberoi (17):

$$\frac{e'}{E} = A_m \frac{u'}{\bar{u}} \pm A_v \frac{v'}{\bar{u}} \quad (2)$$

where A_m is the sensitivity coefficient for axial velocity fluctuation and A_v is the radial velocity fluctuation sensitivity coefficient.

These coefficients are evaluated in the following manner:

$$A_m = \left. \frac{\partial \ln E}{\partial \ln \bar{u}} \right|_{R_w, \phi \text{ constant}}$$

$$A_v = \left. \frac{\partial \ln E}{\partial \phi} \right|_{R_w, \bar{u} \text{ constant}}$$

If a crossed hot-wire is used at the orientation shown in Figure 7, then equation (2) written for each wire becomes:

$$e_1' = E_1 A_{m_1} \frac{u'}{u} + E_1 A_{v_1} \frac{v'}{u}$$

$$e_2' = E_2 A_{m_2} \frac{u'}{u} - E_2 A_{v_2} \frac{v'}{u}$$

Output from each wire can be instantaneously added and subtracted to obtain:

$$(e_1' + e_2') = (E_1 A_{m_1} + E_2 A_{m_2}) \frac{u'}{u} + (E_1 A_{v_1} - E_2 A_{v_2}) \frac{v'}{u}$$

$$(e_1' - e_2') = (E_1 A_{m_1} - E_2 A_{m_2}) \frac{u'}{u} + (E_1 A_{v_1} + E_2 A_{v_2}) \frac{v'}{u}$$

The crossed hot-wires are matched so that the sensitivity coefficients A_m and A_v are approximately the same for both wires and the overheat ratios of the wires are set so that $E_1 \approx E_2$. These simplifications give:

$$(e_1' + e_2') = D_m \frac{u'}{u}$$

where $D_m = (E_1 A_{m_1} + E_2 A_{m_2})$

and

$$(e_1' - e_2') = B_\phi \frac{v'}{u}$$

where $B_\phi = (E_1 A_{v_1} + E_2 A_{v_2})$

Thus, solving for the turbulent velocities

$$u' = \frac{\bar{u} (e_1' + e_2')}{D_m}$$

$$v' = \frac{\bar{u} (e_1' - e_2')}{B_\phi}$$

which may be nondimensionalized via

$$u'/u_o = (u'/\bar{u}) (\bar{u}/u_o)$$

$$v'/u_o = (v'/\bar{u}) (\bar{u}/u_o)$$

To obtain the appropriate D_m or B_ϕ , the sensitivity coefficients A_m and A_v need to be evaluated. That is:

$$A_m = \frac{\partial \ln E}{\partial \ln \bar{u}} = \frac{\bar{u}}{E} \frac{\partial E}{\partial \bar{u}}$$

$$A_v = \frac{\partial \ln E}{\partial \phi} = \frac{1}{E} \frac{\partial E}{\partial \phi}$$

To determine A_{m_1} and A_{m_2} , $\partial E_1/\partial \bar{u}$ and $\partial E_2/\partial \bar{u}$ are calculated from the derivative of E with respect to \bar{u} of Equation (1). Thus,

$$\begin{aligned} \frac{\partial E_1}{\partial \bar{u}} &= \frac{\partial}{\partial \bar{u}} [(A_1 + B_1 \bar{u}^{1/2} + C_1 \bar{u})^{1/2}] \\ &= \frac{2C_1 \bar{u}^{1/2} + B_1}{4(A_1 \bar{u} + B_1 \bar{u}^{3/2} + C_1 \bar{u}^2)^{1/2}} \end{aligned}$$

Similarly for wire 2:

$$\frac{\partial E_2}{\partial \bar{u}} = \frac{2C_2 \bar{u}^{\frac{1}{2}} + B_2}{4(A_2 \bar{u} + B_2 \bar{u}^{\frac{3}{2}} + C_2 \bar{u}^2)^{\frac{1}{2}}}$$

Therefore, an A_{m_1} and A_{m_2} can be determined for a certain number of velocities and with these, a graph of D_m against velocity can be drawn. The relationship between D_m and velocity is a linear one and is shown in Figure 13. Thus any D_m is known within the range of velocities encountered.

The sensitivity to angulation coefficients A_{v_1} and A_{v_2} are obtained by positioning the probe in the X-Z plane of the round free jet and rotating the probe in 1° increments between $+10^\circ$ and -10° yaw angle to the free stream flow direction, shown in Figure 14. Both mean voltages are recorded for each yaw angle ϕ and a linear curve fit is then applied to each voltage versus ϕ . Figure 15 contains examples of these measurements. Because the wires are matched to a high degree, the curves intersect at or very near the zero degree point. The slopes of these plots are $\partial E_1 / \partial \phi$ and $\partial E_2 / \partial \phi$. This procedure is repeated at the same velocities at which the D_m 's are calculated. Thus, the sensitivity coefficients A_{v_1} and A_{v_2} can be determined for each angulation test velocity. A graph of B_ϕ against velocity can then be plotted and again can be approximated by a straight line as illustrated in Figure 13.

A cross correlator can be used to determine the major shear component of the Reynolds stress tensor in a turbulent shear flow by multiplication of the voltages proportional to u'/\bar{u} and v'/\bar{u} . Thus:

$$\frac{\overline{u'v'}}{\overline{u_o}^2} = \frac{\text{Correlator Output}}{B_\phi \cdot D_m} \frac{\overline{u}^2}{\overline{u_o}^2}$$

From the Honeywell SAI-43A correlator manual:

$$\text{Correlator Output} = \frac{X(\text{Volts})}{125} [10^{(dBA + dBB)/20}]$$

where X is the voltage correlation output,

dBA is the attenuation of channel A, and

dBB is the attenuation of channel B.

A factor of $(40)^2$ is introduced because both hot-wire fluctuating signals are amplified by a gain of 40. Therefore:

$$\frac{\overline{u'v'}}{\overline{u_o}^2} = \frac{X(\text{Volts}) [10^{(dBA + dBB)/20}]}{125 \cdot 1600 \cdot B_\phi \cdot D_m} \frac{\overline{u}^2}{\overline{u_o}^2}$$

A computer code was designed to accomplish the reduction of the voltage data from the hot-wires in the technique just discussed. Appendix C contains the User's Guide to the program with sample output listed in Appendix D.

3.2 Turbulent Viscosity Formulation

While the molecular viscosity is a real property of the fluid, existing whether the fluid is in motion or at rest, the eddy viscosity requires some flow of fluid to become effective and is thus not a property of the fluid but a parameter of the fluid motion. This parameter describes the behavior of the turbulent stresses in terms of the mean-velocity gradients implying the assumption that the turbulence transport is of the gradient-type.

The first-order closure (semi-empirical) methods have been applied extensively to the calculation of the eddy viscosity. The first technique, according to the Boussinesq (38) concept, asserts that the eddy viscosity is a scalar quantity (much larger than the laminar viscosity) that relates turbulent shear stress to the time-mean velocity gradients via:

$$\nu_t = \overline{-u'v'} / (\partial \bar{u} / \partial r + \partial \bar{v} / \partial x) \quad (3)$$

and generally varies throughout the flowfield.

Prandtl (39) proposed that the eddy viscosity could be specified in terms of local parameters: a length scale and the time-mean velocity gradient. He suggested:

$$\nu_t = C_\mu l^2 \frac{\partial \bar{u}}{\partial r}$$

where C_μ is a constant and

l is the mixing length.

Both methods require that the flow is not far from equilibrium and that the turbulence Reynolds number is high. The near equilibrium assumption has been shown to be approximately correct for a mixing layer (40) and the Reynolds number at which experiments are conducted in this present study are sufficiently large.

In the present study, measured turbulent shear stress and time-mean velocity gradients are used to deduce values of eddy viscosity via the Boussinesq concept. Because the magnitude of the mean radial velocity \bar{v} is small compared to the mean axial velocity \bar{u} , Equation (3) becomes:

ORIGINAL PAGE IS
OF POOR QUALITY

$$\nu_t = \overline{u'v'} / \partial \bar{u} / \partial r$$

where $\overline{u'v'}$ is the turbulent Reynolds stress and $\partial \bar{u} / \partial r$ is evaluated by finite difference techniques. Thus,

$$\partial \bar{u} / \partial r = \frac{1}{\Delta r} (\bar{u}_{j+1} - \bar{u}_j) \quad \text{for } j = 1$$

$$\partial \bar{u} / \partial r = \frac{1}{2\Delta r} (\bar{u}_{j+1} - \bar{u}_{j-1}) \quad \text{for } j_{\max} > j > 1$$

$$\partial \bar{u} / \partial r = \frac{1}{\Delta r} (\bar{u}_j - \bar{u}_{j-1}) \quad \text{for } j = j_{\max}$$

From inverse analysis of experimental time-mean measurements, Hinze (2) states that the turbulent viscosity in a round free jet is approximately constant in the central part of the fully-developed region and given by the relation:

$$\nu_t = 0.00196 K u_o d$$

where K is a parameter between 5.4 and 6.39. The latter value is used in agreement with earlier measurements (41). In the free jet, a non-dimensionalized turbulent viscosity ν_t^* given by:

$$\nu_t^* = \nu_t / (6.39 u_o d)$$

should approach the value of 0.00196 in the fully-developed region. Later results will confirm this. In the confined jet, the simple normalization

$$\nu_t^* = \nu_t / (u_o d)$$

is used to be consistent with on-going theoretical studies (42). Its

value, corresponding to 0.00196 in the free jet, is 0.0125. Later deduced values will be seen to be below this in low shear regions and above this in high shear regions.

CHAPTER IV

RESULTS AND DISCUSSION

4.1 Measurement Procedures

Nonswirling nonreacting free and confined jet flows, with coordinate systems shown in Figure 16, are investigated by the use of a crossed hot-wire to measure mean velocities \bar{u} and \bar{v} , fluctuating velocities u' and v' , and Reynolds stress $\overline{u'v'}$. The preceding quantities are normalized with the nozzle uniform axial exit velocity u_0 , determined with the probe from an independent measurement at the nozzle exit face. Radial distribution of turbulent viscosity is also deduced. The Reynolds numbers of the flows under investigation are high enough to ensure that the results are in the Reynolds number independent regime.

Prior to any measurements, the crossed hot-wire probes were calibrated in the free jet facility as described in Section 3.1. The voltage divider box and A/D converter were also calibrated by use of a voltage standard. This was to check that no 'drifting' of the electronics had occurred.

Measurements were made in a free jet at axial locations of x/d of 1, 6, 10, and 20. Because published data exists for the free jet using hot-wire anemometry, it was used to validate the experimental procedure and data reduction discussed in Chapter III since little published data is available for confined jet flowfields using the present method and test section geometry. The results are compared with those of Sami et

al. (24). These results in tabular form are contained in Table I, Appendix A.

Measurements were also made in a model of an axisymmetric can combustor (confined jet test section) with an expansion ratio $D/d=2$, an expansion angle α of 90° and axial location increments of 0.5 chamber diameters. The axial location of zero is actually 1 mm downstream of the enlargement face so as to prevent the hot-wire probe from damage. Comparable are measurements by Chaturvedi (33) and Jackson and Lilley (34). A single hot-wire multi-orientation technique was used by Jackson and Lilley (34) in the same test facility. Table II consists of flow-field data for the confined jet without contraction nozzle. Also, a confined jet flowfield was investigated with a contraction nozzle of an area ratio of 4 located at $L/D=2$. The data for this flowfield is contained in Table III. This nozzle, mentioned earlier, has a 45° slope facing upstream. Time-mean flowfield data for this configuration have been presented previously by Yoon and Lilley (43), using a five-hole pitot probe technique.

4.2 Free Jet Results

4.2.1 Mean Velocities

Presented in Figure 17 are measurements of time-mean axial velocity \bar{u} and radial velocity \bar{v} . These results indicate that the present jet is similar but slightly narrower than the one used by Sami et al. (24). The comparability of the jets also indicates that the experimental techniques and data reduction are sound for time-mean axial velocity but the time-mean radial velocity distribution shows large scatter indicating a slight error in the data reduction or experimental techniques.

4.2.2 Turbulence Intensities

Figure 18 shows the radial distribution of axial and radial turbulence intensities. Fair agreement with Sami et al. (24) can be seen in u'_{rms}/u_o . The values measured here tend to be lower than those presented by Sami et al. (24) although the trends are alike. This can be explained by the difficulty in measuring turbulent, low speed flows. Sami et al. did not present v'_{rms} data. However, they asserted that $u'_{\text{rms}} \approx \sqrt{2} v'_{\text{rms}}$. This relationship is found to be approximately true in the present study. Moving further downstream, the distribution of the turbulence intensities become less pointed and more flat. This indicates that the turbulence levels are spreading laterally.

4.2.3 Shear Stress

The plots depicting the turbulent shear stress are shown in Figure 19. Again, fair agreement with Sami et al. (24) is to be noted. The shear stress is the most difficult to experimentally measure. This probably accounts for the slightly higher peak as compared with Sami et al. (24) at $x/d=6$. As before in the plots of the normal stresses, Figure 19 shows the dissipation of turbulence throughout the flowfield. The radial distributions of normal and shear stress also indicate that the present jet is thinner than the one used by Sami et al. and that the nozzle is of slightly different design causing variations in the stresses as compared to the present study.

4.2.4 Turbulent Viscosity

The radial distribution of turbulent viscosity calculated from the

shear stress and axial velocity gradient is shown in Figure 20. As can be seen, the turbulent viscosity grows from a spikey, small magnitude profile to one with a larger magnitude and flat appearance. This flat type of distribution with a magnitude of 0.00196 is deduced by Hinze (2) when in the similarity region. The large scatter of the turbulent viscosity at $x/d=10$ and 20 is due to the high sensitivity of ν_t to a change in the time-mean axial velocity.

4.3 Confined Jet Results

4.3.1 Mean Velocity

Figure 21 shows measured values of time-mean axial and radial velocities. A nearly flat axial velocity profile is seen at the entrance of the test section. Comparisons of the time-mean axial velocity with Chaturvedi (33) and Jackson and Lilley (34) show good agreement except in the expected region of recirculation. This is due to two reasons: although a hot-wire anemometer cannot sense flow direction, Chaturvedi (33) and Jackson and Lilley (34) plotted some negative values of time-mean axial velocity by deducing direction from earlier pitot probe data and because of the "L" shaped probe design (see Figure 14) the hot-wires are hidden from the recirculating flow by the probe supports. Because the time-mean radial velocity is calculated from the subtraction of two large quantities producing a small number, the profiles shown in Figure 21 are almost zero at all axial locations. Bruun (44) states that velocities determined by a crossed hot-wire probe have a very strong yaw dependence, particularly \bar{v} . This also may account for the error in the time-mean radial velocity. Thus, the experimental technique is not adequate for these measurements.

The time-mean velocities in the confined jet with the contraction nozzle at $L/D=2$ are presented in Figure 25. The profiles show that the results change very little from the identical flowfield without a contraction nozzle, as also found elsewhere (34,43).

4.3.2 Turbulence Intensities

Inspection of the radial distributions of u'_{rms}/u_o and v'_{rms}/u_o displayed in Figure 22 shows similar trends to those found earlier (33, 34). The axial turbulence intensity values are lower than previous measurements, but the radial turbulence intensity values are in good agreement. The axial turbulence intensity is slightly larger than the corresponding radial quantity with maximum values on the shear layer between recirculating and nonrecirculating flow. Figure 22 also shows that the radial turbulence intensity is damped to a higher degree than the axial turbulence intensity by the presence of the test facility tube wall.

Figure 26 presents turbulence intensities with the contraction nozzle and shows little change from the non-contracted counterpart.

4.3.3 Shear Stress

Shown in Figure 23 is the radial distribution of turbulent shear stress. As can be seen, Chaturvedi's (33) data indicates lower values of shear stress than the present study. Also, results are similar to Jackson and Lilley's (34) with the present measurements having smoother profiles. The shear layer, which is very thin at the entrance to the test section, grows quickly to encompass a large amount of the flowfield. All shear stress values are plotted as positive, although in the vicinity of the recirculation zone, the gradient of the time-mean

axial velocity in the radial direction might be positive, inferring negative values of $\overline{u'v'}$.

Turbulent shear stress profiles of the confined jet flowfield with contraction nozzle in place are presented in Figure 27. Like the normal stresses, there is insufficient change with respect to the flowfield without the contraction nozzle to warrant any new discussion.

4.3.4 Turbulent Viscosity

Figure 24 shows the radial distribution of turbulent viscosity. As shown, the turbulent viscosity grows in magnitude while progressing downstream with large peaks near the centerline ($r/D = 0$) from 1.0 until 2.5 diameters. Here the peak reduces because the mean velocity gradient near the centerline has increased. Although the change in mean axial velocity is little at small radial and axial positions, the peak is not seen since the shear stress is correspondingly small. The peaks in the vicinity of $r/D = 0.25$ at axial locations of 0.5 and 1.0 give an indication of the position of the recirculation zone. The expected free jet turbulent viscosity of 0.00196 corresponds to 0.5 on the horizontal axis. As can be seen, the values of viscosity are lower than this expected value in the low shear regions and larger in high shear regions. It must be noted that the turbulent viscosity is the most difficult of all the turbulence quantities presented to ascertain.

The radial distribution of turbulent viscosity in the confined jet with contraction nozzle is presented in Figure 28. As before, the results indicate that the contraction nozzle effects little change.

CHAPTER V

CLOSURE

5.1 Summary and Conclusions

A crossed hot-wire probe has been employed to measure the time-mean and fluctuating velocities and shear stress in nonswirling nonreacting free and confined jet flows. The turbulent viscosity is also calculated from these results.

The free jet investigation was used to validate the experimental technique and data reduction. The results of the free jet measurements show good comparison with available data.

Measurements were also made in a model of an axisymmetric can combustor (confined jet test section) with an expansion ratio $D/d=2$, an expansion angle, α of 90° and axial location increments of 0.5 diameters. A contraction nozzle was located at $L/D=2$ for some of the confined jet measurements. Good agreement with previous workers is to be noted. The confined jet investigation shows that the crossed hot-wire probe cannot accurately measure recirculating flow without prior direction knowledge, and that the experimental technique is inadequate for deduction of the time-mean radial velocity. The crossed hot-wire technique should give more accurate results of the turbulent shear stress and thus turbulent viscosity than a multi-orientation single-wire technique. Smoother profiles for turbulent shear stress are seen in the present study than

in the previous single-wire study. Faster development of velocity profiles, higher values of turbulence quantities, and larger time-mean radial velocities produced by the recirculation zone are the effects of confining the free jet. Also, time-mean and turbulence characteristics with the contraction nozzle at $L/D=2$ show little change from that of the corresponding flowfield without a contraction nozzle. This is probably due to the high time-mean axial velocity pushing the effects of the contraction nozzle downstream.

5.2 Recommendations for Further Work

Work continuing with the crossed hot-wire should concentrate on deriving a new method to determine the time-mean radial velocity and the yaw dependence factor. Also, a new crossed hot-wire probe with a different geometry or rotating the probe 180 degrees in recirculation regions might alleviate the flow reversal insensitivity problem. If the probe could be set on the main streamline at a particular location, all turbulence quantities with respect to the probe could be found assuming that the probe could be rotated. Then appropriate coordinate transformations could relate the quantities in the probe coordinate frame to quantities in the facility coordinate frame.

REFERENCES

- (1) Lefebvre, A. H. (ed.), Gas Turbine Combustor Design Problems, Hemisphere-McGraw-Hill, New York, 1980.
- (2) Hinze, J. O., Turbulence, 2nd Edition, McGraw-Hill, New York, 1975.
- (3) Bradshaw, P., An Introduction to Turbulence and It's Measurement, Peghmon Press, New York, 1976.
- (4) Beer, J. M. and Chigier, N. A., Combustion Aerodynamics, Halsted Press Division, John Wiley & Sons, Inc., New York, 1972.
- (5) Syred, N., Beer, J. M. and Chigier, N. A., "Turbulence Measurements in Swirling Recirculating Flows", Proceedings, Salford Symposium on Internal Flows, Inst. of Mechanical Engineering, London, England, 1971, pp. B27-B36.
- (6) Drorak, K. and Syred, N., "The Statistical Analysis of Hot-wire Anemometer Signals in Complex Flow Fields", DISA Conference, University of Leicester, 1972.
- (7) King, C. F., "Some Studies of Vortex Divices - Vortex Amplifier Performance Behavior", Ph.D. Thesis, University College of Wales, Cardiff, Wales, 1978.
- (8) Jorgensen, F. E., "Directional Sensitivity of Wire and Fiber Film Probes", DISA Information No. 11, Franklin Lakes, New Jersey, May, 1971.
- (9) Rhode, D. L., Lilley, D. G. and McLaughlin, D. K., "Mean Flowfields in Axisymmetric Combustor Geometries with Swirl", Paper AIAA 82-0177, Orlando, Florida, Jan. 11-14, 1982.
- (10) Lilley, D. G., "Turbulent Combustor Flowfield Investigation", Paper in Combustion Fundamentals Research Conference, held at NASA Lewis Research Center, Cleveland, Ohio, Oct. 21-22, 1982, pp. 152-168.
- (11) Yoon, H. K., "Five-hole Pitot Probe Time-Mean Velocity Measurements in Confined Swirling Flows", M.S. Thesis, Oklahoma State University, July, 1982.

- (12) Janjua, S. I., McLaughlin, D. K., Jackson, T. W. and Lilley, D. G., "Turbulence Measurements in a Confined Jet Using a Six-Orientation Hot-wire Probe Technique", Paper AIAA 82-1262, Cleveland, Ohio, June 21-23, 1982.
- (13) Lilley, D. G. and Rhode, D. L., "A Computer Code for Swirling Turbulent Axisymmetric Recirculation Flows in Practical Isothermal Combustor Geometries", NASA CR-3442, Feb., 1982.
- (14) Rhode, R. L., Lilley, D. G. and McLaughlin, D. K., "On the Prediction of Swirling Flowfields Found in Axisymmetric Combustor Geometries", ASME Journal of Fluids Engng., Vol. 104, 1982, pp. 378-384.
- (15) Abujelala, M. T. and Lilley, D. G., "Confined Swirling Flow Predictions", Paper AIAA 83-0316, Reno, Nevada, Jan. 10-13, 1983.
- (16) Sander, G. F. and Lilley, D. G., "The Performance of an Annular Vane Swirler", Paper AIAA 83-1326, Seattle, Wash., June 27-29, 1983.
- (17) Corrsin, S. and Uberoi, M. S., "Spectrums and Diffusion in a Round Turbulent Jet", NASA Report 1040, 1949.
- (18) Kolpin, M. A., "The Flow in the Mixing Region of a Jet", Journal of Fluid Mechanics, Vol. 18, 1964, pp. 529-548.
- (19) Davies, P. O. A. L., Fisner, M. J. and Barrett, M. J., "Turbulence in the Mixing Region of a Round Jet", Journal of Fluid Mechanics, Vol. 15, 1963, pp. 337-367.
- (20) Wygnanski, I. and Fiedler, H., "Some Measurements in the Self-preserving Jet", Journal of Fluid Mechanics, Vol. 38, 1969, pp. 577-612.
- (21) Rodi, W., "A New Method of Analysing Hot-wire Signals in Highly Turbulent Flow, and Its Evaluation in a Round Jet", DISA Information, No. 17, 1975.
- (22) Bradshaw, P., Ferris, D. H. and Johnson, R. F., "Turbulence in the Noise Producing Region of a Circular Jet", Journal of Fluid Mechanics, Vol. 19, pp. 591-624, 1964.
- (23) Corrsin, S., "Investigation of Flow in an Axially Symmetrical Heated Jet of Air", NACA Wartime Report W94, 1943.
- (24) Sami, S., Carmody, T., and Rouse, H., "Jet Diffusion in the Region of Flow Establishment", Journal of Fluid Mechanics, Vol. 27, 1967, pp. 231-252.

- (25) Krall, K. M. and Sparrow, E. M., "Turbulent Heat Transfer in the Separated, Reattached, and Redevelopment Regions of a Circular Tube", *Journal of Heat Transfer*, Feb., 1966, pp. 131-136.
- (26) Phaneuf, J. T. and Netzer, D. W., "Flow Characteristics in Solid Fuel Ramjets", Report No. NPS-57Nt74081. Prepared for the Naval Weapons Center by the Naval Postgraduate School, Monterey, California, July, 1974.
- (27) Back, L. H. and Roschke, E. J., "Shear Layer Flow Regimes and Wave Instabilities and Reattachment Lengths Downstream of an Abrupt Circular Channel Expansion", *Journal of Applied Mechanics*, Sept., 1972, pp. 677-681.
- (28) Roschke, E. J. and Back, L. H., "The Influence of Upstream Conditions on Flow Reattachment Lengths Downstream of an Abrupt Circular Channel Expansion", *Journal of Biomechanics*, Vol. 9, 1976, pp. 481-483.
- (29) Feuerstein, I. A., Pike, G. K. and Round G. F., "Flow in an Abrupt Expansion as a Model for Biological Mass Transfer Experiments", *Journal of Biomechanics*, Vol. 8, 1975, pp. 41-51.
- (30) Ha Minh, H. and Chassaing, P., "Perturbations of Turbulent Pipe Flow", *Proceedings, Symposium of Turbulent Shear Flows*, Pennsylvania State University, April, 1977, pp. 13.9-13.17.
- (31) Moon, L. F. and Rudinger, G., "Velocity Distribution in an Abruptly Expanding Circular Duct", *Journal of Fluids Engineering*, March, 1977, pp. 226-230.
- (32) Johnson, B. V. and Bennett, J. C., "Velocity and Concentration Characteristics and Their Cross Correlation for Coaxial Jets in a Confined Sudden Expansion; Part II: Predictions", *Proceedings, ASME Symposium on Fluid Mechanics of Combustion Systems*, Boulder, CO, June 22-23, 1981, pp. 145-160.
- (33) Chaturvedi, M. C., "Flow Characteristics of Axisymmetric Expansions", *Proceedings, Journal Hydraulics Division, ASCE*, Vol. 89, May, 1963, pp. 61-92.
- (34) Jackson, T. W. and Lilley, D. G., "Single-wire Swirl Flow Turbulence Measurements", Paper AIAA 83-1202, Seattle, Wash., June 27-29, 1983.
- (35) Morel, T., "Comprehensive Design of Axisymmetric Wind Tunnel Contractions", ASME Paper 75-FE-17, Minneapolis, May 5-7, 1975.

- (36) Morrison, G. L., "Flow Instability and Acoustic Radiation Measurements of Low Reynolds Number Supersonic Jets", Ph.D. Thesis, Oklahoma State University, 1977.
- (37) Swearingen, J. D., "Crossed Hot-wire Measurements in Low Reynolds Number Supersonic Jets", M.S. Thesis, Oklahoma State University, 1979.
- (38) Boussinesq, J., J. Mem. Pres. Acad. Sci., Paris, Vol. 23, 1877, p. 46.
- (39) Prandtl, L., Z. Angew. Math. Mech., Vol. 5, 1925, pp. 136-139.
- (40) Bradshaw, P., Cebeci, T., and Whitelaw, J. H., Engineering Calculation Methods for Turbulent Flow", Academic Press, New York, 1981.
- (41) Hinze, J. O. and Van Der Hegge Zijnen, B. G., "Transfer of Heat and Matter in the Turbulent Mixing Zone of an Axially Symmetrical Jet", Applied Science Res., A1, 1949, pp. 435-461.
- (42) Abujelala, M. T. and Lilley, D. G., Studies in Progress, Oklahoma State University, Stillwater, Okla., 1983.
- (43) Yoon, H. K. and Lilley, D. G., "Five-Hole Pitot Probe Time-Mean Velocity Measurements in Confined Swirling Flows", Paper AIAA 83-0315, Reno, Nev., Jan. 10-13, 1983.
- (44) Bruun, H. H., "Interpretation of X-Hot-Wire Signals", DISA Information No. 18, Fran'clin Lakes, New Jersey, May, 1971.

APPENDIX A

TABLES

TABLE I
FREE JET FLOWFIELD DATA

r/r_0	x/d			
	1	6	10	20
0	1.01100	0.95400	0.64800	0.32700
0.1	1.01300	0.94400		0.32300
0.2	1.01400	0.92700	0.63600	0.31600
0.3	1.01500	0.90100		
0.4	1.01100	0.87600	0.60000	0.30600
0.5	1.00900	0.83600		
0.6	0.99800	0.79500	0.55700	0.30600
0.7	0.96900	0.73900		
0.8	0.87600	0.69400	0.51000	0.30000
0.9	0.72000	0.64100	0.49600	
1.0	0.52300	0.59200	0.47100	0.26600
1.1	0.36200	0.52400	0.44400	
1.2	0.21200	0.47000	0.42500	0.27300
1.3	0.13500	0.43400		
1.4	0.08100	0.40400	0.37000	0.24100
1.5	0.05500	0.31600		
1.6		0.29200	0.31900	0.22700
1.7		0.30500		
1.8		0.25200	0.27900	0.21300
1.9		0.21200		
2.0		0.16700	0.23600	0.20700
2.2			0.20400	0.20900
2.4			0.17300	0.17100
2.6			0.14600	0.16500
2.8				0.14600
3.0				0.13700

(a) \bar{u}/u_0

TABLE I (Continued)

r/r_0	x/d			
	1	6	10	20
0	-0.01000	-0.00700	-0.00100	-0.00500
0.1	-0.00800	-0.00400		0.00900
0.2	-0.00300	0.00000	0.00500	-0.00400
0.3	-0.00100	-0.00100		
0.4	-0.00600	0.00800	0.00800	0.00600
0.5	0.00200	0.01400		
0.6	0.00700	0.00900	0.01700	0.00600
0.7	0.01500	0.01000		
0.8	0.02000	0.01200	0.00500	0.01000
0.9	0.02400	0.02100	0.00900	
1.0	0.01000	0.01700	0.01300	-0.00300
1.1	0.00000	0.00600	0.00700	
1.2	-0.01800	0.00900	0.00400	0.00100
1.3	-0.01700	0.01400		
1.4	-0.01400	0.02600	0.00800	-0.00600
1.5	-0.01100	0.01300		
1.6		0.00100	-0.00100	-0.01000
1.7		0.00700		
1.8		0.01400	0.00400	0.00000
1.9		0.00500		
2.0		-0.00500	0.00400	-0.00300
2.2			0.00200	0.00000
2.4			0.00300	0.00000
2.6			-0.00500	-0.00300
2.8				-0.00100
3.0				0.00000

(b) \bar{v}/u_0

TABLE I (Continued)

r/r_o	x/d			
	1	6	10	20
0	0.02000	0.09100	0.11600	0.06400
0.1	0.02100	0.09000		0.06400
0.2	0.02400	0.09500	0.11700	0.06300
0.3	0.02700	0.10000		
0.4	0.03300	0.11600	0.11600	0.06200
0.5	0.04200	0.12000		
0.6	0.05700	0.12600	0.11400	0.06200
0.7	0.08100	0.12900		
0.8	0.11400	0.13300	0.10800	0.06300
0.9	0.13800	0.13000	0.10800	
1.0	0.12600	0.12600	0.10600	0.05700
1.1	0.09800	0.12100	0.10100	
1.2	0.06000	0.11400	0.10000	0.05700
1.3	0.03800	0.10700		
1.4	0.01900	0.10100	0.09000	0.05200
1.5	0.00900	0.08500		
1.6		0.07900	0.08100	0.05100
1.7		0.08000		
1.8		0.06900	0.07200	0.04900
1.9		0.06100		
2.0		0.04700	0.06200	0.04500
2.2			0.05400	0.04500
2.4			0.04600	0.03900
2.6			0.03900	0.03800
2.8				0.03300
3.0				0.03000

(c) u'_{rms}/u_o

TABLE I (Continued)

r/r_o	1	6	x/d	10	20
0	0.00800	0.06500		0.08800	0.05100
0.1	0.01000	0.06500			0.04900
0.2	0.01100	0.06800		0.09000	0.05000
0.3	0.01600	0.07200			
0.4	0.02100	0.07700		0.08700	0.04800
0.5	0.03000	0.08200			
0.6	0.04400	0.08700		0.08700	0.04700
0.7	0.07200	0.08900			
0.8	0.10500	0.09200		0.08200	0.04800
0.9	0.12800	0.09200		0.08300	
1.0	0.11900	0.09100		0.08000	0.04500
1.1	0.09100	0.08900		0.07900	
1.2	0.05200	0.08400		0.07600	0.04500
1.3	0.02900	0.08100			
1.4	0.01300	0.07600		0.06900	0.04100
1.5	0.00700	0.06200			
1.6		0.05900		0.06100	0.03900
1.7		0.06000			
1.8		0.05100		0.05500	0.03600
1.9		0.04200			
2.0		0.03300		0.04700	0.03500
2.2				0.04000	0.03500
2.4				0.03300	0.02900
2.6				0.02700	0.02800
2.8					0.02500
3.0					0.02300

(d) v'_{rms}/u_o

TABLE I (Continued)

r/r_0	x/d			
	1	6	10	20
0	0.00000	0.00000	0.00097	0.00115
0.1	0.00000	0.00000		0.00092
0.2	0.00000	0.00000	0.00418	0.00158
0.3	0.00000	0.00338		
0.4	0.00000	0.00539	0.00590	0.00166
0.5	0.00000	0.00852		
0.6	0.00000	0.01071	0.00689	0.00143
0.7	0.00093	0.01143		
0.8	0.01115	0.01163	0.00696	0.00207
0.9	0.01296	0.01067	0.00692	
1.0	0.00896	0.00962	0.00671	0.00229
1.1	0.00477	0.00831	0.00615	
1.2	0.00155	0.00700	0.00598	0.00190
1.3	0.00042	0.00594		
1.4	0.00003	0.00518	0.00487	0.00194
1.5	0.00000	0.00376		
1.6		0.00326	0.00383	0.00191
1.7		0.00342		
1.8		0.00249	0.00306	0.00173
1.9		0.00181		
2.0		0.00111	0.00228	0.00151
2.2			0.00172	0.00157
2.4			0.00100	0.00121
2.6			0.00087	0.00111
2.8				0.00085
3.0				0.00075

(e) $\overline{u^*v^*}/u_0^2$

TABLE 1 (Continued)

r/r_o	x/d			
	1	6	10	20
0	0.00000	0.00000	0.00084	0.00227
0.1	0.00000	0.00000		0.00132
0.2	0.00000	0.00000	0.00234	0.00219
0.3	0.00000	0.00104		
0.4	0.00000	0.00130	0.00207	0.00520
0.5	0.00000	0.00165		
0.6	0.00000	0.00173	0.00248	0.00743
0.7	0.00014	0.00177		
0.8	0.00073	0.00186	0.00303	0.00162
0.9	0.00056	0.00164	0.00230	
1.0	0.00036	0.00129	0.00210	0.00266
1.1	0.00022	0.00107	0.00260	
1.2	0.00010	0.00122	0.00187	0.00475
1.3	0.00005	0.00141		
1.4	0.00001	0.00069	0.00151	0.00132
1.5	0.00000	0.00053		
1.6		0.00463	0.00138	0.00213
1.7		0.00134		
1.8		0.00036	0.00109	0.00271
1.9		0.00033		
2.0		0.00019	0.00098	0.01177
2.2			0.00087	0.00136
2.4			0.00060	0.00139
2.6			0.00137	0.00070
2.8				0.00095
3.0				0.00131

(f) v_t^*

ORIGINAL PAGE IS
OF POOR QUALITY

TABLE II
CONFINED JET FLOWFIELD DATA

R/D	0.0	0.5	X/D 1.0	1.5	2.0	2.5
0.47500	0.13000	0.10400	0.15300	0.15800	0.17100	0.17900
0.45000	0.14900	0.11100	0.15600	0.16500	0.20000	0.18600
0.42500	0.15800	0.11300	0.16700	0.17700	0.21700	0.20800
0.40000	0.17700	0.11600	0.18900	0.19300	0.24100	0.22100
0.37500	0.17700	0.11800	0.22000	0.21600	0.26500	0.25000
0.35000	0.18000	0.12900	0.26400	0.25400	0.29400	0.27000
0.32500	0.18500	0.16100	0.32500	0.28500	0.34500	0.29400
0.30000	0.18800	0.23000	0.40400	0.34900	0.37000	0.32500
0.27500	0.19300	0.39000	0.52000	0.41800	0.43300	0.35600
0.25000	1.07000	0.63000	0.65100	0.47500	0.49800	0.39900
0.22500	1.02100	0.88500	0.76400	0.55100	0.53700	0.42700
0.20000	1.00800	0.97700	0.85500	0.62600	0.59800	0.44900
0.17500	1.00800	0.99400	0.91200	0.70600	0.65900	0.48100
0.15000	1.00200	0.98900	0.95000	0.77300	0.70600	0.51400
0.12500	0.99900	0.98900	0.96400	0.82900	0.75500	0.54800
0.10000	1.00000	0.98900	0.97000	0.86200	0.78800	0.56300
0.07500	0.99700	0.99100	0.97200	0.87600	0.82400	0.58500
0.05000	0.99700	0.99300	0.98100	0.88800	0.84200	0.59600
0.02500	1.00000	0.99500	0.98100	0.89400	0.84900	0.62200
0.00000	1.00000	1.00000	0.97800	0.90000	0.86000	0.63200

(a) \bar{u}/u_0

ORIGINAL FILE IS
OF POOR QUALITY

TABLE II (Continued)

R/D	0.0	0.5	x/D 1.0	1.5	2.0	2.5
0.47500	0.01200	0.00000	0.01000	0.00500	0.00600	0.00800
0.45000	0.00800	0.00300	0.00800	0.00700	0.01500	0.00800
0.42500	0.00300	0.00200	0.00800	0.01100	0.02100	0.01200
0.40000	0.00500	0.00500	0.01800	0.02000	0.01600	0.01500
0.37500	0.00300	0.00900	0.01300	0.01400	0.02500	0.01500
0.35000	0.00700	0.00600	0.02100	0.02200	0.02100	0.01800
0.32500	0.00500	0.00600	0.02100	0.02400	0.02200	0.01400
0.30000	0.00200	0.00800	0.01600	0.02600	0.02400	0.02100
0.27500	0.00600	0.01900	0.02500	0.03100	0.03700	0.02300
0.25000	0.00300	0.01700	0.01400	0.02200	0.03800	0.01500
0.22500	0.00800	0.01100	0.01000	0.02100	0.02900	0.02500
0.20000	0.00500	0.00100	0.00100	0.00600	0.03400	0.02800
0.17500	0.01400	0.01200	0.00300	0.00700	0.02500	0.01700
0.15000	0.02000	0.02100	0.01100	0.00500	0.02300	0.01100
0.12500	0.02600	0.02100	0.01600	0.00200	0.01700	0.00700
0.10000	0.03000	0.02900	0.02800	0.01300	0.01300	0.00300
0.07500	0.02800	0.03500	0.03000	0.01900	0.01300	0.00100
0.05000	0.03300	0.03700	0.03900	0.01900	0.00300	0.00700
0.02500	0.03000	0.04400	0.03300	0.02100	0.00800	0.00200
0.00000	0.03000	0.04400	0.03600	0.02400	0.00400	0.01000

(b) \bar{v}/u_0

TABLE II (Continued)

R/D	0.0	0.5	X/D 1.0	1.5	2.0	2.5
0.47500	0.02700	0.02600	0.04200	0.04500	0.04900	0.04900
0.45000	0.03000	0.02700	0.04400	0.04700	0.05400	0.05100
0.42500	0.03300	0.02900	0.04700	0.05100	0.05900	0.05600
0.40000	0.03700	0.02900	0.05300	0.05600	0.06500	0.06000
0.37500	0.03700	0.03000	0.06200	0.06300	0.07200	0.06700
0.35000	0.03900	0.03400	0.07300	0.07200	0.07800	0.07300
0.32500	0.03900	0.04400	0.08800	0.08000	0.09100	0.07800
0.30000	0.03800	0.06300	0.10200	0.09400	0.09800	0.08400
0.27500	0.03900	0.10000	0.11800	0.10800	0.10600	0.09100
0.25000	0.01400	0.13000	0.13300	0.11900	0.11900	0.10200
0.22500	0.01000	0.10200	0.12500	0.12700	0.12400	0.10600
0.20000	0.01000	0.05600	0.09900	0.12900	0.13400	0.11000
0.17500	0.01000	0.03100	0.08000	0.12800	0.13700	0.11500
0.15000	0.00900	0.02200	0.06100	0.11200	0.13400	0.12100
0.12500	0.01000	0.01700	0.05000	0.10100	0.13000	0.12700
0.10000	0.00900	0.01400	0.04000	0.08700	0.12100	0.12600
0.07500	0.01000	0.01400	0.03700	0.07400	0.11500	0.12500
0.05000	0.00900	0.01200	0.03300	0.06900	0.10500	0.12400
0.02500	0.01000	0.01200	0.03300	0.06600	0.09900	0.12900
0.00000	0.01000	0.01200	0.03100	0.06600	0.09400	0.12600

(c) u'_{rms}/u_o

TABLE II (Continued)

R/D	0.0	0.5	X/D 1.0	1.5	2.0	2.5
0.47500	0.01200	0.01300	0.02800	0.02800	0.02800	0.03000
0.45000	0.01300	0.01600	0.03100	0.03200	0.03600	0.03600
0.42500	0.01500	0.01700	0.03500	0.03600	0.04200	0.04300
0.40000	0.01600	0.01800	0.04000	0.04100	0.04900	0.04800
0.37500	0.01700	0.01900	0.04800	0.04700	0.05500	0.05400
0.35000	0.01700	0.02300	0.05800	0.05600	0.06200	0.06000
0.32500	0.01800	0.03200	0.07000	0.06200	0.07200	0.06400
0.30000	0.01700	0.05000	0.08300	0.07400	0.07900	0.07200
0.27500	0.01600	0.08200	0.09500	0.08400	0.08900	0.07800
0.25000	0.00800	0.10000	0.09700	0.09000	0.09700	0.08400
0.22500	0.00600	0.07900	0.09000	0.09300	0.10100	0.08700
0.20000	0.00700	0.04300	0.07000	0.00920	0.10300	0.09000
0.17500	0.00600	0.02400	0.05400	0.08800	0.10400	0.09400
0.15000	0.00700	0.01500	0.04200	0.08000	0.10200	0.09500
0.12500	0.00600	0.01100	0.03100	0.06900	0.09600	0.09500
0.10000	0.00600	0.00900	0.02500	0.06000	0.08800	0.09600
0.07500	0.00600	0.00700	0.02200	0.05300	0.08300	0.09500
0.05000	0.00600	0.00700	0.01900	0.04600	0.07800	0.09300
0.02500	0.00600	0.00700	0.01600	0.04400	0.07300	0.09600
0.00000	0.00700	0.00700	0.01800	0.04400	0.07200	0.09700

(d) v'_{rms}/u_o

TABLE II (Continued)

R/D	0.0	0.5	x/D 1.0	1.5	2.0	2.5
0.47500	0.00000	0.00000	0.00029	0.00025	0.00033	0.00045
0.45000	0.00000	0.00002	0.00033	0.00032	0.00054	0.00049
0.42500	0.00002	0.00004	0.00043	0.00038	0.00070	0.00072
0.40000	0.00000	0.00008	0.00063	0.00055	0.00104	0.00093
0.37500	0.00001	0.00010	0.00100	0.00084	0.00142	0.00136
0.35000	0.00003	0.00021	0.00161	0.00126	0.00197	0.00172
0.32500	0.00007	0.00063	0.00278	0.00183	0.00284	0.00216
0.30000	0.00010	0.00154	0.00486	0.00312	0.00376	0.00281
0.27500	0.00117	0.00513	0.00839	0.00466	0.00521	0.00335
0.25000	0.00112	0.01252	0.01272	0.00645	0.00694	0.00431
0.22500	0.00029	0.01703	0.01582	0.00879	0.00850	0.00484
0.20000	0.00013	0.00239	0.01443	0.01134	0.01038	0.00527
0.17500	0.00011	0.00004	0.01021	0.01308	0.01210	0.00557
0.15000	0.00007	0.00004	0.00539	0.01353	0.01330	0.00595
0.12500	0.00007	0.00006	0.00056	0.01226	0.01410	0.00631
0.10000	0.00006	0.00007	0.00032	0.00948	0.01367	0.00630
0.07500	0.00006	0.00008	0.00036	0.00769	0.01255	0.00547
0.05000	0.00005	0.00006	0.00041	0.00551	0.01121	0.00459
0.02500	0.00002	0.00007	0.00054	0.00499	0.00942	0.00374
0.00000	0.00002	0.00011	0.00073	0.00487	0.00792	0.00282

(e) $\overline{u'v'}/u_o^2$

TABLE III
 CONFINED JET WITH CONTRACTION
 NOZZLE FLOWFIELD DATA

R/D	X/D				
	0.0	0.5	1.0	1.5	2.0
0.47500	0.15700	0.10100	0.15400	0.18700	0.22600
0.45000	0.16500	0.10400	0.16400	0.19600	0.22700
0.42500	0.16600	0.10700	0.17100	0.21400	0.24100
0.40000	0.18400	0.11000	0.18900	0.23800	0.25700
0.37500	0.19500	0.12000	0.22800	0.27200	0.29300
0.35000	0.19400	0.13900	0.27300	0.30500	0.31400
0.32500	0.20300	0.18000	0.32800	0.35100	0.36000
0.30000	0.21400	0.29100	0.40300	0.42500	0.41300
0.27500	0.21000	0.45600	0.51300	0.50400	0.47400
0.25000	0.20700	0.71400	0.63100	0.57600	0.52300
0.22500	1.02400	0.91800	0.75100	0.64500	0.58000
0.20000	0.99600	0.98700	0.85000	0.73700	0.61800
0.17500	0.99900	0.99000	0.92300	0.78800	0.67600
0.15000	0.99300	0.99300	0.95800	0.83800	0.73300
0.12500	0.98400	0.99300	0.97800	0.87200	0.76600
0.10000	0.98700	0.99300	0.98600	0.89400	0.79800
0.07500	0.98800	0.99600	0.98900	0.90600	0.80900
0.05000	0.99100	0.99400	0.98900	0.92000	0.82500
0.02500	0.98800	0.99600	0.99600	0.92600	0.83500
0.00000	0.99700	1.00000	0.99100	0.92600	0.84000

(a) \bar{u}/u_o

TABLE III (Continued)

R/D	0.0	0.5	X/D 1.0	1.5	2.0
0.47500	0.00200	0.00900	0.00700	0.00800	0.00900
0.45000	0.00200	0.00700	0.00800	0.00800	0.00200
0.42500	0.00200	0.00800	0.00600	0.01400	0.01100
0.40000	0.00400	0.00500	0.00200	0.02700	0.01600
0.37500	0.00400	0.00300	0.00400	0.01500	0.01800
0.35000	0.00700	0.00100	0.00500	0.02200	0.01700
0.32500	0.00800	0.00000	0.00800	0.03800	0.02000
0.30000	0.00400	0.00600	0.00800	0.03100	0.01400
0.27500	0.00200	0.00700	0.01500	0.02900	0.01200
0.25000	0.00800	0.00500	0.01700	0.03600	0.00800
0.22500	0.01200	0.00700	0.00300	0.02900	0.00500
0.20000	0.00600	0.01500	0.01100	0.02400	0.00900
0.17500	0.02100	0.02400	0.01000	0.00700	0.00300
0.15000	0.02700	0.03000	0.02000	0.01000	0.01100
0.12500	0.03600	0.03400	0.02700	0.00000	0.01300
0.10000	0.04300	0.03900	0.03200	0.00900	0.00900
0.07500	0.04500	0.04500	0.03800	0.00400	0.00200
0.05000	0.04800	0.04300	0.04700	0.01800	0.01400
0.02500	0.04500	0.04500	0.04500	0.02500	0.01200
0.00000	0.04600	0.04600	0.05400	0.02500	0.02200

(b) \bar{v}/u_o

TABLE III (Continued)

R/D	0.0	0.5	X/D 1.0	1.5	2.0
0.47500	0.02900	0.02300	0.03900	0.05200	0.06500
0.45000	0.03100	0.02300	0.04300	0.05400	0.06700
0.42500	0.03100	0.02400	0.04400	0.06000	0.06900
0.40000	0.03600	0.02500	0.05100	0.06700	0.00730
0.37500	0.03800	0.02900	0.06000	0.07500	0.08300
0.35000	0.03800	0.03500	0.07100	0.08200	0.08700
0.32500	0.03900	0.05000	0.08300	0.09500	0.09700
0.30000	0.04100	0.07800	0.09900	0.11000	0.10900
0.27500	0.04100	0.11500	0.11900	0.12300	0.12000
0.25000	0.03100	0.14000	0.13600	0.13800	0.12700
0.22500	0.01300	0.10000	0.13300	0.13800	0.13400
0.20000	0.01200	0.05500	0.12100	0.14400	0.13600
0.17500	0.01200	0.03500	0.09500	0.12600	0.13500
0.15000	0.01300	0.02500	0.07600	0.11400	0.13400
0.12500	0.01200	0.02000	0.06000	0.09900	0.12600
0.10000	0.01300	0.01800	0.05100	0.08400	0.12300
0.07500	0.01200	0.01700	0.04400	0.07900	0.11300
0.05000	0.01300	0.01600	0.04300	0.07000	0.11200
0.02500	0.01200	0.01500	0.03900	0.06600	0.10700
0.00000	0.01300	0.01600	0.03700	0.06400	0.10800

(c) u'_{rms}/u_o

TABLE III (Continued)

R/D	X/D				
	0.0	0.5	1.0	1.5	2.0
0.47500	0.01200	0.01200	0.02500	0.03100	0.03600
0.45000	0.01300	0.01400	0.03000	0.03700	0.04000
0.42500	0.01300	0.01500	0.03300	0.04300	0.04500
0.40000	0.01500	0.01600	0.03800	0.05000	0.05000
0.37500	0.01500	0.01800	0.04600	0.05800	0.05900
0.35000	0.01500	0.02400	0.05800	0.06500	0.06600
0.32500	0.01600	0.03700	0.07100	0.07400	0.07400
0.30000	0.01600	0.06400	0.08600	0.08700	0.08500
0.27500	0.01400	0.09900	0.10300	0.09700	0.09400
0.25000	0.00800	0.11500	0.11300	0.10100	0.10000
0.22500	0.00700	0.08200	0.10900	0.10000	0.10400
0.20000	0.00600	0.04500	0.09300	0.09800	0.10300
0.17500	0.00600	0.02500	0.07100	0.08500	0.10100
0.15000	0.00600	0.01700	0.05300	0.07600	0.09700
0.12500	0.00600	0.01200	0.03900	0.06100	0.09400
0.10000	0.00600	0.00900	0.03200	0.05600	0.08600
0.07500	0.00600	0.00800	0.02600	0.04800	0.07900
0.05000	0.00600	0.00800	0.02300	0.04200	0.07700
0.02500	0.00600	0.00700	0.02000	0.04100	0.07600
0.00000	0.00600	0.00700	0.01900	0.03900	0.07500

(d) v'_{rms}/u_o

TABLE III (Continued)

R/D	0.0	0.5	X/D 1.0	1.5	2.0
0.47500	0.00000	0.00008	0.00019	0.00029	0.00039
0.45000	0.00000	0.00009	0.00033	0.00045	0.00046
0.42500	0.00001	0.00015	0.00043	0.00068	0.00069
0.40000	0.00001	0.00020	0.00062	0.00110	0.00095
0.37500	0.00001	0.00026	0.00102	0.00159	0.00164
0.35000	0.00001	0.00039	0.00169	0.00240	0.00226
0.32500	0.00003	0.00090	0.00272	0.00337	0.00350
0.30000	0.00003	0.00271	0.00449	0.00548	0.00511
0.27500	0.00007	0.00707	0.00763	0.00812	0.00731
0.25000	0.00312	0.01594	0.01132	0.01056	0.00927
0.22500	0.00006	0.01476	0.01422	0.01287	0.01100
0.20000	0.00005	0.00026	0.01431	0.01507	0.01270
0.17500	0.00005	0.00004	0.00150	0.01471	0.01410
0.15000	0.00005	0.00004	0.00052	0.01332	0.01419
0.12500	0.00004	0.00001	0.00005	0.00511	0.01407
0.10000	0.00004	0.00004	0.00002	0.00475	0.01331
0.07500	0.00004	0.00006	0.00002	0.00314	0.01155
0.05000	0.00003	0.00005	0.00005	0.00266	0.01035
0.02500	0.00003	0.00005	0.00006	0.00298	0.00900
0.00000	0.00003	0.00005	0.00011	0.00297	0.00720

(e) $\overline{u'v'}/u_o^2$

TABLE III (Continued)

R/D	0.0	0.5	X/D 1.0	1.5	2.0
0.47500	0.00002	0.00140	0.00098	0.00164	0.01878
0.45000	0.00005	0.00145	0.00195	0.00167	0.00307
0.42500	0.00003	0.00254	0.00175	0.00163	0.00233
0.40000	0.00003	0.00151	0.00109	0.00191	0.00136
0.37500	0.00007	0.00091	0.00123	0.00240	0.00223
0.35000	0.00009	0.00057	0.00170	0.00307	0.00331
0.32500	0.00015	0.00050	0.00211	0.00283	0.00368
0.30000	0.00042	0.00103	0.00245	0.00361	0.00486
0.27500	0.00095	0.00168	0.00337	0.00542	0.00715
0.25000	0.00039	0.00348	0.00480	0.00756	0.00935
0.22500	0.00001	0.00545	0.00654	0.00806	0.01260
0.20000	0.00021	0.00036	0.00839	0.01063	0.01376
0.17500	0.00182	0.00070	0.00140	0.01468	0.01367
0.15000	0.00033	0.00126	0.00095	0.01598	0.01932
0.12500	0.00074	0.00000	0.00016	0.00920	0.02086
0.10000	0.00109	0.00149	0.00020	0.01407	0.03629
0.07500	0.00026	0.00594	0.00058	0.01219	0.05544
0.05000	0.00000	0.00000	0.00075	0.01347	0.03157
0.02500	0.00053	0.00078	0.00284	0.05014	0.00000
0.00000	0.00018	0.00065	0.00109	0.00000	0.00070

(f) v_t^*

APPENDIX B

FIGURES

ORIGINAL PAGE IS
OF POOR QUALITY

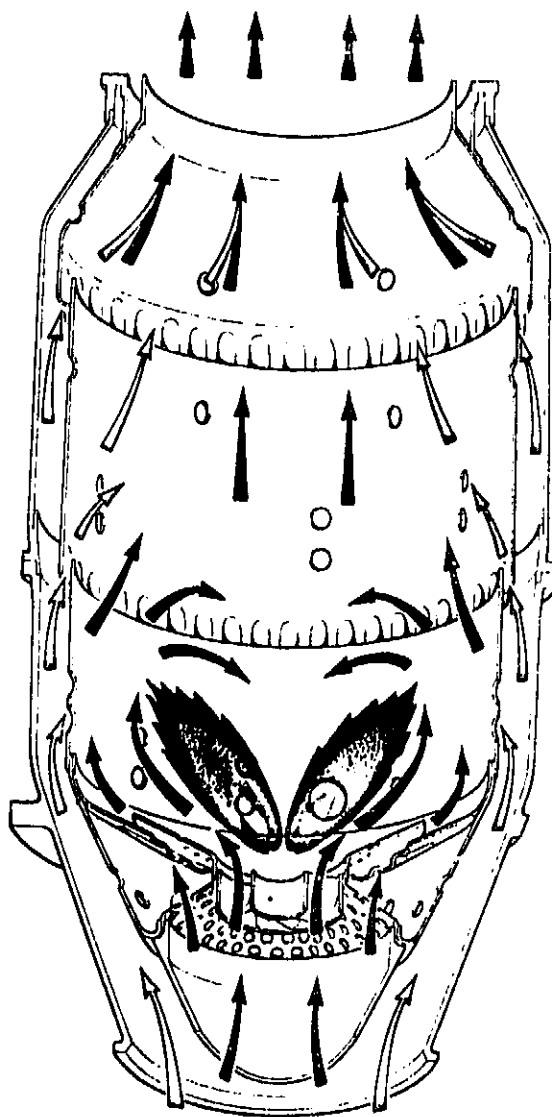


Figure 1. Axisymmetric Combustor of a Gas Turbine (Ref. 11)

ORIGINAL PAGE IS
OF POOR QUALITY

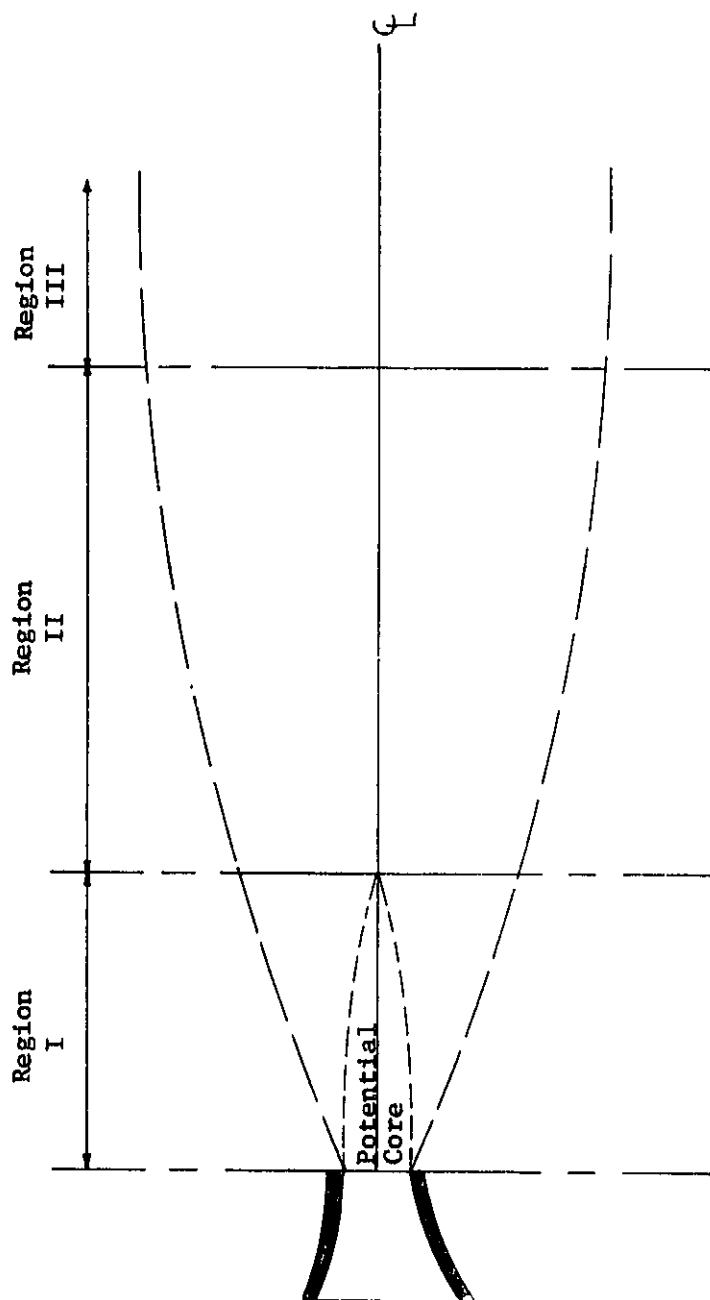


Figure 2. Different Regions in a Turbulent Jet

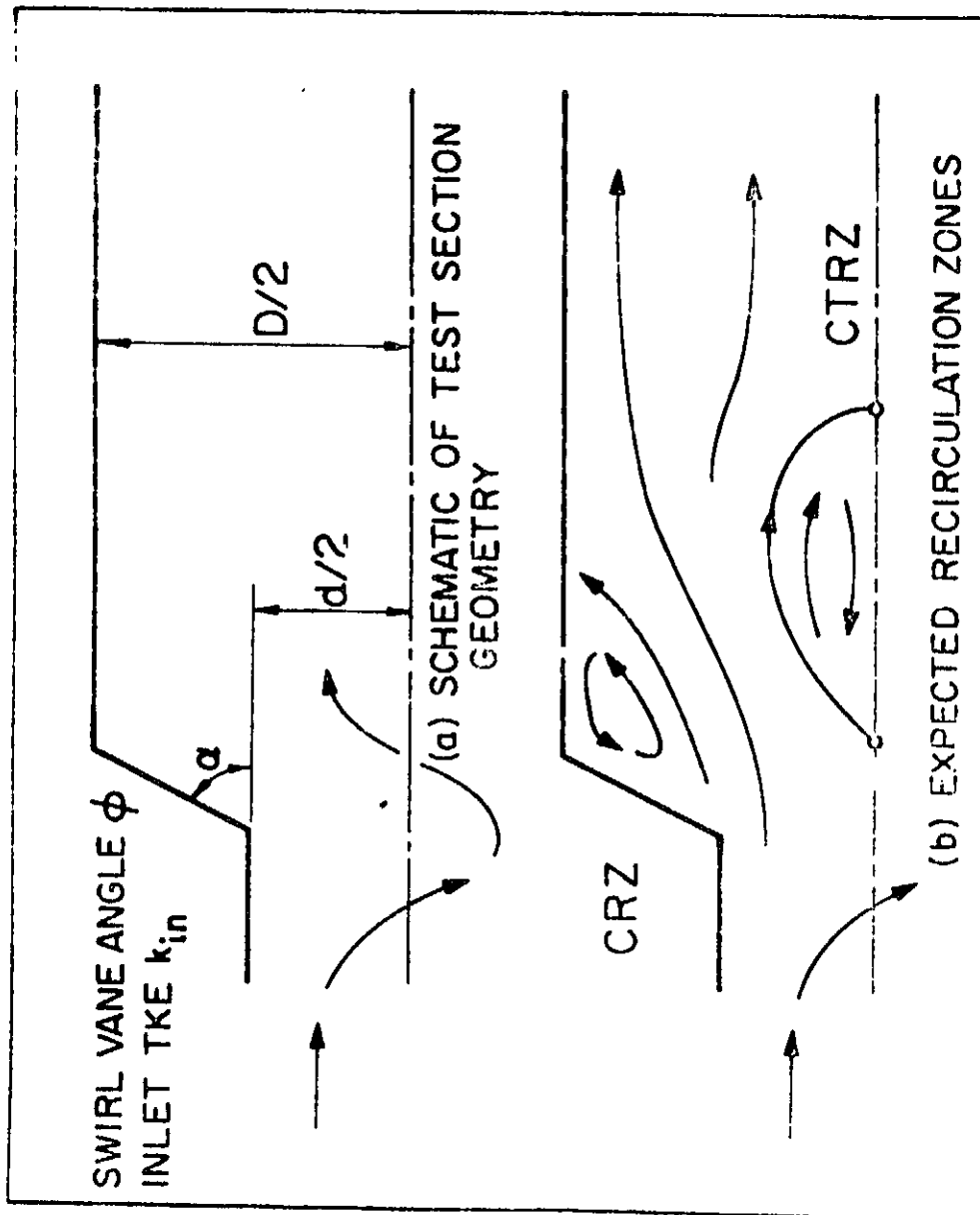


Figure 3. The Confined Jet Flowfield

ORIGINAL PAGE IS
OF POOR QUALITY

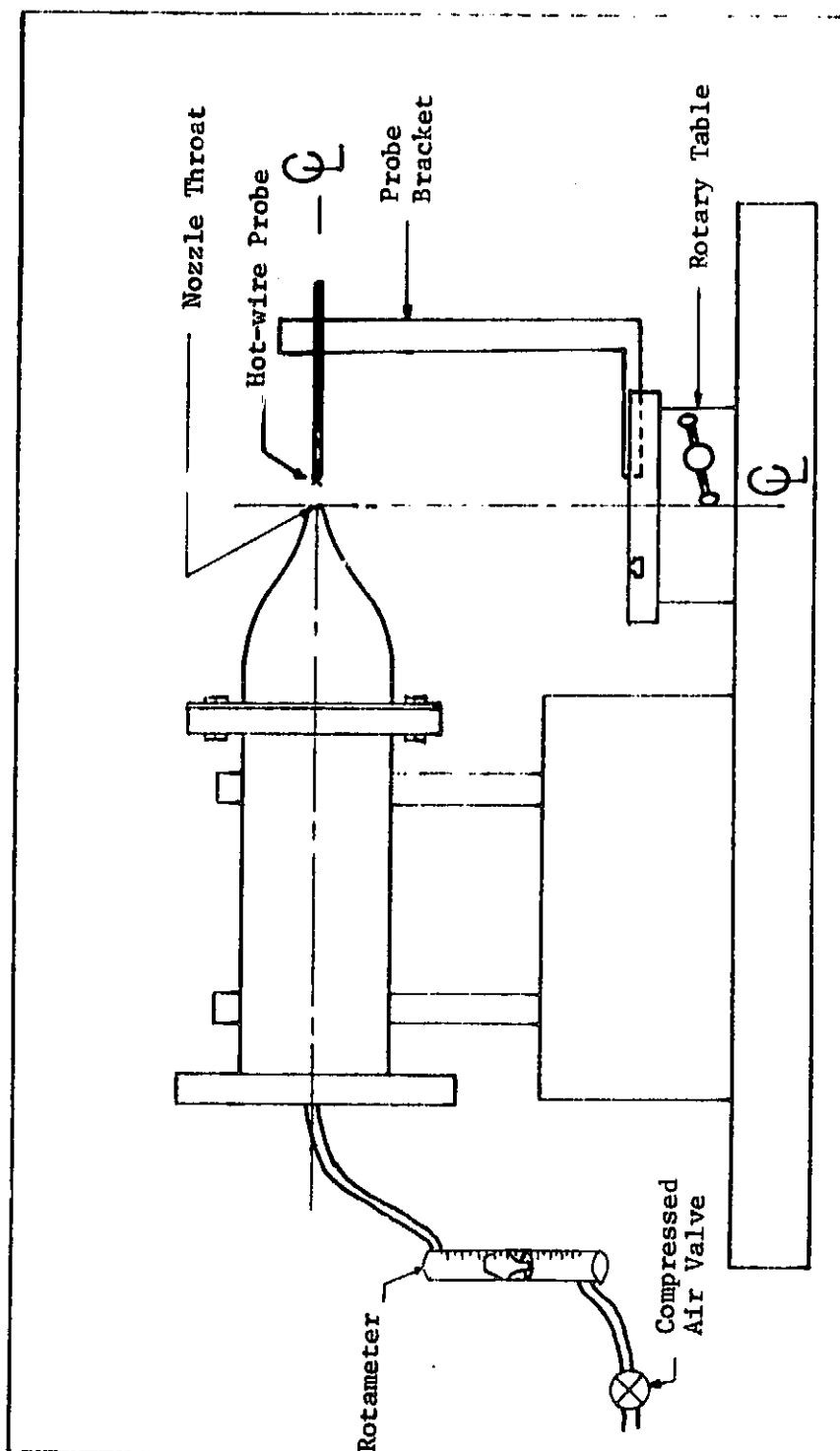


Figure 4. Free Jet Apparatus

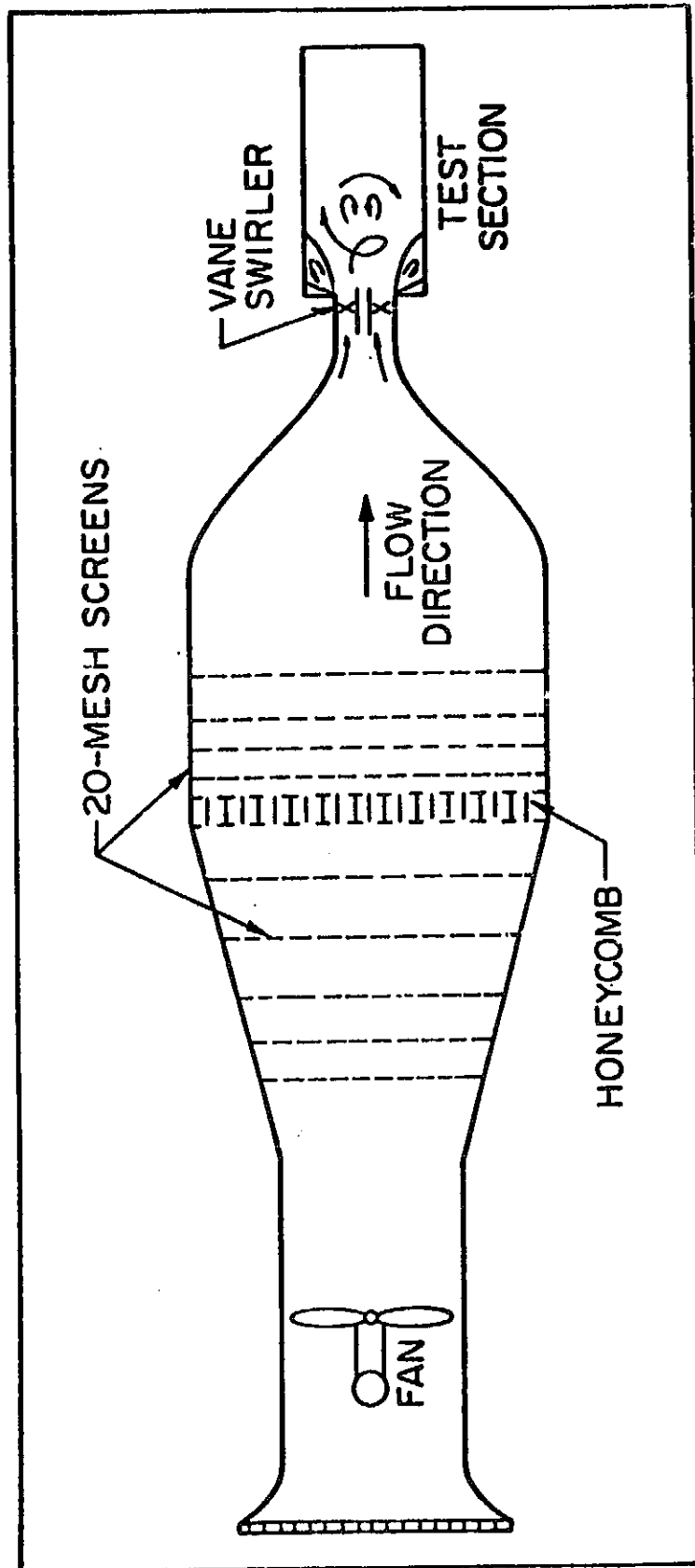


Figure 5. Schematic of the Overall Experimental Facility

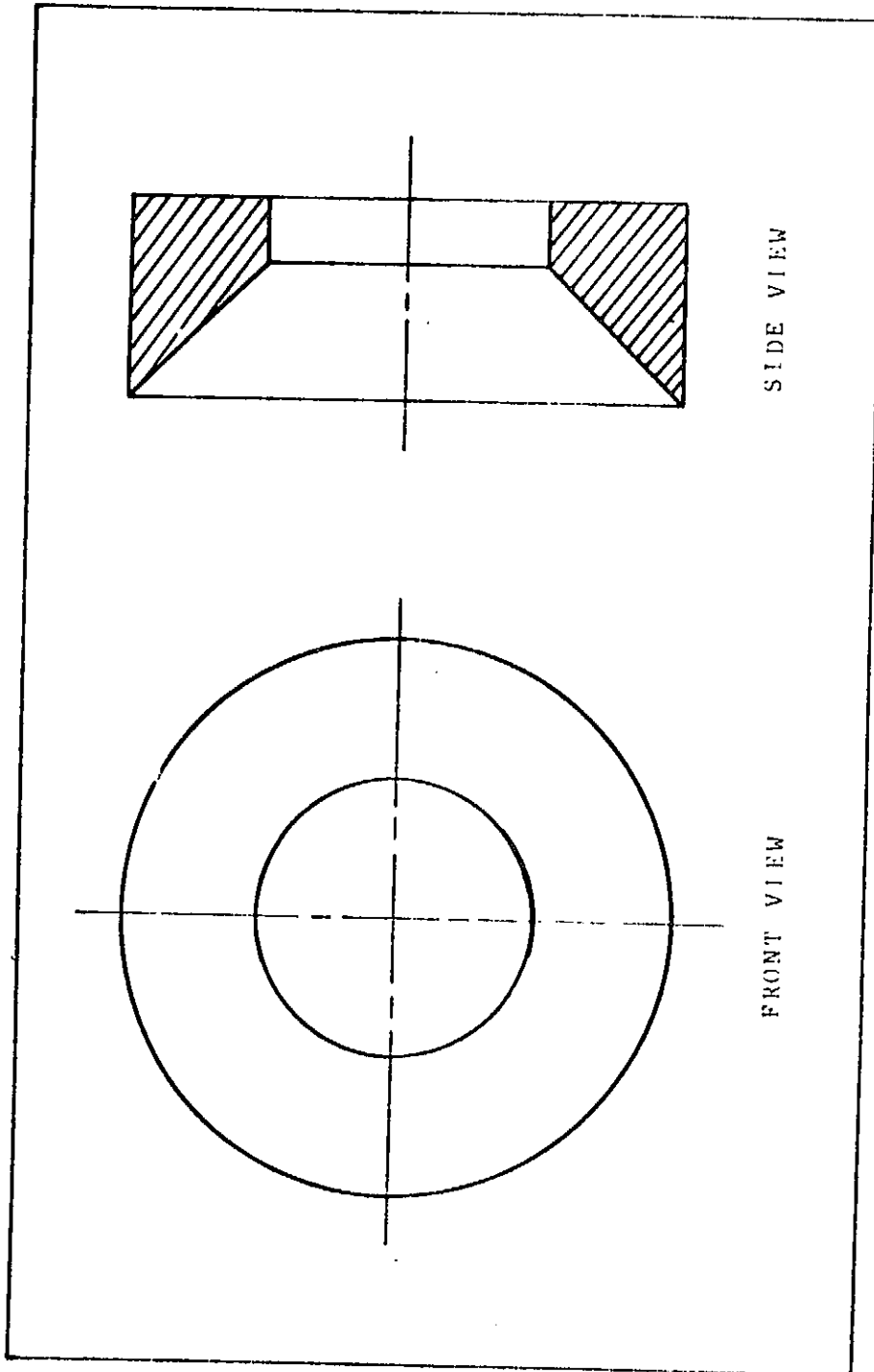


Figure 6. The Contraction Nozzle with Area Ratio of 4 (Ref. II)

ORIGINAL PAGE IS
OF POOR QUALITY

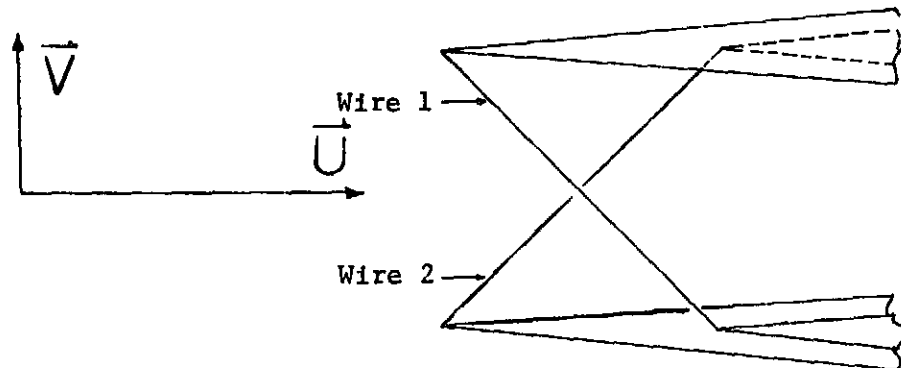


Figure 7. Hot-wire Orientation

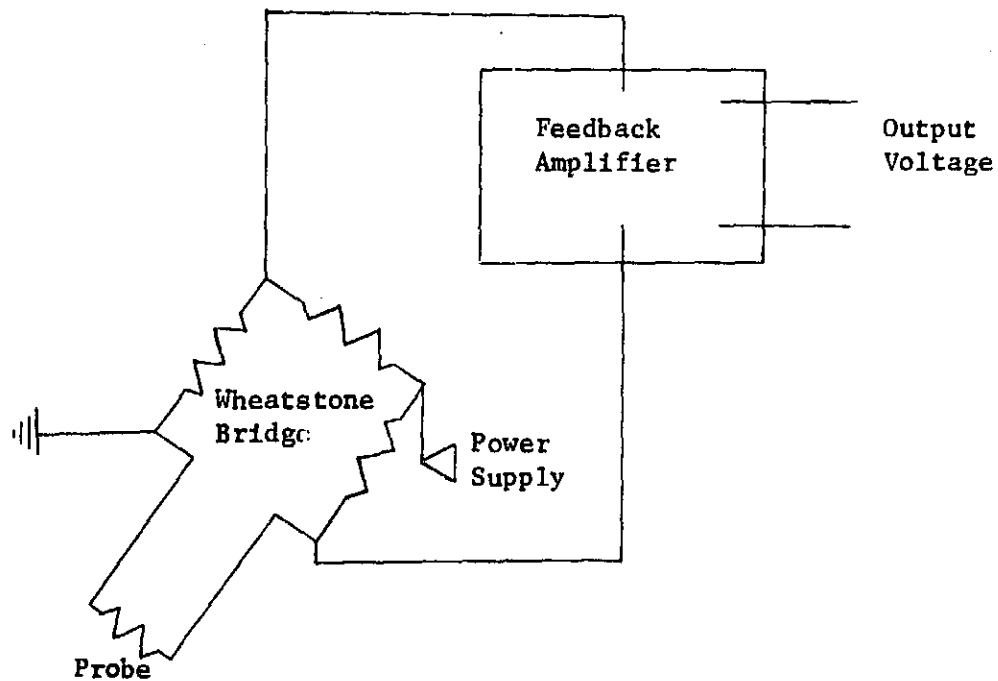
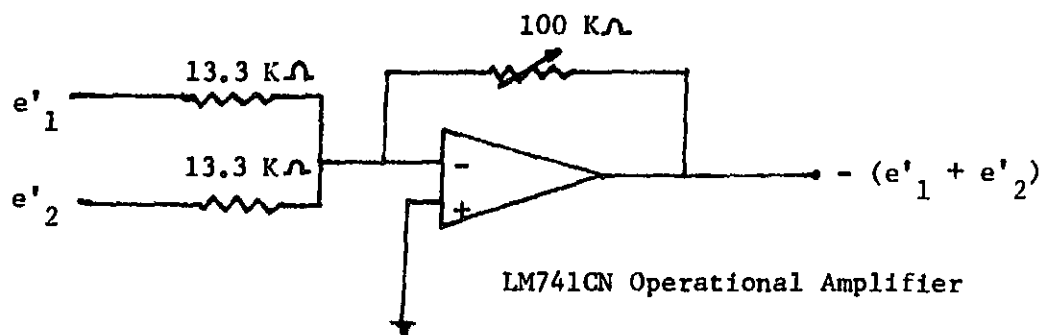
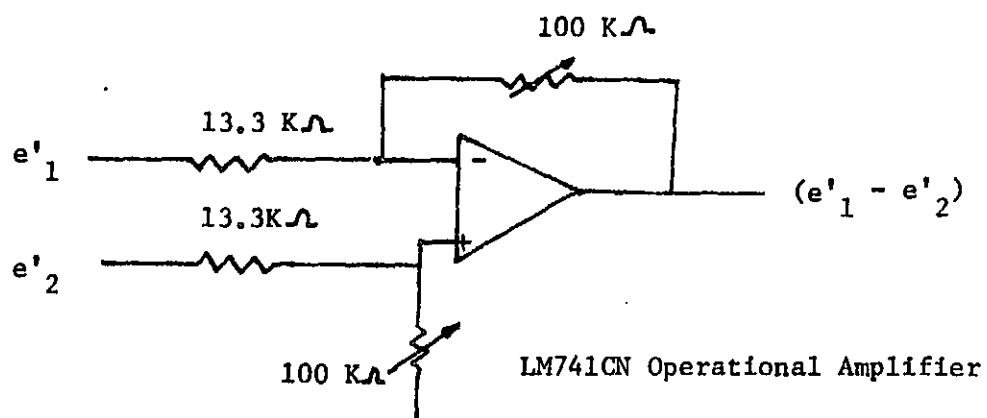


Figure 8. Constant Temperature Anemometer

ORIGINAL PAGE 7
OF POOR QUALITY



Adder Circuit



Subtractor Circuit

Figure 9. Schematic of the Constructed Devices

ORIGINAL PAGE IS
OF POOR QUALITY

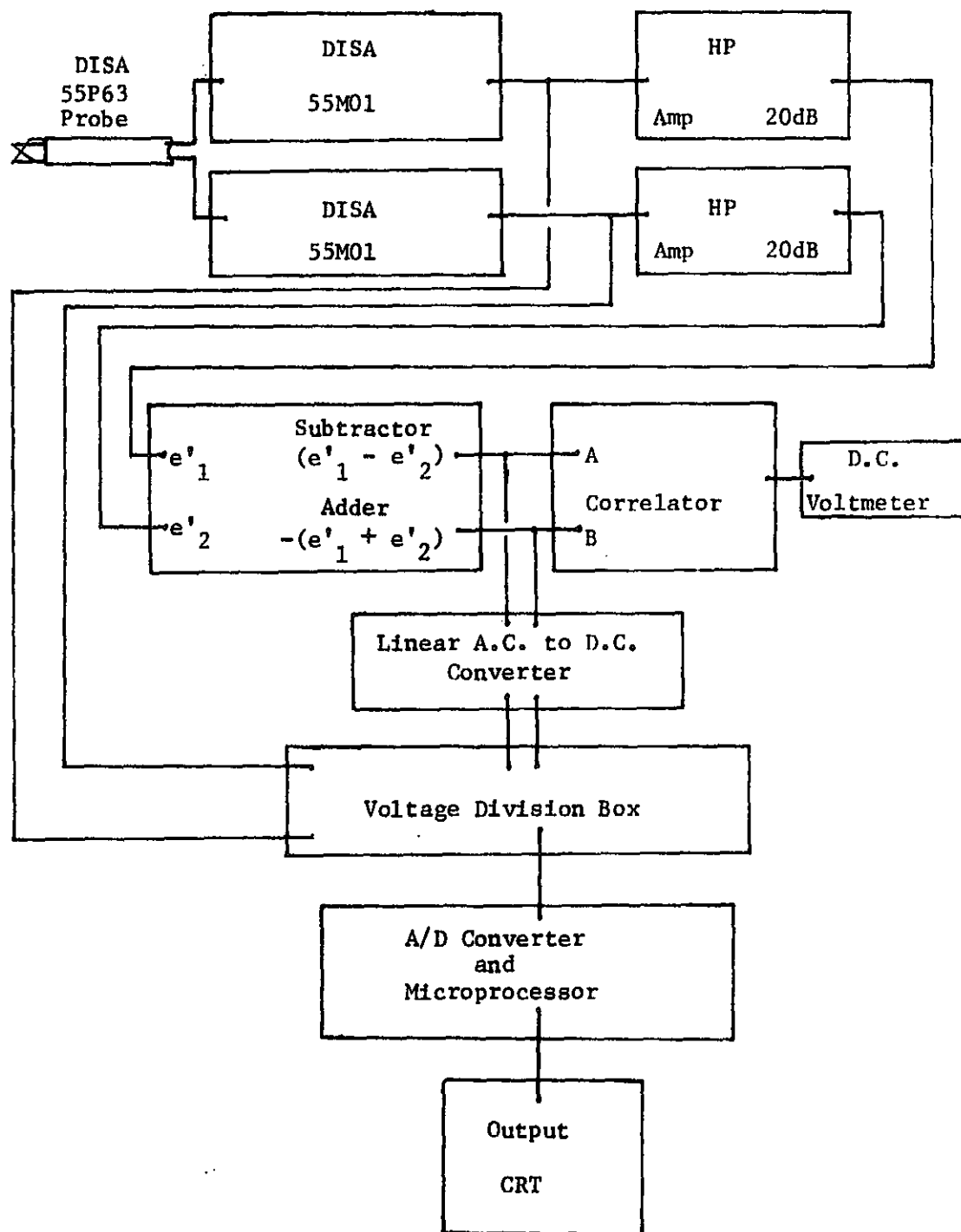


Figure 10. Instrumentation Layout

ORIGINAL PAGE IS
OF POOR QUALITY

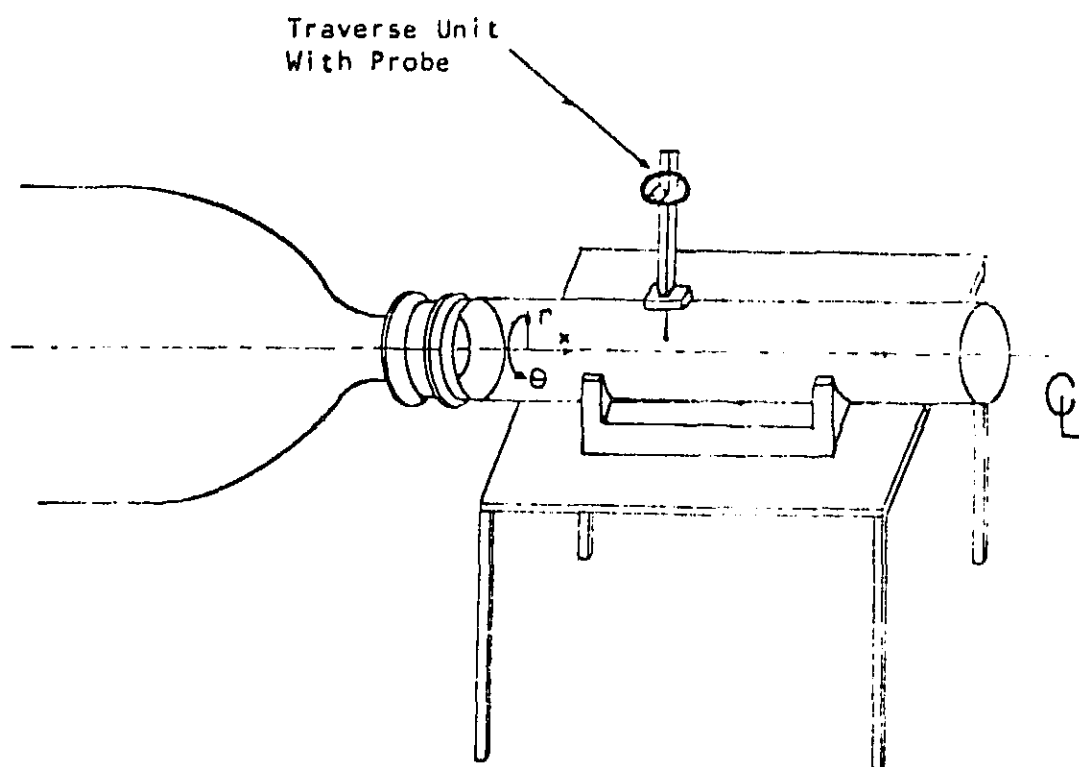


Figure 11. Hot-wire Probe Mounted on the Confined Jet Test Section (Ref. 12)

ORIGINAL PAGE IS
OF POOR QUALITY

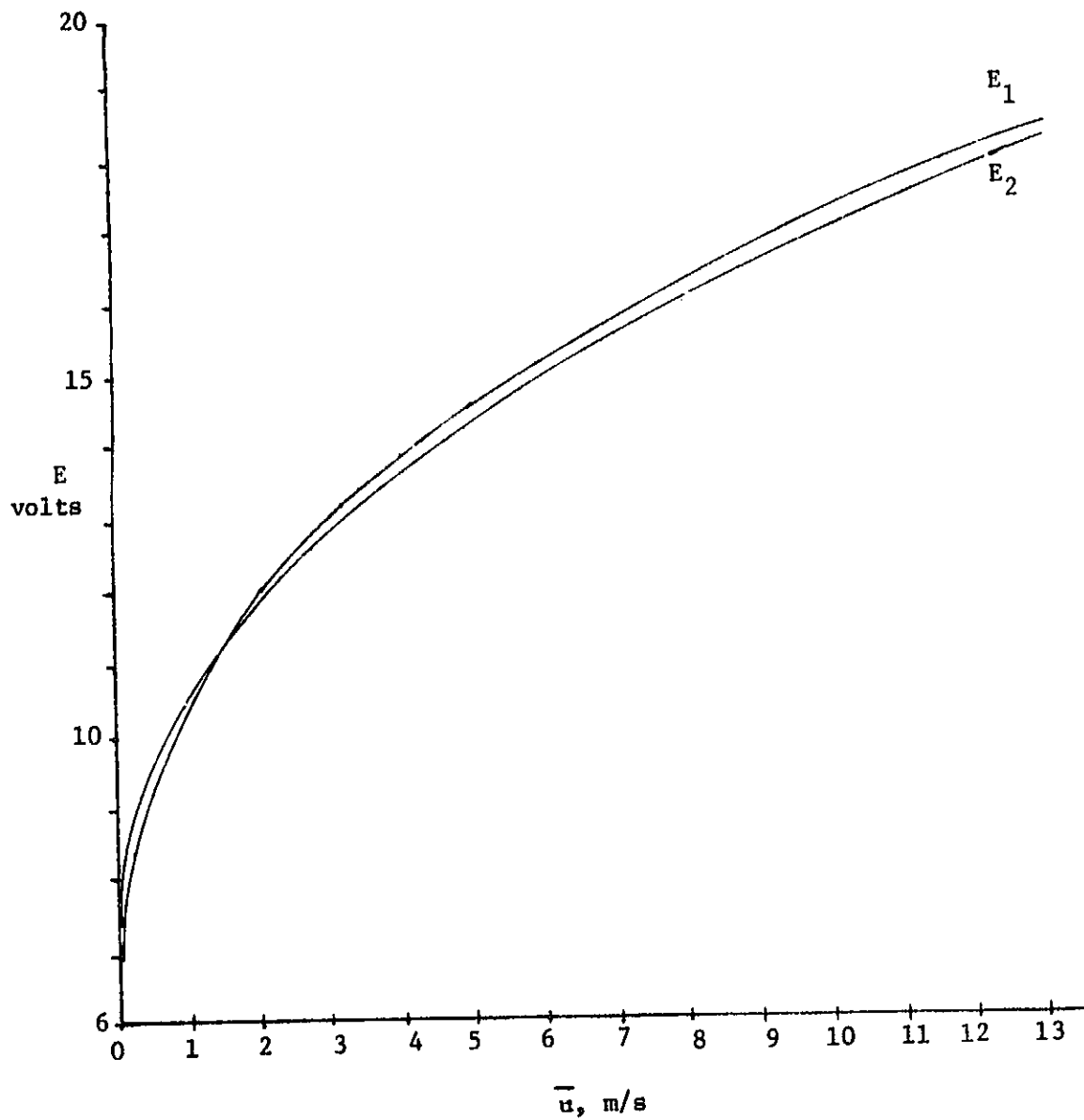


Figure 12. Hot-wire Calibration Curves

ORIGINAL PAGE IS
OF POOR QUALITY

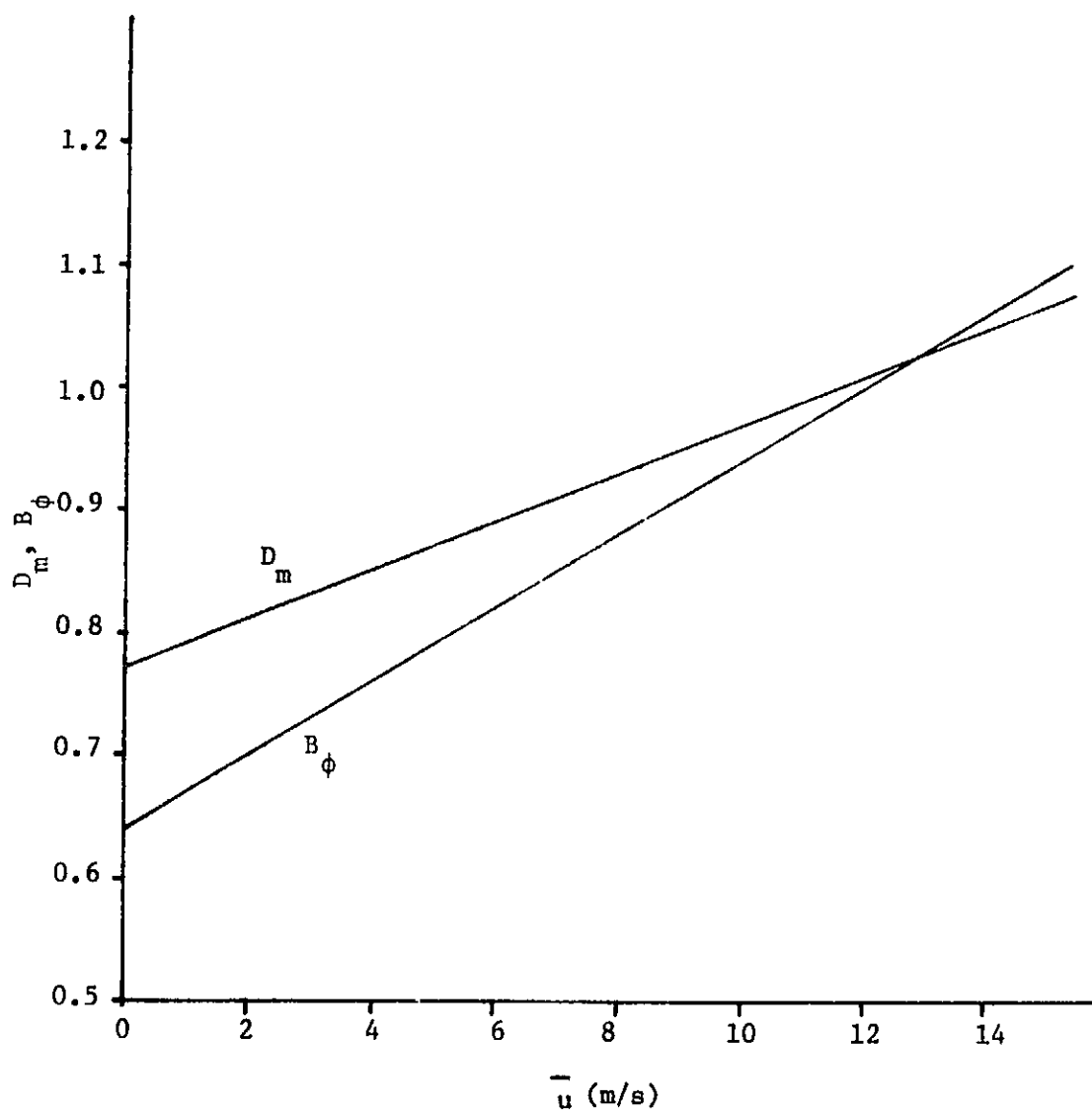


Figure 13. Sensitivity Parameters D_m and B_ϕ versus \bar{u}

ORIGINAL PAGE IS
OF POOR QUALITY

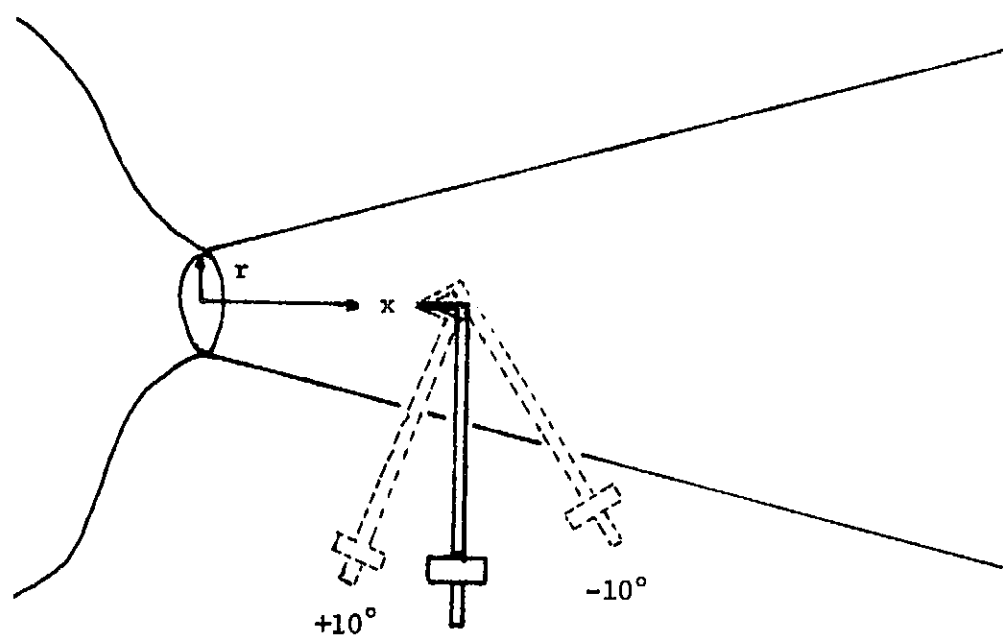


Figure 14. Angulation Test Coordinate System

ORIGINAL PAGE IS
OF POOR QUALITY

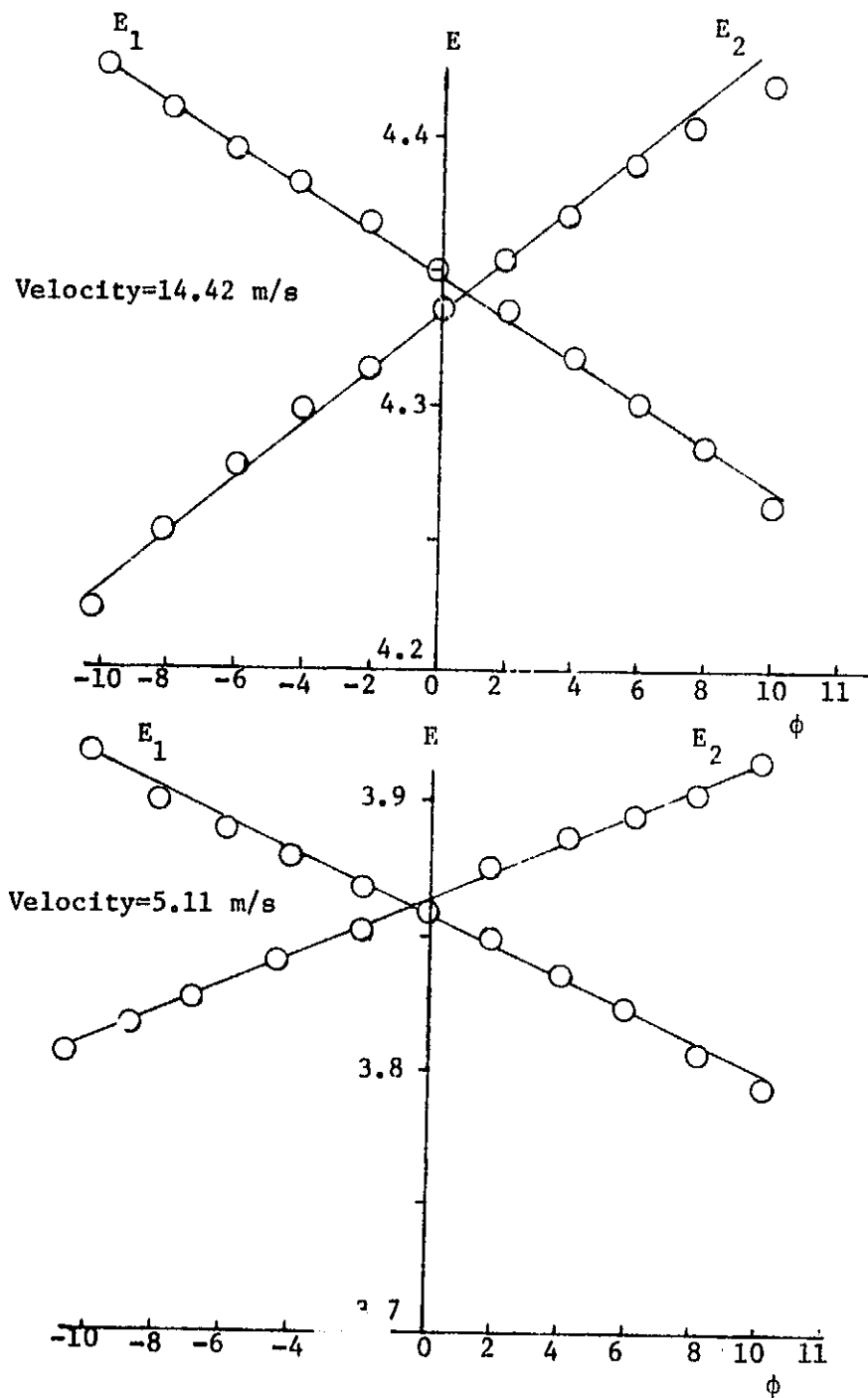


Figure 15. Calibration Plot for Sensitivity to Angulation

ORIGINAL PAGE 19
OF POOR QUALITY

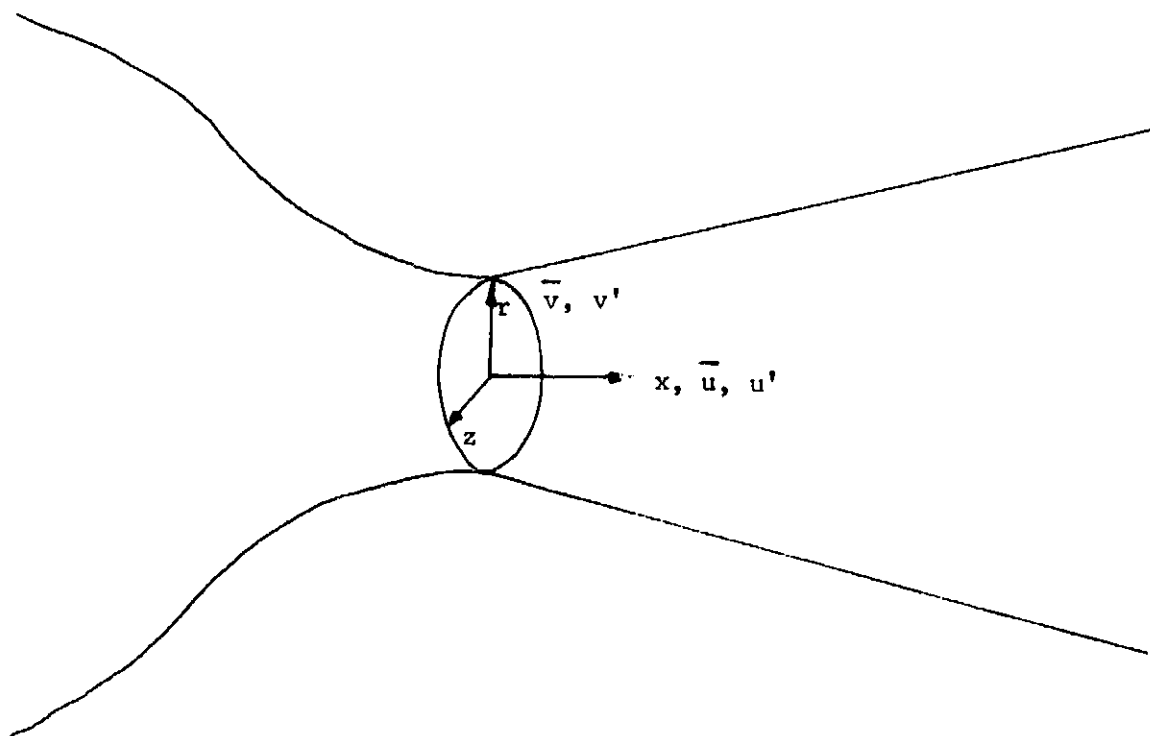


Figure 16. Free and Confined Jet Coordinate System

ORIGINAL PAGE IS
OF POOR QUALITY

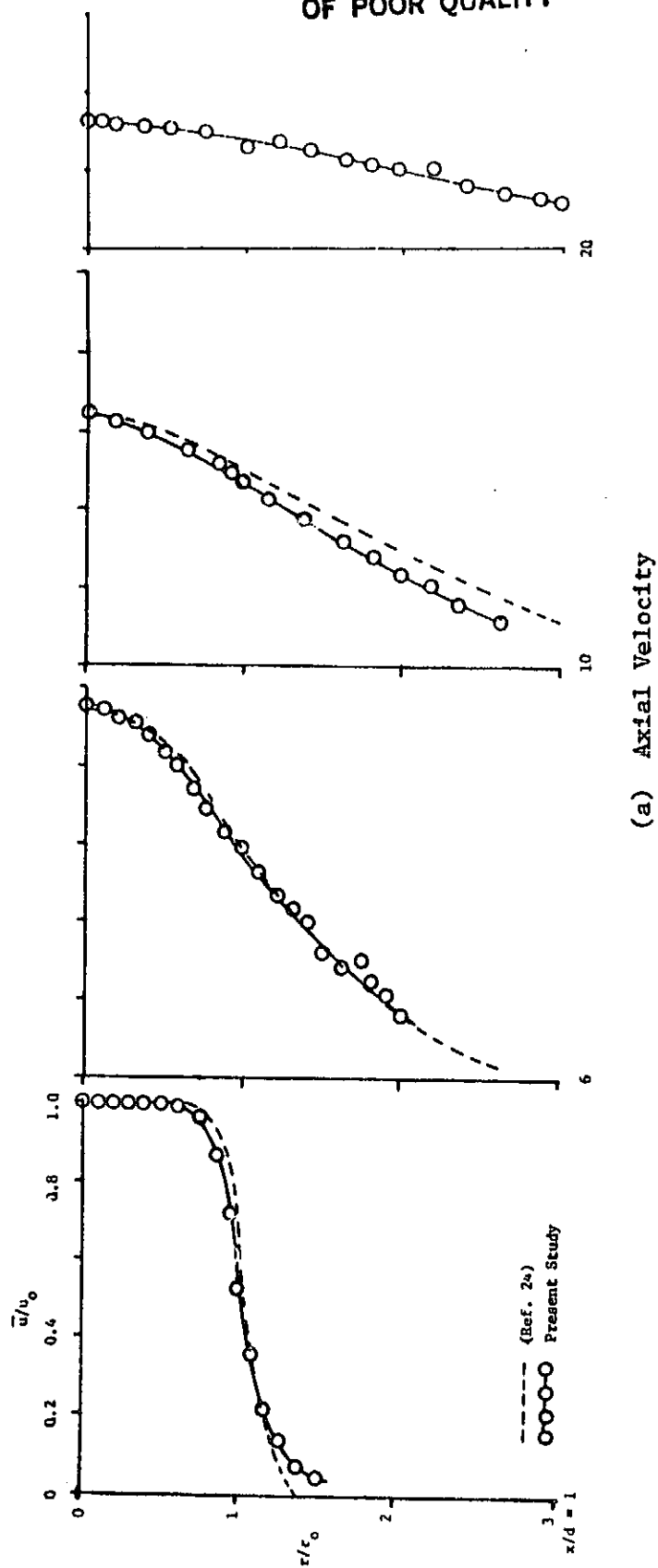
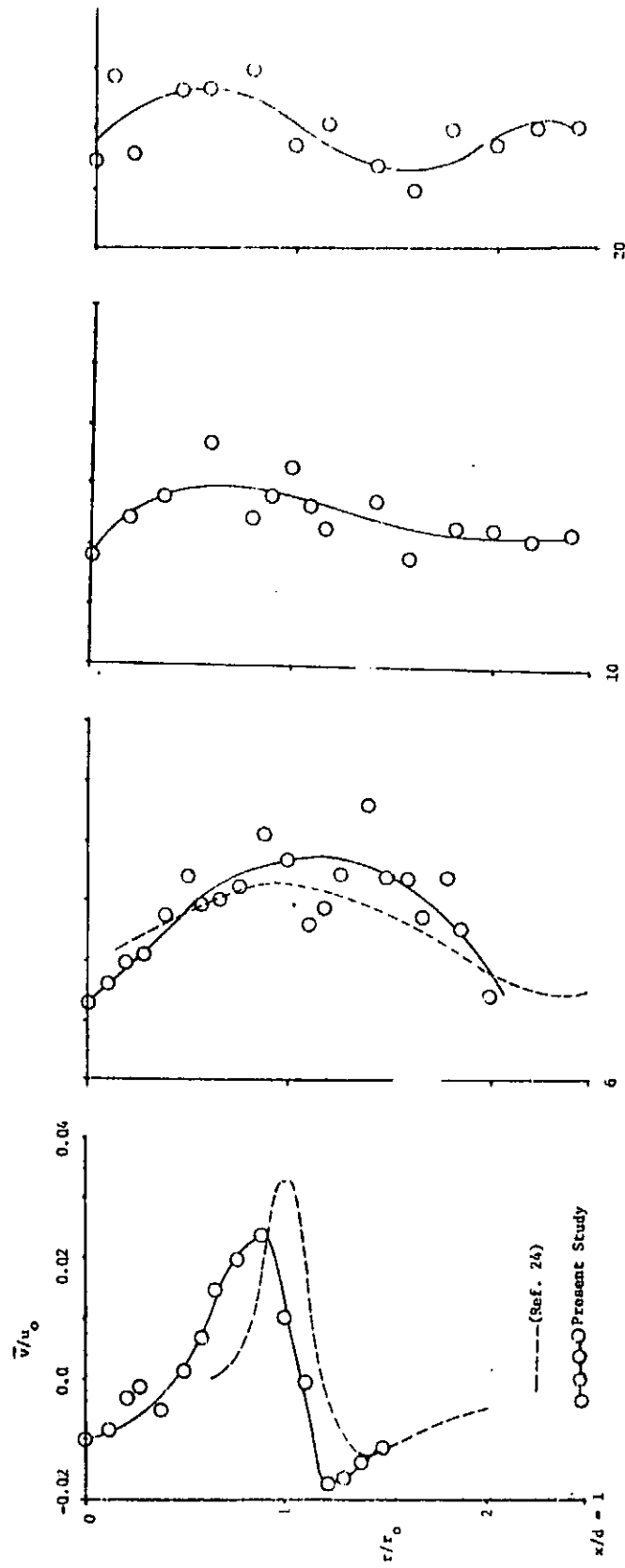


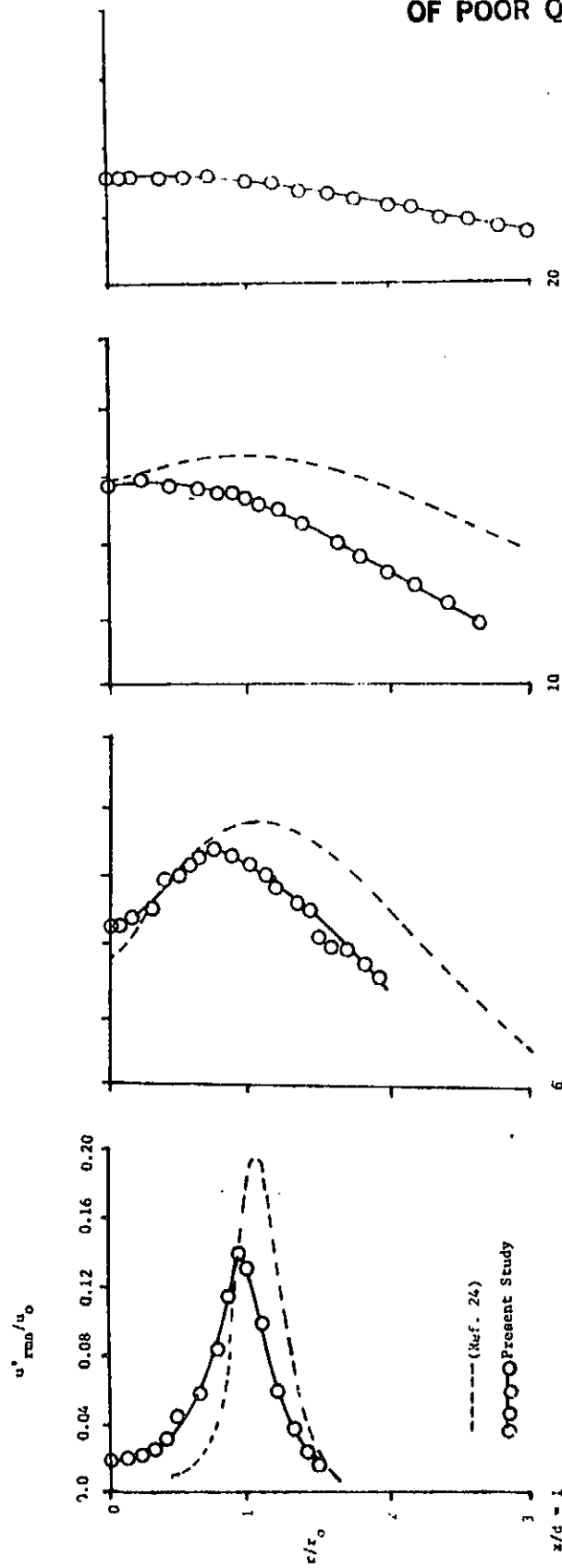
Figure 17. Free Jet Radial Distribution of Time-Mean Velocities



(b) Radial Velocity

Figure 17. (continued)

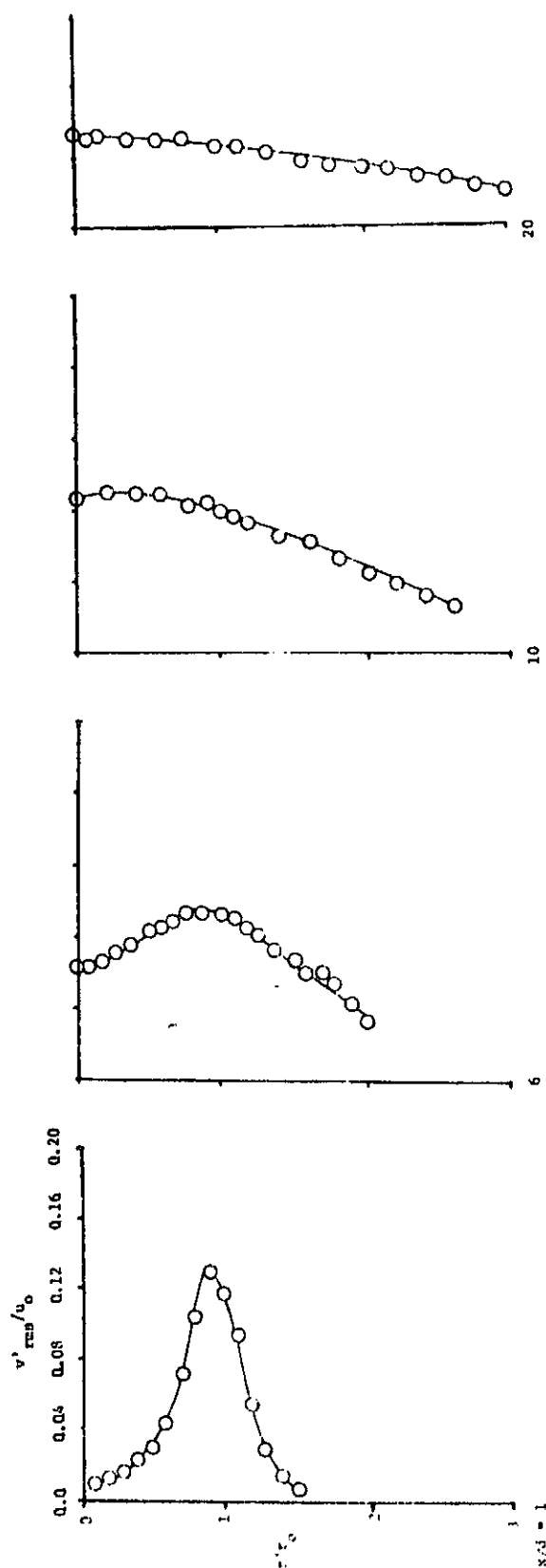
ORIGINAL PAGE 18
OF POOR QUALITY



(a) Axial Intensity

Figure 18. Free Jet Radial Distribution of Turbulence Intensities

ORIGINAL PAGE 18
OF POOR QUALITY



(b) Radial Intensity

Figure 18. (continued)

ORIGINAL PAGE NO.
OF PCOR QUALITY

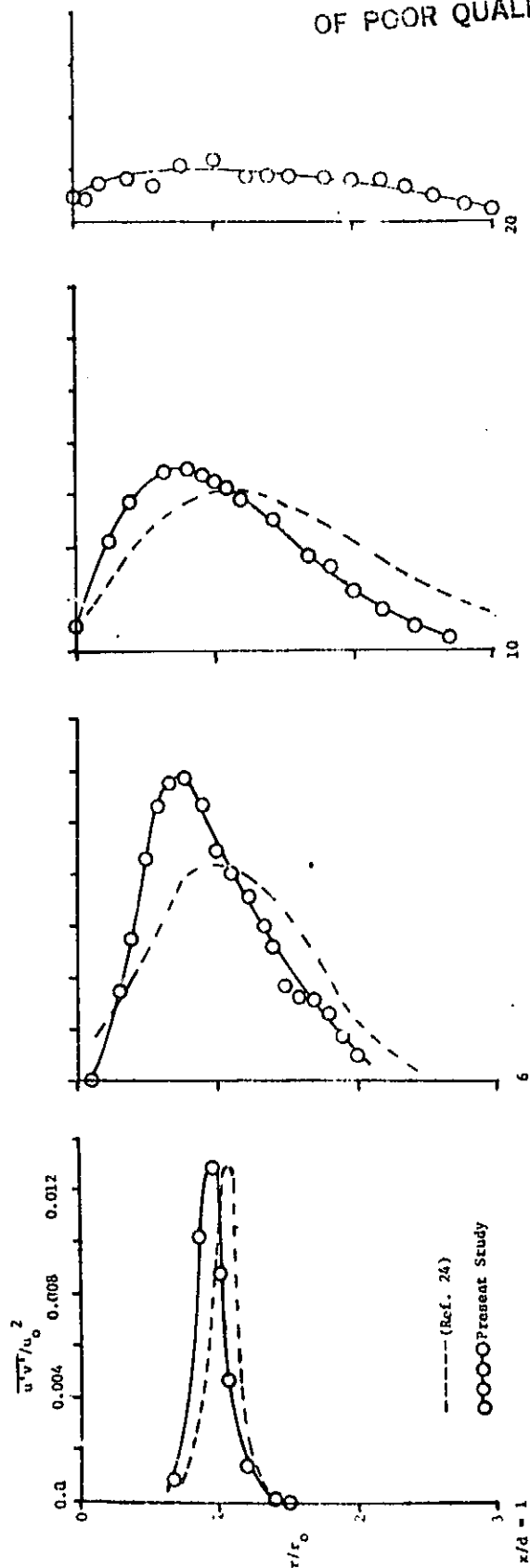


Figure 19. Free Jet Radial Distribution of Turbulent Shear Stress

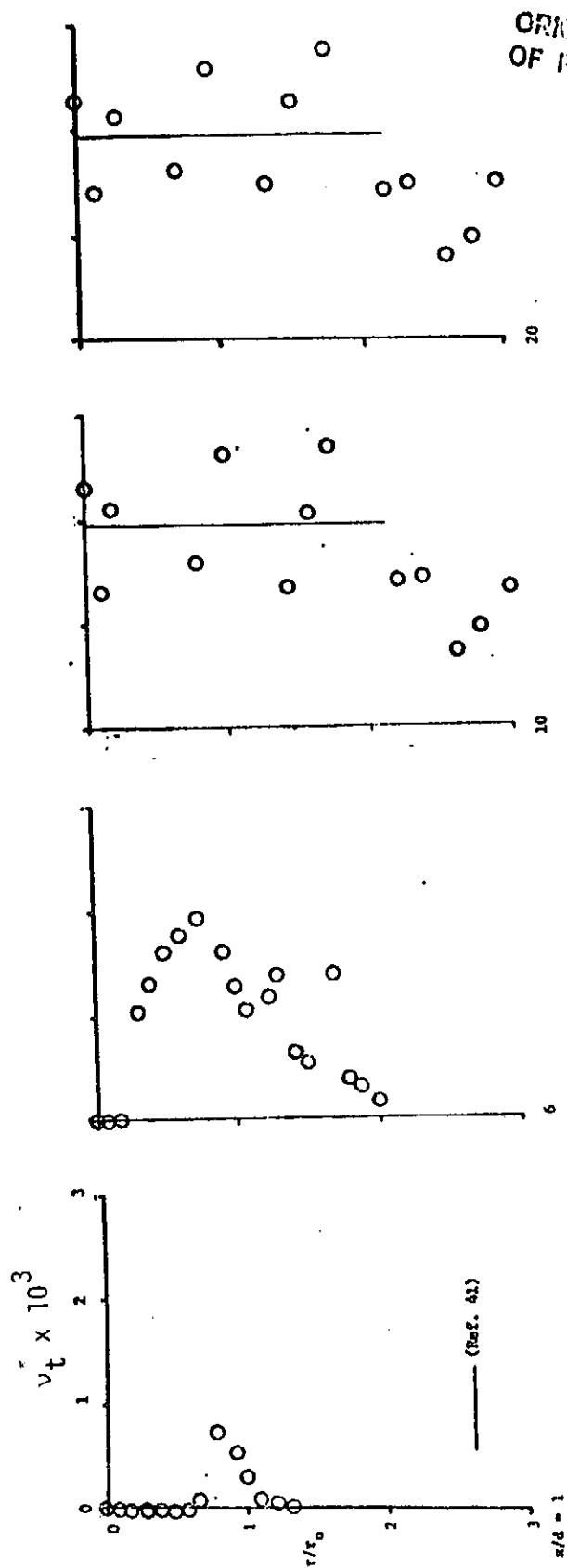


Figure 20. Free Jet Radial Distribution of Turbulent Viscosity

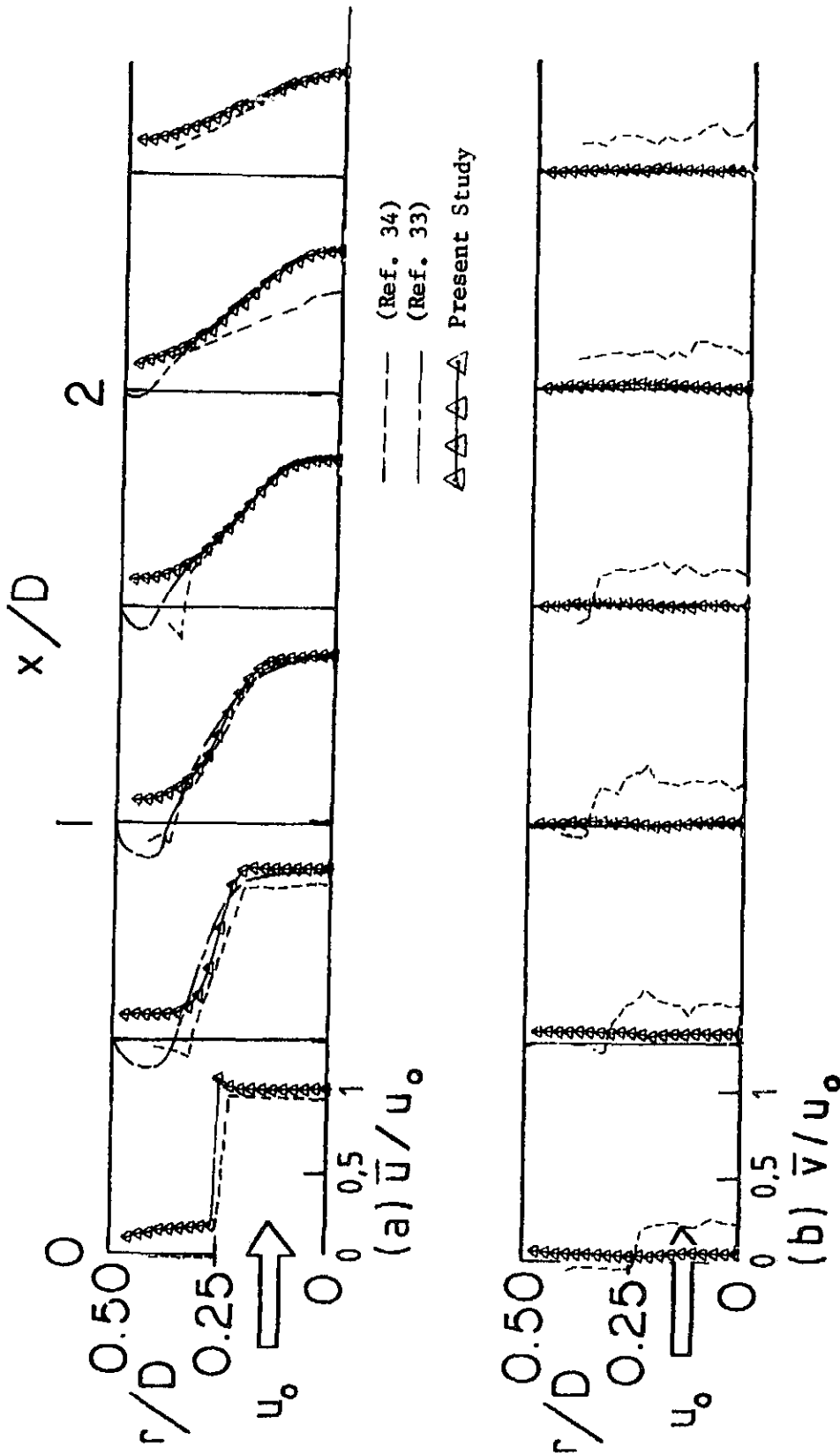


Figure 21. Confined Jet Radial Distribution of Time-Mean (a) Axial and (b) Radial Velocities

ORIGINAL PAGE 111
OF PODR QUALITY

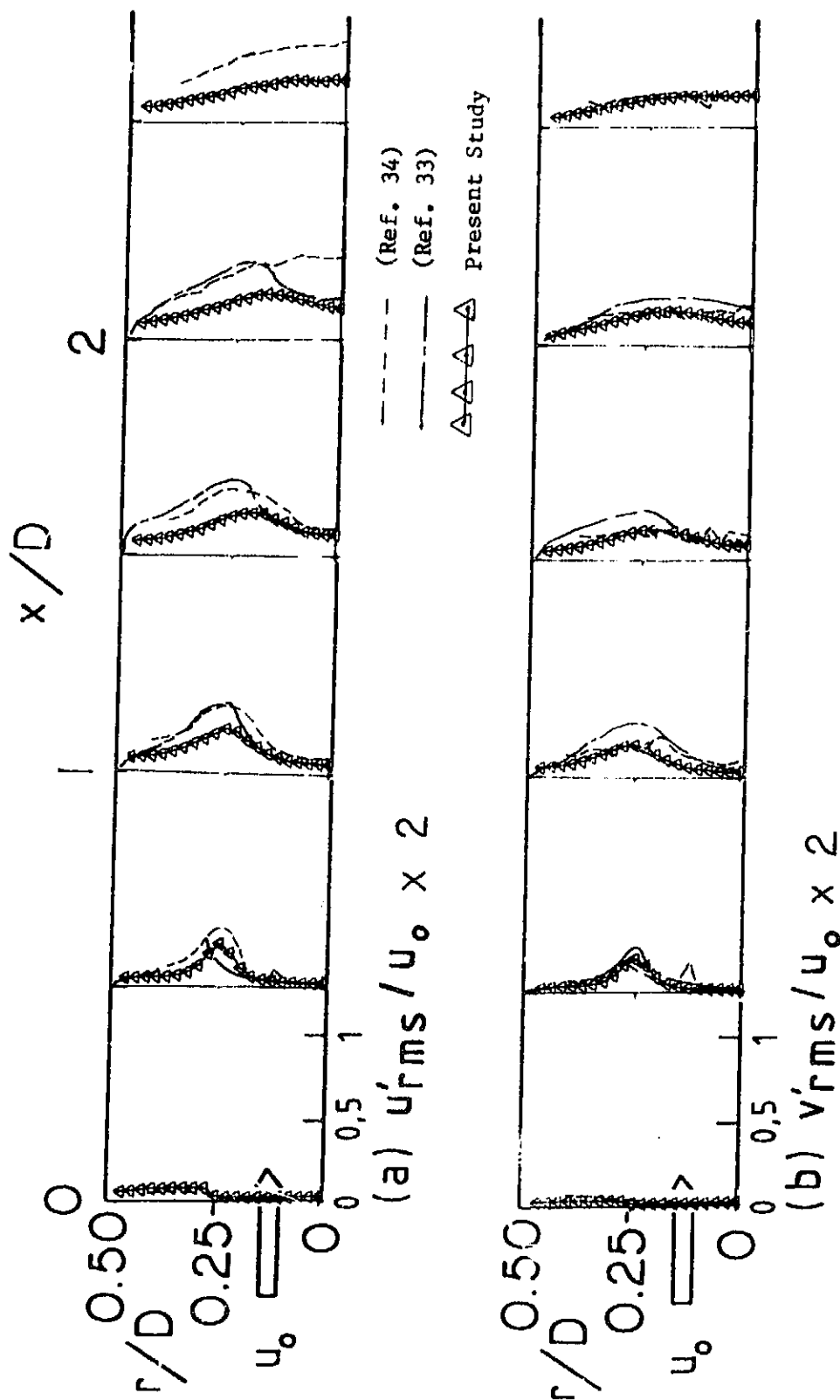


Figure 22. Confined Jet Radial Distribution of (a) Axial and (b) Radial Turbulence Intensities

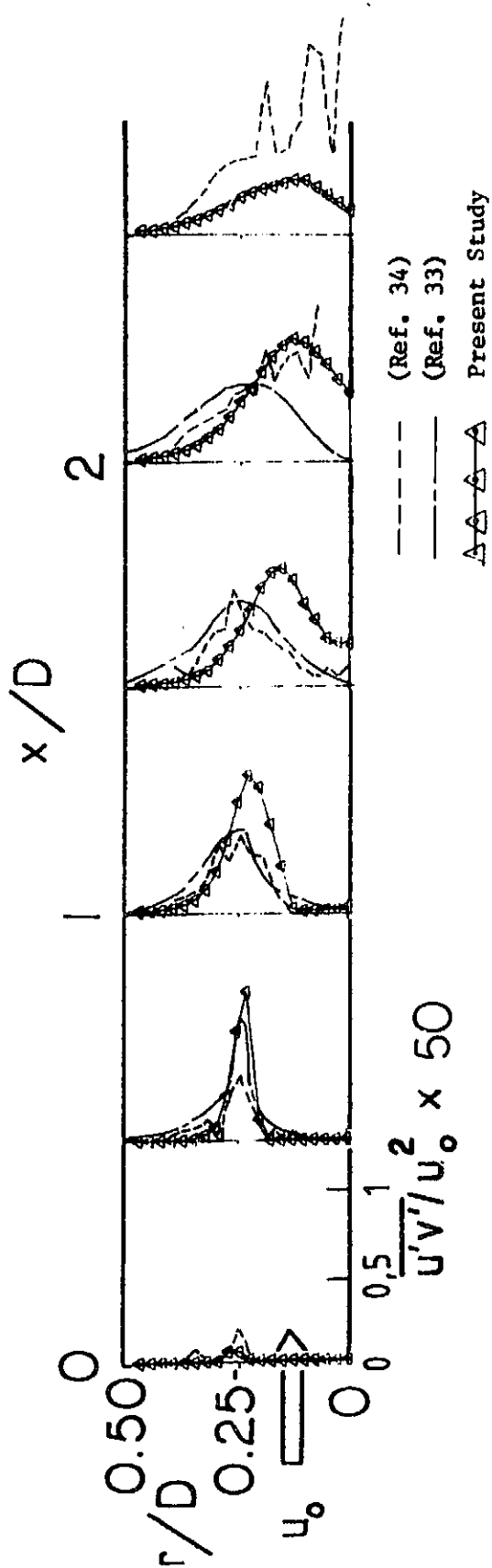


Figure 23. Confined Jet Radial Distribution of Turbulent Shear Stress

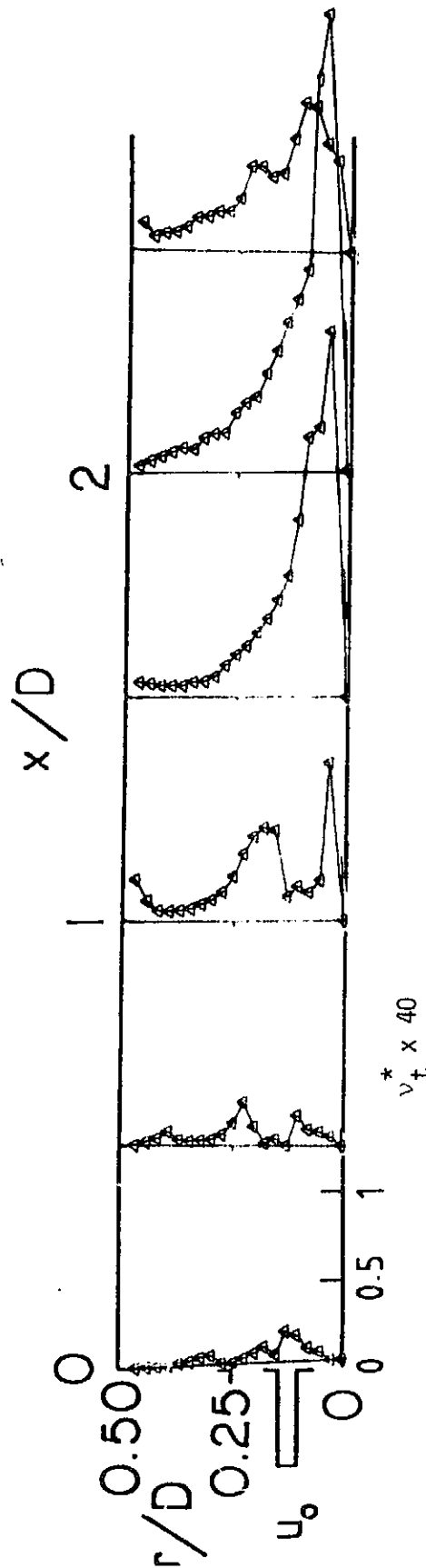


Figure 24. Confined Jet Radial Distribution of Turbulent Viscosity

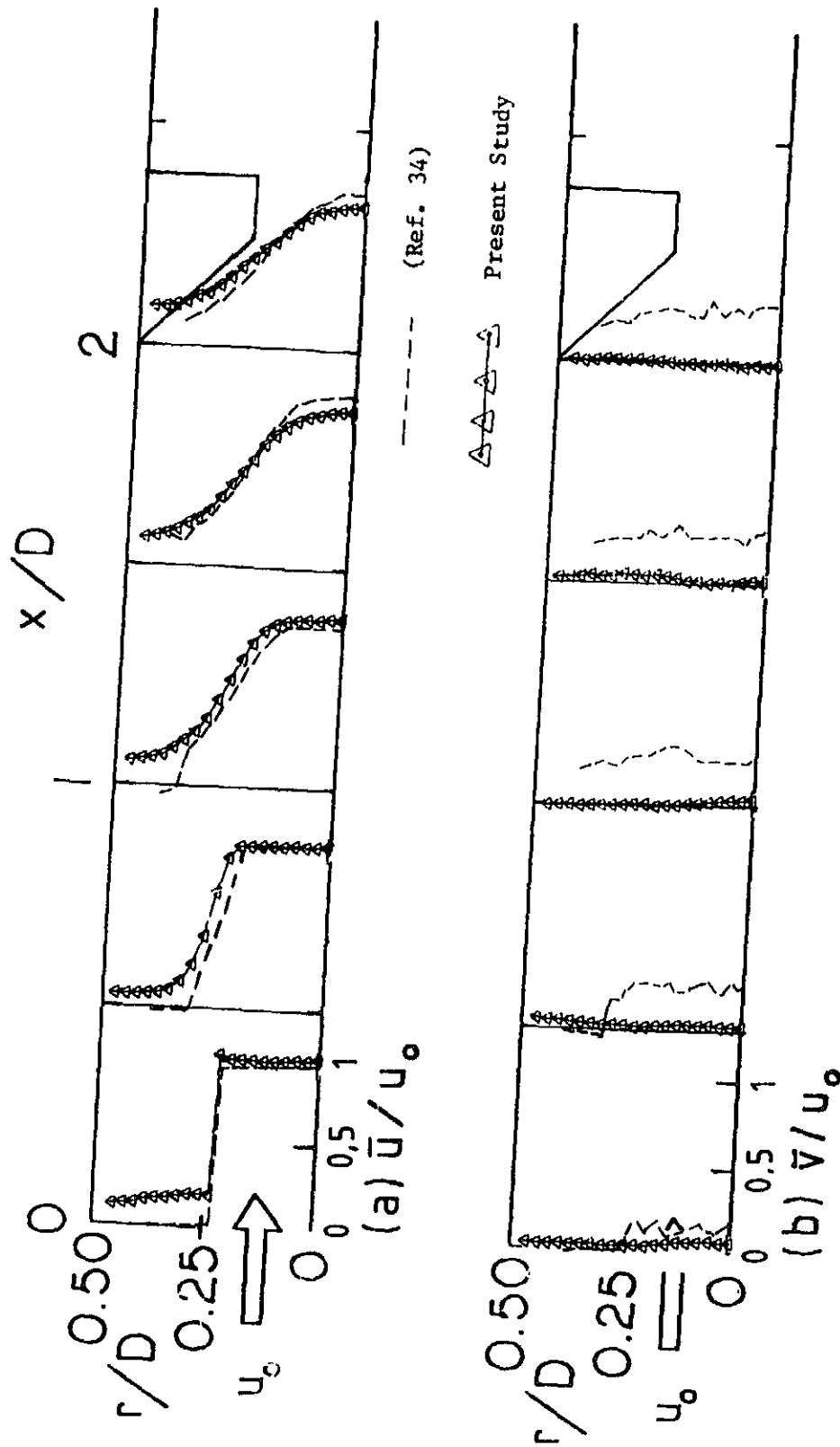


Figure 25. Confined Jet with Contraction Nozzle Radial Distribution of Time-Mean
(a) Axial and (b) Radial Velocities

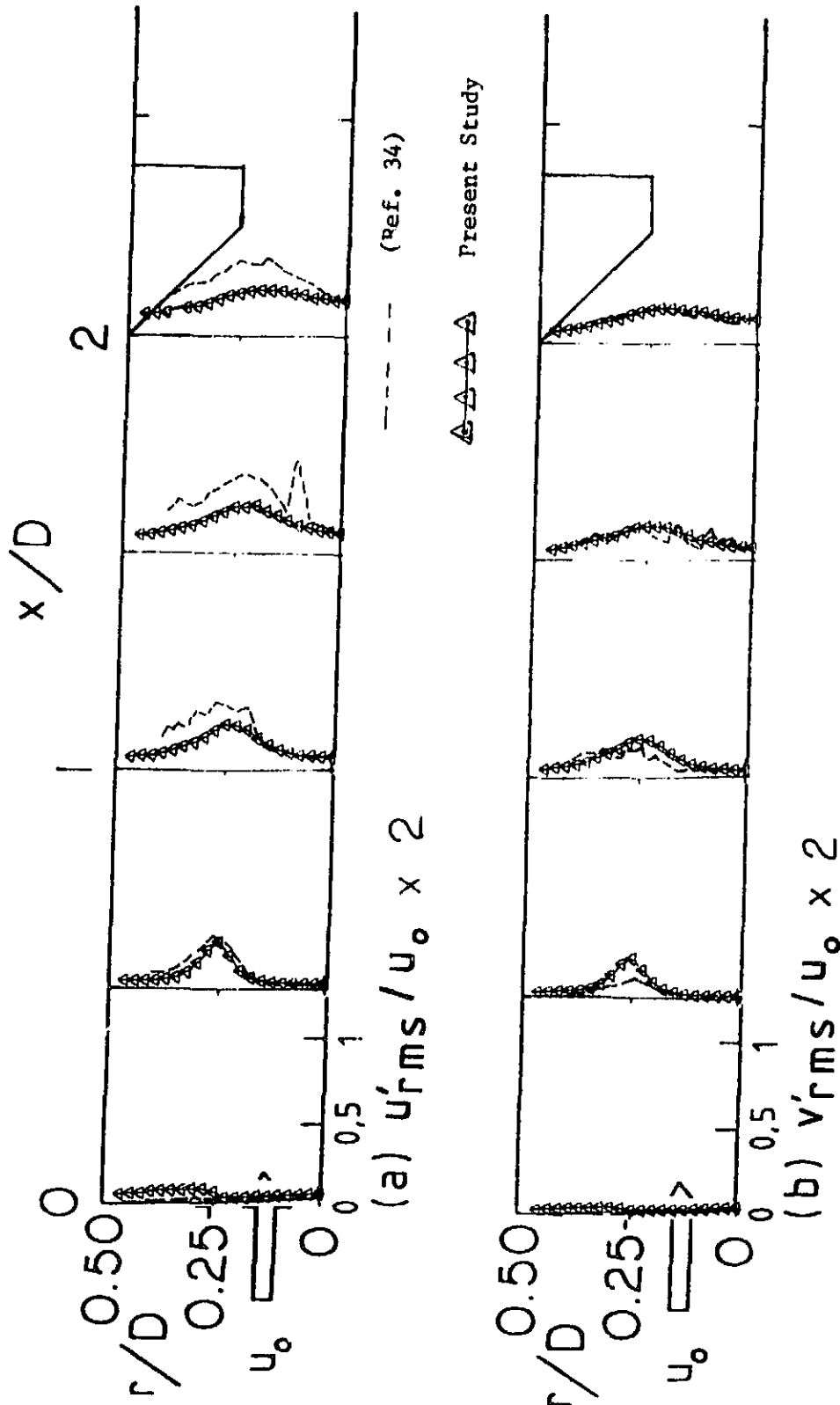


Figure 26. Confined Jet with Contraction Nozzle Radial Distribution of (a) Axial and (b) Radial Turbulence Intensities

ORIGINAL PAGE IS
OF POOR QUALITY

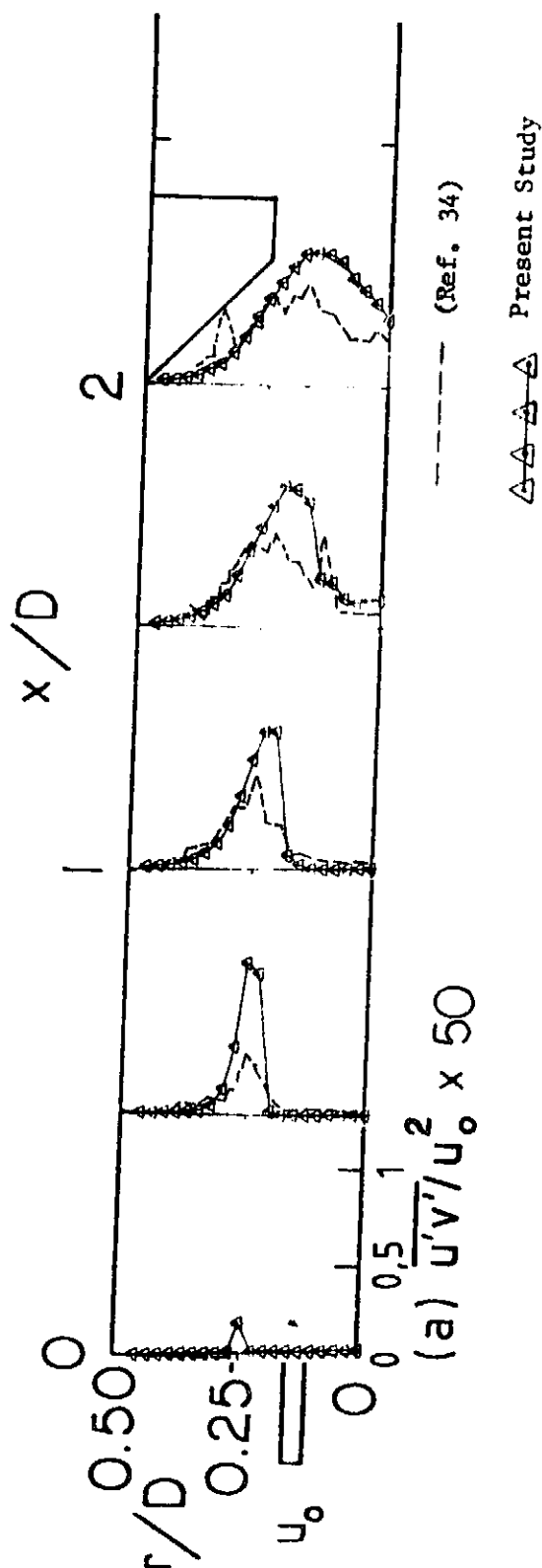


Figure 27. Confined Jet with Contraction Nozzle Radial Distribution of Turbulent Shear Stress

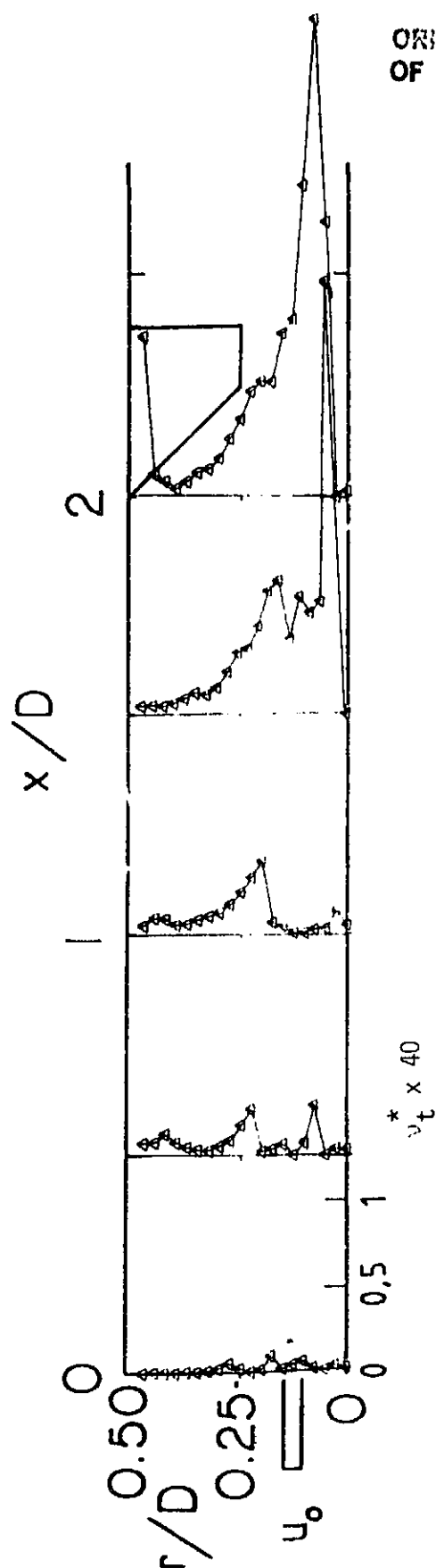


Figure 28. Confined Jet with Contraction Nozzle Radial Distribution of Turbulent Viscosity

ORIGINAL PAGE IS
OF POOR QUALITY

APPENDIX C

COMPUTER PROGRAM USER'S GUIDE

A listing for the computer program discussed in this Appendix and sample addressed data files are contained in Appendix D. Included at the end of this user's guide are the nomenclature employed in the program and a sample output.

The X-wire arrangement used for data input into this code is assumed to be the standard mutually perpendicular, 45° to probe axis wire orientation. The hot-wires are assumed to obey an extension of King's Law. That is:

$$E^2 = A + B\bar{u}^{1/2} + C\bar{u}$$

where, A, B, and C are constants determined a priori by a calibration experiment.

Four main data sets are needed as input to generate the data reduction. They are:

1. Calibration data
2. Experimental data
3. Miscellaneous data consisting of the date, experiment parameters and ambient conditions.
4. Angulation data

and are now itemized in detail.

Calibration

The calibration is accomplished as discussed in section 3.1. Thus, the calibration data set contains a number (NMAX) of selected velocities and the corresponding mean voltages from wire 1, CALE1 and wire 2, CALE2.

Experimental

This data is the information from the test section. At each radial position, r/d or r/D , seven quantities are measured. They are:

1. Mean voltage of wire 1, E_1
2. Mean voltage of wire 2, E_2
3. Adder voltage ($e_1' + e_2'$), ADDE
4. Subtractor voltage ($e_1' - e_2'$), SUBE
5. Attenuation of channel A of the correlator, ATTA
6. Attenuation of channel B of the correlator, ATTB
7. Correlator output voltage (millivolts, DC), EMVDC

There are jmax of each seven quantities.

Miscellaneous

The miscellantous data set is just that, miscellaneous. It contains:

1. Month, day, year - the date of the experiment
2. XDD - the downstream location of the probe in diameters
3. LDD - the downstream position of the contraction block in diameters
4. ALPHA - the expansion block angle in degrees
5. FE - the swirl angle, should equal zero
6. PAMB - the ambient pressure, cm of hg
7. TAMB - the ambient temperature, °C
8. E01 - nozzle exit velocity voltage of wire 1, volts
9. E02 - nozzle exit velocity voltage of wire 2, volts
10. E01 - no flow voltage of wire 1, volts
11. E02 - no flow voltage of wire 2, volts

C-2

Angulation

Because the angulation test is only done once, the slopes of E_1 and E_2 versus yaw angle, ϕ are not calculated inside this computer code. Therefore, this data consists of a series of the two slopes $\partial E_1 / \partial \phi$ and $\partial E_2 / \partial \phi$ and their corresponding velocities.

Computer Code

This computer code consists of a main program and three subroutines. Each is separated into chapters and sections. Thus, itemized by chapters:

Main

1. Inputing Data
2. Curve Fitting the Calibration Data (calls CFIT)
3. Calculating the Sensitivity Coefficients
4. Curve Fitting D_m and B_ϕ (calls C2FIT)
5. Calculating the Jet Nozzle Exit Velocity
6. Calculating All Output Variables
7. Data Output in Tabular Form
8. Data Output in Graphic Form (calls SUBPLT)

Subroutines CFIT and C2FIT

1. Initializing the Variables
2. Repackaging the Curve Fitting Variables
3. Calculation of A, B, and C, Calibration Constants,
in CFIT and Slope, B and Y-intercept, A in C2FIT

Subrouting Subplt

1. Line Plot Graph Routine

The following is an explanation of each chapter and section. Refer to Appendix D for a code listing. Nomenclature for the computer code is at the end of this appendix.

Main

Chapter 1

Section 1

This section inputs the code parameters of the number of velocities used in calibration; NMAX, the number of velocities used in the angulation tests; IMAX, and the number of measuring positions used on a cross section in the test section experiment, JMAX.

Section 2

CALU is inputted through a data statement because the calibration of the probe is done at these velocities every time. The data of the calibration voltages from the hot-wires is read from a separate data file which is called into the code using statement 4240.

Section 3

Like CALU, RDD doesn't vary. Thus, RDD is contained in a data statement. The seven quantities measured at each location in the test section are entered in a data set. As before, this data is called in the code using statement 4250.

Section 4

The data from the angulation tests is contained in this section. Data statements are used as the input medium because these tests are done once per probe.

Section 5

Miscellaneous data is input here through a allocation statement that addresses the miscellaneous data file (statement 4260).

Chapter 2

Section 1

The calibration data for wire 1 from Chapter 1, Section 2, is curve fit using a second order least squares routine (CFIT) so that:

$$CALE1^2 = A1 + B1\bar{u}^{\frac{1}{2}} + C1\bar{u}$$

Section 2

The calibration data for wire 2 is curve fit as wire 1 so that:

$$CALE2^2 = A2 + B2\bar{u}^{\frac{1}{2}} + C2\bar{u}$$

Chapter 3

In this chapter, D_m and B_ϕ are calculated for the velocities given in the angulation experiment.

Chapter 4

Section 1

The D_m 's of the previous chapter are linearly curve fit so that:

$$D_m = A3 + B2 \bar{u}$$

Section 2

The B_ϕ 's of the previous chapter are linearly curve fit so that:

$$B_\phi = A4 + B4 \bar{u}$$

Chapter 5

The nozzle exit velocity, u_o , used to nondimensionalize all turbulent quantities is calculated here from two hot-wire mean voltages determined from positioning the probe at the nozzle exit face.

Chapter 6

The outputs: \bar{u}/u_o , \bar{v}/u_o , u'/u_o , v'/u_o and $\overline{u'v'}/u_o^2$ are calculated.

Chapter 7

Section 1

Miscellaneous data is written out here with appropriate headings.

Section 2

This section writes the headings for the major output.

Section 3

Section 3 writes the turbulent quantities in tabular form.

Chapter 8

This chapter then graphs each turbulent quantity using a line printer plotting routine that is a library function in the machine for which this code was written. To do the plots, a subroutine (SUBPLT) is called to access the library plotting function.

Subroutine CFITChapter 1

The variables are initialized to zero.

Chapter 2

The x and y are repackaged so that the subroutine curve fits $CALE1^2$ versus $\bar{u}^{\frac{1}{2}}$ the first time it is called and $CALE2^2$ versus $\bar{u}^{\frac{1}{2}}$ the second.

Chapter 3

The necessary calculation are done using the least square technique. The last part of this chapter uses Cramer's Rule to solve for the A, B, and C constants.

Subroutine C2FITChapter 1

The variables are initialized to zero.

Chapter 2

The x and y are repackaged so that the subroutine curve fits D_m versus \bar{u} the first time it is called and B_ϕ versus \bar{u} the second.

Chapter 3

A linear curve fit is applied to D_m and B_ϕ versus \bar{u} to calculate slopes and y-intercepts.

Implementation

To use this computer code, the following cards have to be changed.

1. NMAX (line 380)
2. IMAX (line 390)
3. JMAX (line 400)
4. Line 4240 will be changed to address the file of calibration data that corresponds to the particular experiment.
5. Line 4250 will be changed to address the file of experiment data that corresponds with the particular experiment.
6. Line 4260 will be changed to address the file of miscellaneous data that corresponds to the particular experiment.
7. If one has crossed-wires that produce different $\partial E / \partial \phi$'s, then lines 800 and 810 will have to be modified.

It must be remembered that the code has the following restrictions:

1. Non-swirling flow
2. Wires obey King's Law
3. Wires are matched so that $(e_1' + e_2')$ and $(e_1' - e_2')$ can be simplified.
4. The hot-wire geometry is the same as shown in Figure 7.

NOMENCLATURE

<u>Code</u>	<u>Theory</u>	<u>Meaning</u>
ADDE	$(e_1' + e_2')$	Adder voltage, volts
ALPHA	α	Wall expansion angle, degrees
AM1	A_{m_1}	Axial velocity fluctuation sensitivity coefficient of wire 1
AM2	A_{m_2}	Axial velocity fluctuation sensitivity coefficient of wire 2
ANGU	-	Angulation experiment velocity, m/sec
ATTA	ATTA	Attenuation of channel A
ATTB	ATTB	Attenuation of channel B
AV1	A_{v_1}	Radial velocity fluctuation sensitivity coefficient of wire 1
AV2	A_{v_2}	Radial velocity fluctuation sensitivity coefficient of wire 2
A1, A2, etc.	$A_1, A_2, \text{etc.}$	Y-intercept of linear curve fit
BO	B_ϕ	$(E_1 A_{v_1} + E_2 A_{v_2})$
B1, B2, etc.	$B_1, B_2, \text{etc.}$	Slope of linear curve fit
CALE1	Cale1	Calibration voltage of wire 1, volts
CALE2	Cale2	Calibration voltage of wire 2, volts
CALU	-	Calibration velocity, m/sec
DM	D_m	$(E_1 A_{m_1} + E_2 A_{m_2})$
TAMB	TAMB	Temperature of atmosphere, °C
U	-	Axial velocity, m/sec
UAVG	-	Average of nondimensional axial velocity

UPDUO	u'/u_o	Nondimensionalized rms axial velocity fluctuation
UPRMS	u'	RMS axial velocity fluctuation, u' rms, m/sec
UO	u_o	Nozzle exit velocity, m/sec
U1	\bar{u}_1	Time mean axial velocity of wire 1, m/sec
U2	\bar{u}_2	Time mean axial velocity of wire 2, m/sec
U1DUO	\bar{u}_1/u_o	Nondimensional axial velocity, wire 1
U2DUO	\bar{u}_2/u_o	Nondimensional axial velocity, wire 2
VPDUO	v'/u_o	Nondimensionalized rms radial velocity fluctuation
VPRMS	v'	RMS radial velocity fluctuation, v' rms, m/sec
XDD	x/d or x/D	Nondimensionalized distance from jet exit
XDL	x/L	Nondimensionalized position of constriction block
E	-	Variable defined by call statement
EMVDC	EMVDC	Correlator output, millivolts, D.C.
EO1	-	Voltage of wire 1; no flow
EO2	-	Voltage of wire 2; no flow
E1	E_1	Mean voltage of wire 1, volts
E2	E_2	Mean voltage of wire 2, volts
E1DFE	$\partial E_1 / \partial \phi$	The slope of E_1 versus ϕ , volts/rad
E2DFE	$\partial E_2 / \partial \phi$	The slope of E_2 versus ϕ , volts/rad
E1D2U	$\partial E_1 / \partial \bar{u}$	The slope of E_1 versus \bar{u} , volts/m/sec
E2D2U	$\partial E_2 / \partial \bar{u}$	The slope of E_2 versus \bar{u} , volts/m/sec

E01	-	Nozzle exit velocity voltage of wire 1, volts
E02	-	Nozzle exit velocity voltage of wire 2, volts
FE	ϕ	Swirl angle (zero for this program), degrees
IMAX	IMAX	Number of points in angulation experiment
JMAX	JMAX	Number of points in test section experiment
NMAX	NMAX	Number of points in calibration experiment
PAMB	PAMB	Pressure of atmosphere, psia
REYSTR	$\frac{u'v'}{u_o^2}$	Nondimensional rx component of Reynolds stress tensor
RDD	r/d or r/D	Nondimensionalized distance from center line
SUBE	$(e_1' - e_2')$	Subtractor voltage, volts

Subroutine CFIT

AA0, AA1, etc.	-	Constants for Cramer's rule
A, B, etc.	-	Curve fit variables
B1, C1, etc.	-	Determinate constants
DET	-	Value of determinate used in Cramer's rule
E	-	Voltage
SI	-	Value of NMAX
SX	-	Sum of x
SXY	-	Sum of x times y
SX2	-	Sum of u
SX3	-	Sum of u times x
SX4	-	Sum of u^2
SX2Y	-	Sum of x^2 times y

SY	-	Sum of E^2
U	-	Time-mean axial velocity
X	-	Abcissa value - $u^{1/2}$
X2	-	Dummy variable
X3	-	u times x
X4	-	u^2
XY	-	x times y
X2Y	-	x^2 times y
Y	-	Ordinate value - E^2

Subroutine C2FIT

ANGU	-	Angulation test velocities
CONST	-	Variable defined by call statement
SX	-	Sum of x
SXY	-	Sum of x times y
SX2	-	Sum of x^2
SY	-	Sum of y
U	-	Variable defined by call statement
X	-	Abcissa axis values
XMEAN	-	Mean value of abcissa values
Y	-	Ordinate axis values
YMEAN	-	Mean value of ordinate values

Subroutine SUBPLOT

IM	-	Field size
NLAST	-	Number of points to be plotted
X	-	Abcissa plot variable

XMAX	-	Maximum abscissa value
XX	-	Value of abscissa to be plotted
Y	-	Ordinate plot variable
YMAX	-	Maximum ordinate value
YX	-	Value of ordinate to be plotted

ORIGINAL PAGE IS
OF POOR QUALITY

SAMPLE OUTPUT

DATA TAKEN 8/23/83

X/D: 1.5

L/D: 2.0

ALPHA: 90.0

FE: 0.0

PAMB: 74.2

TAMB: 27.0

UO: 18.3438

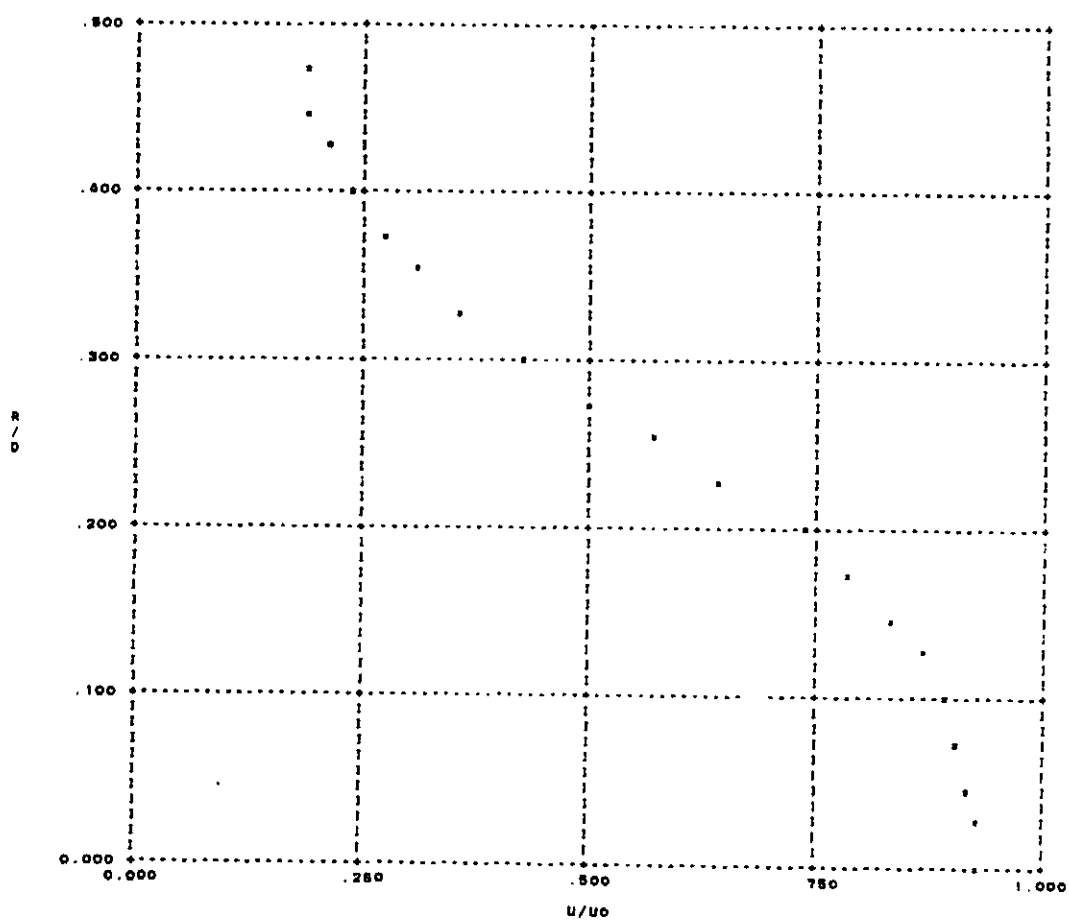
E01: 2.61

E02: 2.67

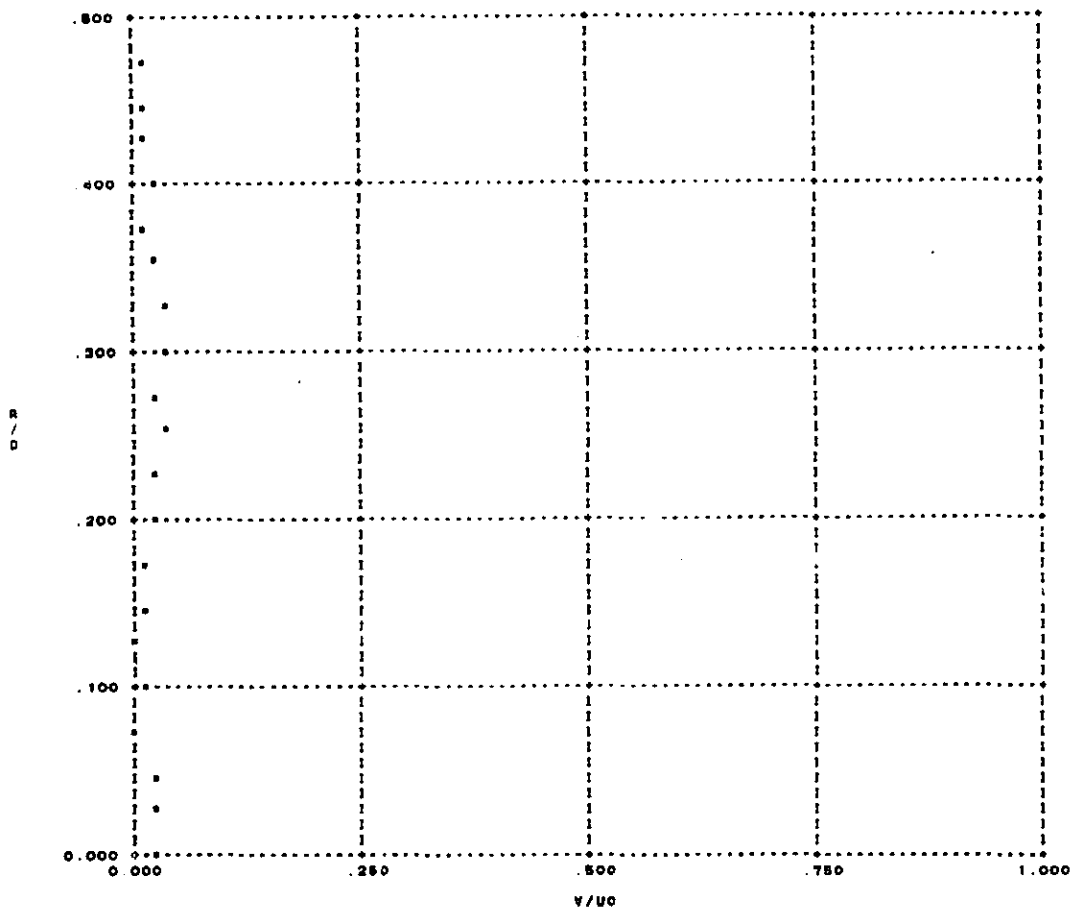
R/D	U1/U0	U2/U0	U/U0	V/U0	U*/U0	V*/U0	U* V*/U0**2
0.000	0.851	0.801	0.826	0.026	0.064	0.036	0.002730
0.025	0.851	0.801	0.826	0.026	0.066	0.036	0.002761
0.050	0.838	0.801	0.820	0.016	0.070	0.038	0.002440
0.075	0.810	0.801	0.806	0.004	0.076	0.046	0.002690
0.100	0.803	0.886	0.894	0.008	0.084	0.051	0.004382
0.125	0.872	0.872	0.872	0.000	0.090	0.056	0.004697
0.150	0.828	0.846	0.836	0.010	0.114	0.070	0.012238
0.175	0.781	0.786	0.788	0.007	0.126	0.078	0.013511
0.200	0.713	0.761	0.737	0.024	0.144	0.090	0.013840
0.225	0.616	0.873	0.846	0.020	0.136	0.092	0.011811
0.250	0.641	0.812	0.876	0.036	0.136	0.092	0.009706
0.275	0.670	0.633	0.804	0.020	0.123	0.089	0.007446
0.300	0.394	0.457	0.425	0.031	0.110	0.080	0.006022
0.325	0.314	0.360	0.361	0.036	0.096	0.068	0.003088
0.350	0.282	0.327	0.306	0.022	0.087	0.080	0.002202
0.375	0.256	0.267	0.272	0.016	0.076	0.053	0.001480
0.400	0.211	0.264	0.236	0.027	0.087	0.046	0.001006
0.425	0.201	0.220	0.214	0.014	0.080	0.039	0.000823
0.450	0.188	0.204	0.196	0.008	0.064	0.034	0.000410
0.475	0.178	0.196	0.187	0.006	0.052	0.029	0.000268

ORIGINAL PAGE IS
OF POOR QUALITY

R/D	U/U0
0.000	0.876
0.025	0.826
0.050	0.820
0.075	0.808
0.100	0.804
0.125	0.872
0.150	0.838
0.175	0.788
0.200	0.737
0.225	0.843
0.250	0.878
0.275	0.804
0.300	0.426
0.325	0.381
0.350	0.305
0.375	0.272
0.400	0.238
0.425	0.214
0.450	0.186
0.475	0.187

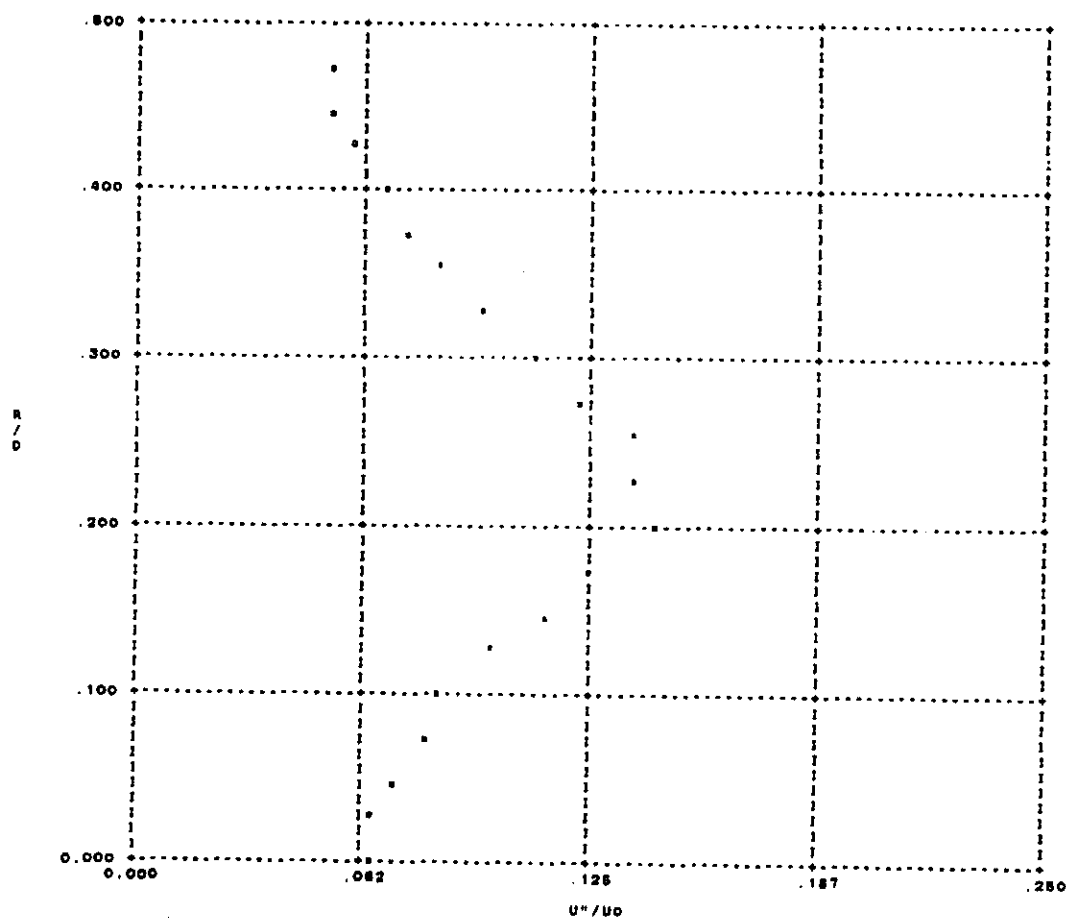


R/D	V/UO
0.000	0.028
0.025	0.028
0.050	0.018
0.075	0.004
0.100	0.008
0.125	0.000
0.150	0.010
0.175	0.007
0.200	0.024
0.225	0.028
0.250	0.038
0.275	0.028
0.300	0.031
0.325	0.038
0.350	0.022
0.375	0.015
0.400	0.027
0.425	0.014
0.450	0.008
0.475	0.008

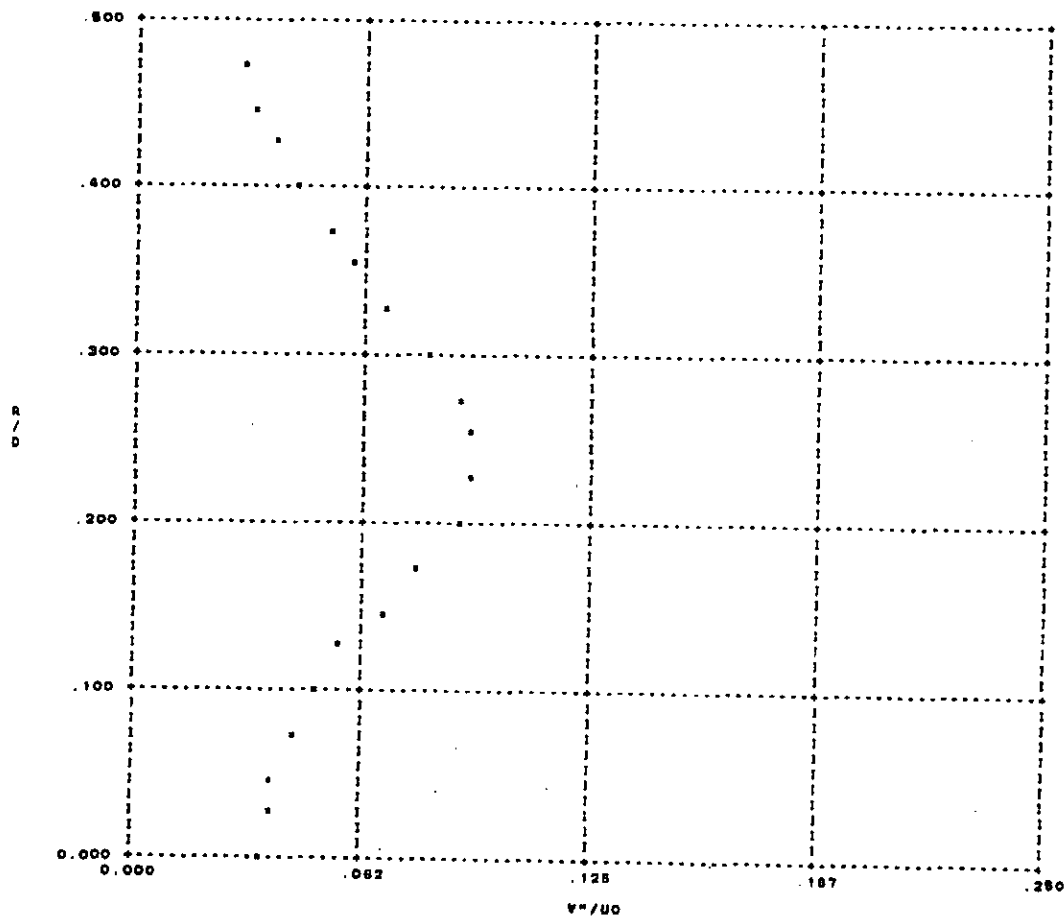


ORIGINAL PAGE IS
OF POOR QUALITY

R/D	U^*/U_0
0.000	0.084
0.025	0.086
0.050	0.070
0.075	0.078
0.100	0.084
0.125	0.089
0.150	0.114
0.175	0.128
0.200	0.144
0.225	0.131
0.250	0.138
0.275	0.123
0.300	0.110
0.325	0.086
0.350	0.082
0.375	0.078
0.400	0.087
0.425	0.080
0.450	0.084
0.475	0.082



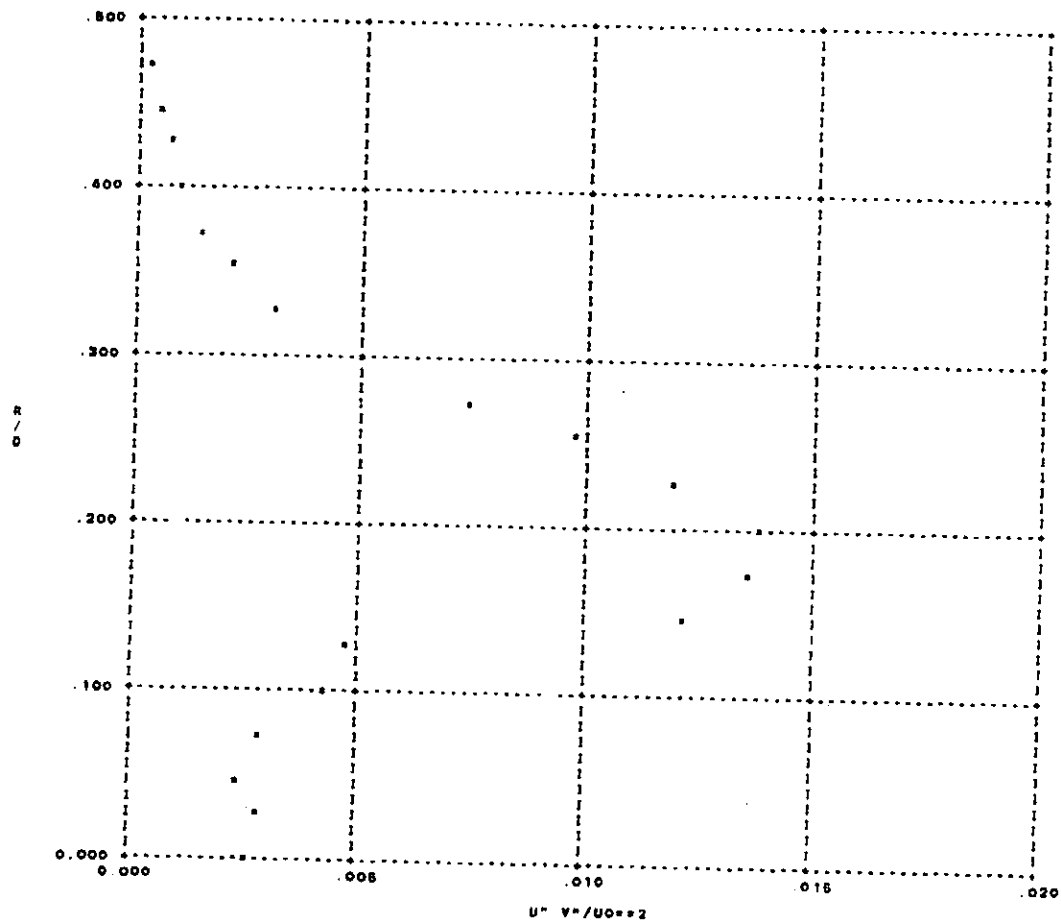
R/D	V''/U0
0.000	0.036
0.025	0.036
0.050	0.039
0.075	0.045
0.100	0.051
0.125	0.058
0.150	0.070
0.175	0.078
0.200	0.080
0.225	0.082
0.250	0.082
0.275	0.089
0.300	0.080
0.325	0.086
0.350	0.080
0.375	0.053
0.400	0.048
0.425	0.029
0.450	0.024
0.475	0.020



ORIGINAL PAGE IS
OF POOR QUALITY

103

R/D	$U^* V^*/U_0^{*2}$
0.000	0.002730
0.025	0.002741
0.050	0.002440
0.075	0.002890
0.100	0.004262
0.125	0.004887
0.150	0.012238
0.175	0.013511
0.200	0.013840
0.225	0.011811
0.250	0.008706
0.275	0.007448
0.300	0.008022
0.325	0.003086
0.350	0.002202
0.375	0.001480
0.400	0.001006
0.425	0.000823
0.450	0.000410
0.475	0.000288



ORIGINAL PAGE IS
OF POOR QUALITY

APPENDIX D

COMPUTER CODE LISTING

ORIGINAL PAGE IS
OF POOR QUALITY

NUMBERED LISTING

```

00060 C
00070 C *****
00080 C *
00090 C * THIS PROGRAM REDUCES THE 1/4 IN X-WIRE PROBE DATA IN *
00100 C * *
00110 C * NON SWIRLING FLOW. IT IS ASSUMED THAT THE WIRES *
00120 C * *
00130 C * FOLLOW KING'S LAW. *
00140 C * *
00150 C * BY *
00160 C * BRIAN McKILLOP *
00170 C * *
00180 C * LAST ITERATION ON COMPUTER CODE 6-10-83 *
00190 C *
00200 C *****
00210 C
00220 C
00230 C DIMENSION CALU(50),CALE1(50),CALE2(50),FDD(50),L1(50),L2(50),
00240 C XADDF(50),SUBF(50),ATTAC(50),ATTB(50),EMUD(50),ANGU(50),
00250 C REIDFE(50),E2FE(50),F1DPR(50),F2DPR(50),AM1(50),AM2(50),AV1(50),
00260 C XAV2(50),DM(50),BD(50),HRRBS(50),HRRBS(50),UPDIO(50),VPDIO(50),
00270 C BREYSTR(50),U1(50),U2(50),U1DUO(50),U2DUO(50),HRRD(50),VDUO(50),
00280 C XY(50),UC(50),ABSREY(50)
00290 C INTEGER DAY, YEAR
00300 C REAL LDD
00310 C
00320 C ----- CHAPTER 1 -----
00330 C ----- SECTION 1 -----
00340 C
00350 C INPUTTING THE NUMBER OF POINTS FROM CALIBRATION, ANGULATION,
00360 C AND TEST SECTION EXPERIMENTS, RESPECTIVELY.
00370 C
00380 C NMAX=15
00390 C IMAX=5
00400 C JMAX=20
00410 C
00420 C ----- SECTION 2 -----
00430 C
00440 C
00450 C INPUTTING DATA FROM CALIBRATION EXPERIMENT
00460 C
00470 C DATA CALU/2.43,2.76,3.38,3.95,4.63,5.11,5.92,6.72,7.65,
00480 C 8.62,9.57,10.7,11.8,13.05,14.42/
00490 C READ(14,*) (CALE1(N),N=1,NMAX)
00500 C READ(14,*) (CALE2(N),N=1,NMAX)
00510 C WRITE(6,*) (CALE1(N),N=1,NMAX)
00520 C WRITE(6,*) (CALE2(N),N=1,NMAX)
00530 C
00540 C ----- SECTION 3 -----
00550 C
00560 C INPUTTING DATA FROM EXPERIMENT IN TEST SECTION
00570 C
00580 C DATA RMD/0.0,0.025,0.05,0.075,0.1,0.125,0.15,0.175,0.2,0.225,
00590 C 0.25,0.275,0.3,0.325,0.35,0.375,0.4,0.425,0.45,0.475,0.5/
00600 C READ(15,*) (E1(J),J=1,JMAX)
00610 C READ(15,*) (E2(J),J=1,JMAX)
00620 C READ(15,*) (XADDF(J),J=1,JMAX)
00630 C READ(15,*) (SUBF(J),J=1,JMAX)
00640 C READ(15,*) (ATTAC(J),J=1,JMAX)
00650 C READ(15,*) (ATTB(J),J=1,JMAX)
00660 C READ(15,*) (EMUD(J),J=1,JMAX)

```

ORIGINAL PAGE IS
OF POOR QUALITY

```

00670      WRITE(6,*) (F1(J),J=1,JMAX)
00680      WRITE(6,*) (E2(J),J=1,JMAX)
00690      WRITE(6,*) (ADDE(J),J=1,JMAX)
00700      WRITE(6,*) (SURE(J),J=1,JMAX)
00710      WRITE(6,*) (ATTAC(J),J=1,JMAX)
00720      WRITE(6,*) (ATTB(J),J=1,JMAX)
00730      WRITE(6,*) (EMVDC(J),J=1,JMAX)
00740 C
00750 C-----SECTION 4-----
00760 C
00770 C      INPUTING DATA FROM ANGULATION EXPERIMENT
00780 C
00790      DATA ANGU/14.42,11.82,9.57,7.60,5.11/
00800      DATA E1DFF/0.4018,0.4744,0.4543,0.3963,0.3527/
00810      DATA E2DFF/0.5867,0.5461,0.5041,0.4822,0.4282/
00820 C
00830 C-----SECTION 5-----
00840 C
00850 C      INPUTING MISCELLANEOUS DATA
00860 C
00870      READ(16,*) MONTH, DAY, YEAR, XDD, LDD, ALPHA, FE, FAMB, TAMR, E01, E02,
00880      &E01, E02
00890      WRITE(6,*) MONTH, DAY, YEAR, XDD, LDD, ALPHA, FE, FAMB, TAMR, E01, E02,
00900      &E01, E02
00910 C
00920 C-----CHAPTER 2-----
00930 C
00940 C-----SECTION 1-----
00950 C
00960 C
00970 C      THIS STATEMENT TAKES CALIBRATION VOLTAGE ONE AND DOES A
00980 C      SECOND ORDER LEAST SQUARES CURVE FIT SUCH THAT:
00990 C      CALE1**2=A1+B1*U**0.5+C1*U
01000 C
01010      CALL CE11(NMAX,CALU,CALE1,A1,B1,C1)
01020      WRITE(6,100) A1, B1, C1
01030 100  FORMAT(///20X, 'CALE1 SQUARED=', F8.3, '  +', F8.3, 2X, 'CALU TO 1/2',
01040      &'  +', F8.3, 2X, 'CALU')
01050 C
01060 C-----SECTION 2-----
01070 C
01080 C      THIS STATEMENT TAKES CALIBRATION VOLTAGE TWO AND DOES A
01090 C      SECOND ORDER LEAST SQUARES CURVE FIT SUCH THAT:
01100 C      CALE2**2=A2+B2*U**0.5+C2*U
01110 C
01120      CALL CE11(NMAX,CALU,CALE2,A2,B2,C2)
01130      WRITE(6,110) A2, B2, C2
01140 110  FORMAT(///20X, 'CALE2 SQUARED=', F8.3, '  +', F8.3, 2X, 'CALU TO 1/2',
01150      &'  +', F8.3, 2X, 'CALU')
01160 C
01170 C-----CHAPTER 3-----
01180 C
01190 C      DO LOOP USING ANGULATION EXPERIMENT DATA TO COMPUTE
01200 C      SENSITIVITY COEFFICIENTS
01210 C
01220      DO 300 I=1,IMAX
01230          E1D2U(I)=(B1+2.0*C1*ANGU(I)**0.5)/(4.0*(A1+ANGU(I)+B1*ANGU(I)**1.5
01240      &+C1*ANGU(I)**2)**0.5)
01250          E2D2U(I)=(B2+2.0*C2*ANGU(I)**0.5)/(4.0*(A2+ANGU(I)+B2*ANGU(I)**1.5
01260      &+C2*ANGU(I)**2)**0.5)
01270          WRITE(6,1234) E1D2U(I), E2D2U(I)
01280 1234  FORMAT(///10X, F10.6, 10X, F10.6)
01290          AM1(I)=ANGU(I)*E1D2U(I)
01300          AM2(I)=ANGU(I)*E2D2U(I)
01310          AV1(I)=E1DFF(I)
01320          AV2(I)=E2DFF(I)

```

ORIGINAL PAGE IS
OF POOR QUALITY

```

01350      DM(I)=AM(I)+AM2(I)
01360      RM(I)=AV1(I)+AV2(I)
01370      CONTINUE
01380      -----CHAPTER 4-----
01390      -----SECTION 1-----
01400      C
01410      C      THIS STATEMENT TAKES DM AND DOES A LINEAR CURVE FIT SUCH THAT:
01420      C      DM=A3+B3*U
01430      C
01440      CALL CDFIT(IMAX,ANGU,DM,A3,B3)
01450      C      A3=0.535
01460      C      B3=0.0632
01470      WRITE(6,202) A3,B3
01480      202  FORMAT(///20X,'DM=' ,F8.3, ' ' ,F8.3,2X,'U')
01490      C
01500      C      THIS STATEMENT TAKES BU AND DOES A LINEAR CURVE FIT SUCH THAT:
01510      C      BU=A4+B4*U
01520      C
01530      C      -----SECTION 2-----
01540      C
01550      CALL CDFIT(IMAX,ANGU,BU,A4,B4)
01560      C      WRITE(6,203) A4,B4
01570      203  FORMAT(///20X,'BU=' ,F8.3, ' ' ,F8.3,2X,'U')
01580      C
01590      C      -----CHAPTER 5-----
01600      C
01610      C      CALCULATING THE NOZZLE EXIT VELOCITY
01620      C
01630      U01=((-B1+(B1**2-4.0*C1*(A1-F1**2))**0.5)/(2.0*C1))**2
01640      U02=((-B2+(B2**2-4.0*C2*(A2-L02**2))**0.5)/(2.0*C2))**2
01650      U0=(U01+U02)/2.0
01660      C
01670      C      -----CHAPTER 6-----
01680      C
01690      C      NO LOOP TO GENERATE OUTPUT DATA ,CALCULATIONS ARE PERFORMED
01700      C      AT EACH R/D POSITION
01710      C
01720      DO 1000 J=1,JMAX
01730      U1(J)=((-B1+(B1**2-4.0*C1*(A1-F1(J)**2))**0.5)/(2.0*C1))**2
01740      U2(J)=((-B2+(B2**2-4.0*C2*(A2-L02(J)**2))**0.5)/(2.0*C2))**2
01750      U1DUO(J)=U1(J)/U0
01760      U2DUO(J)=U2(J)/U0
01770      UDUO(J)=(U1DUO(J)+U2DUO(J))/2.0
01780      VDUO(J)=ABS(U1DUO(J)-U2DUO(J))/2.0
01790      U(J)=UDUO(J)*U0
01800      DM(J)=A3+B3*U(J)
01810      RO(J)=A4+B4*U(J)
01820      UFRMS(J)=ADDE(J)/DM(J)
01830      VFRMS(J)=SUBE(J)/RO(J)
01840      UFDUO(J)=UFRMS(J)*U(J)/U0
01850      VFDUO(J)=VFRMS(J)*U(J)/U0
01860      REYSTR(J)=(VDUO(J)*10.0**((ALFA(J)+ATTE(J))/20.0)*U(J)**2/
01870      *(U0**2*125.0*1600.0*RO(J)*BH(J))*0.001
01880      1000  CONTINUE
01890      C      WRITE(6,9112) (U1(J),J=1,JMAX)
01900      C      WRITE(6,9113) (U2(J),J=1,JMAX)
01910      112  FORMAT( ,5X,16F10.4)
01920      C      WRITE(6,9113)U0
01930      9113  FORMAT( ,///,35X,F10.4)
01940      C
01950      C      -----CHAPTER 7-----
01960      C
01970      C      -----SECTION 1-----
01980      C

```


ORIGINAL PAGE IS
OF POOR QUALITY

```

01990 C
02000 WRITE(A,250)
02010 J50 FORMAT(1H1)
02020 C
02030 C WRITE STATEMENTS FOR MISCELLANEOUS DATA
02040 C
02050 WRITE(A,251) MONTH, DAY, YEAR
02060 J51 FORMAT(//,45X, 'DATA TAKEN', 2X, 12, '/', 12, '/', 12)
02070 WRITE(A,252) XBD, LDD
02080 J52 FORMAT(//,30X, 'X/D=', F4.1, 30X, 'L/D=', F4.1)
02090 WRITE(A,253) ALPHA, FE
02100 J53 FORMAT(//,30X, 'ALPHA=', F4.1, 30X, 'FE=', F4.1)
02110 WRITE(A,254) PAMB, TAMB, UO, EO1, EO2
02120 J54 FORMAT(//,25X, 'PAMB=', F4.1, 5X, 'TAMB=', F5.1, 5X, 'UO=', F5.3,
02130 5X, 'EO1=', F4.2, 5X, 'EO2=', F4.2)
02140 C
02150 C -----SECTION 2-----
02160 C
02170 C WRITE STATEMENT FOR HEADINGS
02180 C
02190 WRITE(A,255)
02200 J55 FORMAT(///,13X, 'R/D', 7X, 'U1/U0', 6X, 'U2/U0', 5X, 'U/U0', 8X, 'U/U0',
02210 8X, 'U*U0', 7X, 'U*/U0', 9X, 'U*U*/U0*2')
02220 C
02230 C -----SECTION 3-----
02240 C
02250 C WRITE STATEMENT FOR GENERATED OUTPUT
02260 C
02270 WRITE(A,1001) (RDD(J), U1DUO(J), U2DUO(J), UDUO(J), VDUO(J),
02280 XUFDUO(J), VPDFDUO(J), REYSTR(J), J=1, JMAX)
02290 1001 FORMAT(//,10X, F8.3, 2X, F8.3, 3X, F8.3, 2X, F8.3, 4X, F8.3, 5X,
02300 4X, F8.3, 4X, F8.3, 9X, F10.6)
02310 C
02320 C -----CHAPTER B-----
02330 C
02340 C PLOTTING THE OUTPUT DATA
02350 C
02360 WRITE(A,8020)
02370 8020 FORMAT(1H1)
02380 WRITE(A,8021)
02390 8021 FORMAT(//,30X, 'R/D', 20X, 'U/U0')
02400 WRITE(A,8022) (RDD(J), UDUO(J), J=1, JMAX)
02410 8022 FORMAT(//,27X, F8.3, 15X, F8.3)
02420 YMAX=0.5
02430 XMAX=1.0
02440 CALL SUBPLT(Y, XMAX, YMAX, UDUO, RDD, JMAX)
02450 WRITE(A,8000)
02460 8000 FORMAT(//,51X, 'U/U0')
02470 WRITE(A,8020)
02480 WRITE(A,8023)
02490 8023 FORMAT(//,30X, 'R/D', 20X, 'U/U0')
02500 WRITE(A,8022) (Y(J), VDUO(J), J=1, JMAX)
02510 DO 1670 J=1, JMAX
02520 RDD(J)=Y(J)
02530 1670 CONTINUE
02540 CALL SUBPLT(Y, XMAX, YMAX, VDUO, RDD, JMAX)
02550 WRITE(A,8001)
02560 8001 FORMAT(//,54X, 'U/U0')
02570 WRITE(A,8020)
02580 WRITE(A,8028)
02590 8028 FORMAT(//,30X, 'R/D', 20X, 'U/U0')
02600 WRITE(A,8022) (Y(J), UPDFDUO(J), J=1, JMAX)
02610 DO 1673 J=1, JMAX
02620 RDD(J)=Y(J)
02630 1673 CONTINUE
02640 CALL SUBPLT(Y, XMAX, YMAX, UPDFDUO, RDD, JMAX)

```

ORIGINAL PAGE IS
OF POOR QUALITY

```

02670      WRITE(6,B004)
02680      FORMAT(2,54X,'U*/U0')
02690      WRITE(6,B020)
02700      WRITE(6,B029)
02710      FORMAT(2,30X,'R/D',20X,'U*/U0')
02720      WRITE(6,B022)(Y(J),V(DUO(J)),J=1,JMAX)
02730      DO 1674 J=1,JMAX
02740      RUD(J)=Y(J)
02750      CONTINUE
02760      CALL SUBPLT(Y,XMAX,YMAX,V(DUO),RUD,JMAX)
02770      WRITE(6,B005)
02780      FORMAT(2,54X,'V*/U0')
02790      WRITE(6,B020)
02800      WRITE(6,B030)
02810      FORMAT(2,30X,'R/D',17X,'U*/U0**2')
02820      WRITE(6,B031)(Y(J),REYSTR(J),J=1,JMAX)
02830      FORMAT(2,27X,F8.3,4X,F10.6)
02840      DO 1675 J=1,JMAX
02850      RUD(J)=Y(J)
02860      CONTINUE
02870      XMAX=0.02
02880      DO 1700 J=1,JMAX
02890      ARSREY(J)=ARS(REYSTR(J))
02900      CONTINUE
02910      CALL SUBPLT(Y,XMAX,YMAX,ARSREY,RUD,JMAX)
02920      WRITE(6,B006)
02930      FORMAT(2,51X,'U*/U0**4')
02940      *****
02950      *****
02960      L
02970      STOP
02980      END
02990      SUBROUTINE CFIT(NMAX,U,F,A,B,C)
03000      C      THE PROGRAM DOES A SECOND ORDER CURVE FIT TO GIVEN
03010      C      HOTWIRE CALIBRATION DATA.
03020      C      THE EQUATION IS OF THE FORM C**2 A+B*SOR(U)+C*U
03030      C
03040      C
03050      DIMENSION E(50),U(50),Y(50),Y2(50),X3(50),X4(50),XY(50),
03060      *X2Y(50),X(50)
03070      C
03080      C-----CHAPTER 1-----
03090      C
03100      SI=0
03110      SX=0
03120      SX2=0
03130      SX3=0
03140      SX4=0
03150      SY=0
03160      SXY=0
03170      SX2Y=0
03180      C
03190      C-----CHAPTER 2-----
03200      C
03210      C      REFRAGRADING X AND Y
03220      C
03230      DO 10 I=1,NMAX
03240      Y(I)=F(I)**2
03250      X(I)=SOR(U(I))
03260      C
03270      C-----CHAPTER 3-----
03280      C
03290      X2(I)=U(I)
03300      X3(I)=U(I)*X(I)

```

ORIGINAL PAGE IS
OF POOR QUALITY

```

03310      X4(I) =X(I)**2
03320      XY(I) =X(I)*Y(I)
03330      X2Y(I) =X(I)*X(I)
03340      S1=1
03350      SX=SX+X(I)
03360      SX2=SX2+X2(I)
03370      SX3=SX3+X3(I)
03380      SX4=SX4+X4(I)
03390      SY=SY+Y(I)
03400      SXY=SXY+XY(I)
03410      SX2Y=SX2Y+X2Y(I)
03420 C      USE LEAST SQUARE CURVE FIT METHOD
03430 C      APPLY CRAMER'S RULE TO SOLVE THE THREE EQUATIONS FOR
03440 C      A,B, AND C.
03450 10  CONTINUE
03460      C1=SX2*SX4-SX3*SX3
03470      C2=SX1*SX4-SX2*SX3
03480      C3=SX1*SX3-SX2*SX2
03490      DET=S1*C1-SX*C2+SX2*C3
03500      B1=SXY*SX4-SX2Y*SX3
03510      B2=SXY*SX3-SX2Y*SX2
03520      AA0=SY*C1-SX*B1+SX2Y*B2
03530      A=AA0/DET
03540      D1=SX*SX2Y-SX2*SXY
03550      AA1=S1*B1-SY*C2+SX2*D1
03560      B=AA1/DET
03570      E1=SX*SX2Y-SX2*SXY
03580      AA2=S1*(-B2)-SX*E1+SY*B3
03590      C=AA2/DET
03600      RETURN
03610      END
03620      SUBROUTINE C2FIT(IMAX,ANGU,CONST,A,B)
03630 C
03640 C      THIS SUBROUTINE DOES A LINEAR CURVE FIT TO THE DATA
03650 C      SET OF ANGU AND CONST. THE EQUATION IS OF THE FORM:
03660 C      WHERE A IS THE POINT WHERE X=0(Y=INTERCEPT) AND B IS
03670 C      THE SLOPE OF THE LINE.
03680 C
03690 C-----CHAPTER 1-----
03700 C
03710      DIMENSION CONST(50),ANGU(50),X(50),Y(50)
03720 C
03730 C      SXY IS THE SUM OF X TIMES Y
03740 C      SX IS THE SUM OF X
03750 C      SY IS THE SUM OF Y
03760 C      SX2 IS THE SUM OF X SQUARED
03770 C
03780      SXY=0.0
03790      SX=0.0
03800      SY=0.0
03810      SX2=0.0
03820 C
03830 C-----CHAPTER 2-----
03840 C
03850 C      REPACKAGING X AND Y
03860 C
03870      DO 100 I=1,IMAX
03880      X(I)=ANGU(I)
03890      Y(I)=CONST(I)
03900 100  CONTINUE
03910 C
03920 C-----CHAPTER 3-----
03930 C
03940      DO 101 I=1,IMAX
03950      SXY=SXY+X(I)*Y(I)
03960      SX=SX+X(I)

```


UNNUMBERED LISTING

```

C
C *****
C
C *
C * THIS PROGRAM REDUCES THE INPUT X-WIRE PROBE DATA IN *
C *
C * NON SWIRLING FLOW. IT IS ASSUMED THAT THE WIRES *
C *
C * FOLLOW KING'S LAW. *
C *
C * BY *
C * BRIAN MCKILLOP *
C *
C * LAST ITERATION ON COMPUTER CODE 6-10-83 *
C *
C *****
C
C DIMENSION CALU(50),CALE1(50),CALE2(50),RDD(50),E1(50),E2(50),
&ADDE(50),SUBE(50),ATTA(50),ATTB(50),EMVDC(50),ANGU(50),
&E1DFE(50),E2DFE(50),E1D2U(50),E2D2U(50),AM1(50),AM2(50),AV1(50),
&AV2(50),DM(50),BO(50),UPRMS(50),VPRMS(50),UPDUO(50),VPDUO(50),
&REYSTR(50),U1(50),U2(50),U1DUO(50),U2DUO(50),UDUO(50),VDUO(50),
&Y(50),U(50),ABSREY(50)
C INTEGER DAY, YEAR
C REAL LDD
C
C -----CHAPTER 1-----
C -----SECTION 1-----
C
C INPUTING THE NUMBER OF POINTS FROM CALIBRATION, ANGULATION,
C AND TEST SECTION EXPERIMENTS, RESPECTIVELY.
C
C NMAX=15
C IMAX=5
C JMAX=20
C
C -----SECTION 2-----
C
C INPUTING DATA FROM CALIBRATION EXPERIMENT
C
C DATA CALU/2.43,2.76,3.38,3.95,4.63,5.11,5.92,6.72,7.65,
&8.62,9.57,10.7,11.82,13.05,14.42,35*0.0/
C READ(14,*) (CALE1(N),N=1,NMAX)
C READ(14,*) (CALE2(N),N=1,NMAX)
C WRITE(6,*) (CALE1(N),N=1,NMAX)
C WRITE(6,*) (CALE2(N),N=1,NMAX)
C
C -----SECTION 3-----
C
C INPUTING DATA FROM EXPERIMENT IN TEST SECTION
C
C DATA RDD/0.0,0.025,0.05,0.075,0.1,0.125,0.15,0.175,0.2,0.225,
&0.25,0.275,0.3,0.325,0.35,0.375,0.4,0.425,0.45,0.475,0.5,29*0.0/

```

ORIGINAL PAGE IS
OF POOR QUALITY

```

READ(15,*) (E1(J),J=1,JMAX)
READ(15,*) (E2(J),J=1,JMAX)
READ(15,*) (ADDE(J),J=1,JMAX)
READ(15,*) (SUBE(J),J=1,JMAX)
READ(15,*) (ATTA(J),J=1,JMAX)
READ(15,*) (ATTB(J),J=1,JMAX)
READ(15,*) (EMVDC(J),J=1,JMAX)
WRITE(6,*) (E1(J),J=1,JMAX)
WRITE(6,*) (E2(J),J=1,JMAX)
WRITE(6,*) (ADDE(J),J=1,JMAX)
WRITE(6,*) (SUBE(J),J=1,JMAX)
WRITE(6,*) (ATTA(J),J=1,JMAX)
WRITE(6,*) (ATTB(J),J=1,JMAX)
WRITE(6,*) (EMVDC(J),J=1,JMAX)

```

C
C-----SECTION 4-----

C
C INPUTING DATA FROM ANGULATION EXPERIMENT

```

DATA ANGU/14.42,11.82,9.57,7.65,5.11,45*0.0/
DATA E1DFE/0.6142,0.5737,0.5368,0.4996,0.4569,45*0.0/
DATA E2DFE/0.5592,0.5306,0.4938,0.4636,0.4011,45*0.0/

```

C
C-----SECTION 5-----

C
C INPUTING MISCELLANEOUS DATA

```

READ(16,*) MONTH,DAY,YEAR,XDD,LDD,ALPHA,FE,PAMB,TAMB,E01,E02,
&E01,E02
WRITE(6,*) MONTH,DAY,YEAR,XDD,LDD,ALPHA,FE,PAMB,TAMB,E01,E02,
&E01,E02

```

C
C-----CHAPTER 2-----

C
C-----SECTION 1-----

C
C THIS STATEMENT TAKES CALIBRATION VOLTAGE ONE AND DOES A
C SECOND ORDER LEAST SQUARES CURVE FIT SUCH THAT:
C $CALE1^{**2}=A1+B1*U^{**0.5}+C1*U$

```

CALL CFIT(NMAX,CALU,CALE1,A1,B1,C1)
WRITE(6,100)A1,B1,C1
100 FORMAT(///20X,'CALE1 SQUARED=',F8.3,' +',F8.3,2X,'CALU TO 1/2',
&' +',F8.3,2X,'CALU')

```

C
C-----SECTION 2-----

C
C THIS STATEMENT TAKES CALIBRATION VOLTAGE TWO AND DOES A
C SECOND ORDER LEAST SQUARES CURVE FIT SUCH THAT:
C $CALE2^{**2}=A2+B2*U^{**0.5}+C2*U$

```

CALL CFIT(NMAX,CALU,CALE2,A2,B2,C2)
WRITE(6,110) A2,B2,C2

```

```

110  FORMAT(///20X,'CALE2 SQUARED=',F8.3,'  ',F8.3,2X,'CALU TO 1/2',
      &'  ',F8.3,2X,'CALU')
C
C-----CHAPTER 3-----
C
C      DO LOOP USING ANGULATION EXPERIMENT DATA TO COMPUTE
C      SENSITIVITY COEFFICIENTS
C
      DO 300 I=1,IMAX
      E1D2U(I)=(B1+2.0*C1*ANGU(I)**0.5)/(4.0*(A1*ANGU(I)+B1*ANGU(I)**1.5
&+C1*ANGU(I)**2)**0.5)
      E2D2U(I)=(B2+2.0*C2*ANGU(I)**0.5)/(4.0*(A2*ANGU(I)+B2*ANGU(I)**1.5
&+C2*ANGU(I)**2)**0.5)
      WRITE(6,1234) E1D2U(I),E2D2U(I)
1234  FORMAT(// 10X,F10.6,10X,F10.6)
      AM1(I)=ANGU(I)*E1D2U(I)
      AM2(I)=ANGU(I)*E2D2U(I)
      AV1(I)=E1DFE(I)
      AV2(I)=E2DFE(I)
      DM(I)=AM1(I)+AM2(I)
      BO(I)=AV1(I)+AV2(I)
300   CONTINUE
C-----CHAPTER 4-----
C
C-----SECTION 1-----
C
C      THIS STATEMENT TAKES DM AND DOES A LINEAR CURVE FIT SUCH THAT:
C      DM=A3+B3*U
C
      CALL C2FIT(IMAX,ANGU,DM,A3,B3)
C      A3=0.535
C      B3=0.0632
      WRITE(6,202) A3,B3
202   FORMAT(///20X,'DM=',F8.3,'  ',F8.3,2X,'U')
C
C      THIS STATEMENT TAKES BO AND DOES A LINEAR CURVE FIT SUCH THAT:
C      BO=A4+B4*U
C
C-----SECTION 2-----
C
      CALL C2FIT(IMAX,ANGU,BO,A4,B4)
      WRITE(6,203) A4,B4
203   FORMAT(///20X,'BO=',F8.3,'  ',F8.3,2X,'U')
C
C-----CHAPTER 5-----
C
C      CALCULATING THE NOZZLE EXIT VELOCITY
C
      U01=(((-B1+(B1**2-4.0*C1*(A1-E01**2))**0.5)/(2.0*C1))**2
      U02=(((-B2+(B2**2-4.0*C2*(A2-E02**2))**0.5)/(2.0*C2))**2
      U0=(U01+U02)/2.0
C
C-----CHAPTER 6-----

```

ORIGINAL PAGE IS
OF POOR QUALITY

```

C
C      DO LOOP TO GENERATE OUTPUT DATA ,CALCULATIONS ARE PREFORMED
C      AT EACH R/D POSITION
C
      DO 1000 J=1,JMAX
      U1(J)=((-B1+(B1**2-4.0*C1*(A1-E1(J)**2))**0.5)/(2.0*C1))**2
      U2(J)=((-B2+(B2**2-4.0*C2*(A2-E2(J)**2))**0.5)/(2.0*C2))**2
      U1DU0(J)=U1(J)/U0
      U2DU0(J)=U2(J)/U0
      UDU0(J)=(U1DU0(J)+U2DU0(J))/2.0
      VDU0(J)=ABS(U1DU0(J)-U2DU0(J))/2.0
      U(J)=UDU0(J)*U0
      DM(J)=A3+B3*U(J)
      BO(J)=A4+B4*U(J)
      UPRMS(J)=ADDE(J)/DM(J)
      VPRMS(J)=SUBE(J)/BO(J)
      UPDU0(J)=UPRMS(J)*U(J)/U0
      VPDU0(J)=VPRMS(J)*U(J)/U0
      REYSTR(J)=(EMVDC(J)*10.0**((ATTA(J)+ATTB(J))/20.0)*U(J)**2/
&(U0**2*125.0*1600.0*BO(J)*DM(J)))*0.001
1000  CONTINUE
      WRITE(6,8113)U0
8113  FORMAT(/////,35X,F10.4)
C
C-----CHAPTER 7-----
C
C-----SECTION 1-----
C
C
      WRITE(6,250)
250  FORMAT(1H1)
C
C      WRITE STATEMENTS FOR MISCELLANEOUS DATA
C
      WRITE(6,251) MONTH,DAY,YEAR
251  FORMAT(//,45X,'DATA TAKEN',2X,I2,'/',I2,'/',I2)
      WRITE(6,252) KDD,LDD
252  FORMAT(/,30X,'X/D=',F4.1,30X,'L/D=',F4.1)
      WRITE(6,253) ALPHA,FE
253  FORMAT(/,30X,'ALPHA=',F4.1,28X,'FE=',F4.1)
      WRITE(6,254) PAMB,TAMB,U0,E01,E02
254  FORMAT(/,25X,'PAMB=',F4.1,5X,'TAMB=',F5.1,5X,'U0=',F8.4,
&5X,'E01=',F4.2,5X,'E02=',F4.2)
C
C-----SECTION 2-----
C
C      WRITE STATEMENT FOR HEADINGS
C
      WRITE(6,255)
255  FORMAT(///,13X,'R/D',7X,'U1/U0',6X,'U2/U0',5X,'U/U0',8X,'V/U0',
&9X,'U"/U0',7X,'V"/U0',9X,'U" V"/U0**2')
C
C-----SECTION 3-----
C

```


C WRITE STATEMENT FOR GENERATED OUTPUT

C

```

      WRITE(6,1001) (RDD(J),U1DUO(J),U2DUO(J),UDUO(J),VDUO(J),
&UPDUO(J),VPDUO(J),REYSTR(J),J=1,JMAX)
1001 FORMAT(/,10X,F8.3,2X,F8.3,3X,F8.3,2X,F8.3,4X,F8.3,5X,
&F8.3,4X,F8.3,9X,F10.6)

```

C

C-----CHAPTER 8-----

C

C PLOTTING THE OUTPUT DATA

C

```

      WRITE(6,8020)
8020  FORMAT(1H1)
      WRITE(6,8021)
8021  FORMAT(/,30X,'R/D',20X,'U/UO')
      WRITE(6,8022) (RDD(J),UDUO(J),J=1,JMAX)
8022  FORMAT(/,27X,F8.3,15X,F8.3)
      YMAX=0.5
      XMAX=1.0
      CALL SUBPLT(Y,XMAX,YMAX,UDUO,RDD,JMAX)
      WRITE(6,8000)
8000  FORMAT(/54X,'U/UO')
      WRITE(6,8020)
      WRITE(6,8023)
8023  FORMAT(/,30X,'R/D',20X,'V/UO')
      WRITE(6,8022) (Y(J),VDUO(J),J=1,JMAX)
      DO 1670 J=1,JMAX
      RDD(J)=Y(J)
1670  CONTINUE
      CALL SUBPLT(Y,XMAX,YMAX,VDUO,RDD,JMAX)
      WRITE(6,8001)
8001  FORMAT(/54X,'V/UO')
      WRITE(6,8020)
      WRITE(6,8028)
8028  FORMAT(/,30X,'R/D',20X,'U"/UO')
      WRITE(6,8022) (Y(J),UPDUO(J),J=1,JMAX)
      XMAX=0.25
      DO 1673 J=1,JMAX
      RDD(J)=Y(J)
1673  CONTINUE
      CALL SUBPLT(Y,XMAX,YMAX,UPDUO,RDD,JMAX)
      WRITE(6,8004)
8004  FORMAT(/54X,'U"/UO')
      WRITE(6,8020)
      WRITE(6,8029)
8029  FORMAT(/,30X,'R/D',20X,'V"/UO')
      WRITE(6,8022) (Y(J),VPDUO(J),J=1,JMAX)
      DO 1674 J=1,JMAX
      RDD(J)=Y(J)
1674  CONTINUE
      CALL SUBPLT(Y,XMAX,YMAX,VPDUO,RDD,JMAX)
      WRITE(6,8005)
8005  FORMAT(/54X,'V"/UO')
      WRITE(6,8020)

```

ORIGINAL PAGE IS
OF POOR QUALITY

```

      WRITE(6,8030)
8030  FORMAT(/,30X,'R/D',17X,'U" V"/U0**2')
      WRITE(6,8031)(Y(J),REYSTR(J),J=1,JMAX)
8031  FORMAT(/,27X,F8.3,14X,F10.6)
      DO 1675 J=1,JMAX
      RDD(J)=Y(J)
1675  CONTINUE
      XMAX=0.02
      DO 1700 J=1,JMAX
      ABSREY(J)=ABS(REYSTR(J))
1700  CONTINUE
      CALL SUBPLT(Y,XMAX,YMAX,ABSREY,RDD,JMAX)
      WRITE(6,8006)
8006  FORMAT(/51X,'U" V"/U0**2')
C
C-----
C*****
C-----
C
      STOP
      END
      SUBROUTINE CFIT(NMAX,U,E,A,B,C)
C      THIS PROGRAM DOES A SECOND ORDER CURVE FIT TO GIVEN
C      HOTWIRE CALIBRATION DATA.
C      THE EQUATION IS OF THE FORM  $E^{**2}=A+B*SQR(U)+C*U$ 
C
C      DIMENSION E(50),U(50),Y(50),X2(50),X3(50),X4(50),XY(50),
      *X2Y(50),X(50)
C
C-----CHAPTER 1-----
C
      SI=0
      SX=0
      SX2=0
      SX3=0
      SX4=0
      SY=0
      SXY=0
      SX2Y=0
C
C-----CHAPTER 2-----
C
      REPACKAGING X AND Y
C
      DO 10 I=1,NMAX
      Y(I)=E(I)**2
      X(I)=SQRT(U(I))
C
C-----CHAPTER 3-----
C
      X2(I)=U(I)
      X3(I)=U(I)*X(I)
      X4(I)=U(I)**2

```

ORIGINAL PAGE IS
OF POOR QUALITY

```

XY(I)=X(I)*Y(I)
X2Y(I)=XY(I)*X(I)
SI=I
SX=SX+X(I)
SX2=SX2+X2(I)
SX3=SX3+X3(I)
SX4=SX4+X4(I)
SY=SY+Y(I)
SKY=SKY+XY(I)
SX2Y=SX2Y+X2Y(I)
C      USE LEAST SQUARE CURVE FIT METHOD
C      APPLY CRAMERS RULE TO SOLVE THE THREE EQUATIONS FOR
C      A,B,AND C.
10    CONTINUE
      C1=SX2*SX4-SX3*SX3
      C2=SX*SX4-SX2*SX3
      C3=SX*SX3-SX2*SX2
      DET=SI*C1-SX*C2+SX2*C3
      B1=SKY*SX4-SX2Y*SX3
      B2=SKY*SX3-SX2Y*SX2
      AAO=SY*C1-SX*B1+SX2*B2
      A=AAO/DET
      D1=SX*SX2Y-SX2*SKY
      AA1=SI*B1-SY*C2+SX2*D1
      B=AA1/DET
      E1=SX*SX2Y-SX2*SKY
      AA2=SI*(-B2)-SX*E1+SY*C3
      C=AA2/DET
      RETURN
      END
      SUBROUTINE C2FIT(IMAX,ANGU,CONST,A,B)
C
C      THIS SUBROUTINE DOES A LINEAR CURVE FIT TO THE DATA
C      SET OF ANGU AND CONST. THE EQUATION IS OF THE FORM Y=A+BX
C      WHERE A IS THE POINT WHERE X=0(Y-INTERCEPT) AND B IS
C      THE SLOPE OF THE LINE.
C-----CHAPTER 1-----
C
      DIMENSION CONST(50),ANGU(50),X(50),Y(50)
C
C      SKY IS THE SUM OF X TIMES Y
C      SX IS THE SUM OF X
C      SY IS THE SUM OF Y
C      SX2 IS THE SUM OF X SQUARED
C
      SKY=0.0
      SX=0.0
      SY=0.0
      SX2=0.0
C-----CHAPTER 2-----
C
      REPACKAGING X AND Y

```

```

C
DO 100 I=1,IMAX
X(I)=ANGU(I)
Y(I)=CONST(I)
100 CONTINUE
C
C-----CHAPTER 3-----
C
DO 101 I=1,IMAX
SXY=SXY+X(I)*Y(I)
SX=SX+X(I)
SY=SY+Y(I)
SX2=SX2+X(I)**2
101 CONTINUE
XMEAN=SX/IMAX
YMEAN=SY/IMAX
B=IMAX*SXY-SX*SY
B=B/(IMAX*SX2-SX**2)
A=YMEAN-B*XMEAN
RETURN
END
SUBROUTINE SUBPLT(Y,XMAX,YMAX,XX,YY,NLAST)
C
C-----CHAPTER 1-----
C
DIMENSION IM(1400),XX(50),YY(50),X(50),Y(50)
DO 1200 J=1,NLAST
X(J)=XX(J)
Y(J)=YY(J)
1200 CONTINUE
WRITE(6,1500)
1500 FORMAT(1H1)
CALL PLOT1(0,6,10,5,20)
CALL PLOT2(IM,XMAX,0.0,YMAX,0.0)
CALL PLOT3(1H*,X,Y,NLAST,4)
CALL PLOT4(3,'R/D')
RETURN
END

```

SAMPLE ADDRESSED DATA FILES

U12382A.DECBM.CAL.D10523.DATA

3.487,3.563,3.631,3.697,3.761,3.817,3.876,3.929,3.988,4.042,
4.098,4.151,4.210,4.259,4.310
3.502,3.568,3.634,3.700,3.761,3.817,3.873,3.924,3.981,4.032,
4.088,4.142,4.198,4.247,4.298

U12382A.DECBM.EXP.D10523.P15.DATA

4.344,4.344,4.337,4.322,4.318,4.300,4.274,4.244,4.198,4.125,
4.061,3.998,3.910,3.807,3.761,3.719,3.639,3.619,3.595,3.575
4.305,4.305,4.305,4.305,4.296,4.288,4.274,4.242,4.220,4.159,
4.112,4.046,3.973,3.900,3.824,3.768,3.734,3.675,3.631,3.614
0.0725,0.0742,0.0798,0.0904,0.0975,0.1166,0.1395,0.1612,
0.1943,0.2086,0.2282,0.2288,0.2384,0.2431,0.2396,0.2447,
0.2466,0.2424,0.2386,0.2399
0.0466,0.0492,0.0510,0.0589,0.0685,0.0759,0.0968,0.1125,
0.1348,0.1500,0.1629,0.1729,0.1749,0.1725,0.1693,0.1653,
0.1587,0.1494,0.1386,0.1227
35.0,35.0,35.0,35.0,36.0,36.0,39.0,39.0,39.0,39.0,39.0,39.0,
39.0,39.0,39.0,39.0,39.0,39.0,39.0,39.0
35.0,35.0,35.0,35.0,36.0,36.0,39.0,39.0,39.0,39.0,39.0,39.0,
39.0,39.0,39.0,39.0,39.0,39.0,39.0,39.0
254.0,255.0,230.0,277.0,338.0,377.0,520.0,626.0,706.0,734.0,
715.0,676.0,599.0,505.0,459.0,372.0,324.0,241.0,186.0,133.0

U12382A.DECBM.MISC.D10523.P15.DATA

5,23,83,1.5,2.0,90.0,0.0,74.2,27.0,4.396,4.330,2.81,2.87